8-1-2010

# Mechanisms of hardening in HCP structures through dislocation transmutation and accommodation effects by glide twinning: application to magnesium

A L Oppedal

# MECHANISMS OF HARDENING IN HCP STRUCTURES THROUGH DISLOCATION TRANSMUTATION AND ACCOMMODATION EFFECTS BY GLIDE TWINNING: APPLICATION TO MAGNESIUM

By

Andrew Lars Oppedal

A Dissertation
Submitted to the Faculty of
Mississippi State University
in Partial Fulfillment of the Requirements
for the Degree of Doctor of Philosophy
in Mechanical Engineering
in the Department of Mechanical Engineering

Mississippi State, Mississippi

August 2010

MECHANISMS OF HARDENING IN HCP STRUCTURES THROUGH DISLOCATION TRANSMUTATION AND ACCOMMODATION EFFECTS BY GLIDE TWINNING: APPLICATION TO MAGNESIUM

By

Andrew Lars Oppedal

Approved:

Haitham El Kadiri
Assistant Professor of Mechanical Engineering
(Co-Major Professor)

Mark F. Horstemeyer
Professor of Mechanical Engineering
(Co-Major Professor)

Carlos N. Tomé
Los Alamos National Laboratory
Technical Staff Member
(Committee Member)

Douglas J. Bammann
Professor of Mechanical Engineering
(Committee Member)

John T. Berry
Professor of Mechanical Engineering
(Committee Member)

Philip M. Gullett
Assistant Professor of Civil and Environmental Engineering
(Committee Member)

Esteban B. Marin
Center for Advanced Vehicular Systems
Research Professor
(Committee Member)

David L. Marcum
Professor of Mechanical Engineering
(Graduate Coordinator)

Sarah A. Rajala
Dean of the James Worth Bagley College of Engineering

Name: Andrew Lars Oppedal

Date of Degree: August 7, 2010

Institution: Mississippi State University

Major Field: Mechanical Engineering

Co-Major Professor: Dr. Haitham El Kadiri

Co-Major Professor: Dr. Mark F. Horstemeyer

Title of Study: MECHANISMS OF HARDENING IN HCP STRUCTURES THROUGH DISLOCATION TRANSMUTATION AND ACCOMMODATION EFFECTS BY GLIDE TWINNING: APPLICATION TO MAGNESIUM

Pages in Study: 140

Candidate for Degree of Doctor of Philosophy

At low temperatures, glide twinning activates in HCP structures easier than non-close packed slip necessary to accommodate strain along the c-axis. In contrast to slip, twinning occurs as an accumulation of successive stacking faults that properly report reconstruction of the stacking sequence in a new crystal-reorientated lenticular lamella. These faults are spread by partial dislocations known as twinning dislocations, forcing atoms to switch positions by shear into new crystal planes. As the twinning dislocations thread the faults, the new crystal lamella grows at the expense of the parent. Grain texture changes upon strain, and a strong non-linear trend marks the strain hardening rate. The strain hardening rate changes to a point where it switches sign upon strain. Since activation of these twinning dislocations obey Schmid's law, twinning could be precluded or exhaustively promoted in sharp textures upon slight changes in loading orientations, so strong anisotropy arises. Moreover, a twinning

shear can only reproduce the stacking sequence in one direction, unless the twin mode changes or the c/a ratio crosses a certain ratio. When a twin mode arises with reversed sign, the reorientation is different and more importantly, the strength is different and also the growth rate. Therefore, in addition to strain anisotropy, twin polarity induces a strong asymmetry in textured HCP structures, e.g. wrought HCP metals. This anisotropy/asymmetry is still a barrier to the great economic gain expected from the industrialization of low density, high specific strength and stiffness, HCP Magnesium. This barrier has stimulated efforts to identify the missing links in current scientific knowledge to proper prediction of Magnesium anisotropy. The effect of twinning-induced texture change on the mechanical response is of a major concern. Mesoscale modelers still struggle, without success to predict simultaneously twinning and strain hardening rates upon arbitrary loading directions. We propose a new mechanism that relies on admitting dislocation populations of the twin by dislocations transmuted from the parent when they intersect twinning disconnections. These dislocations interact with original dislocations created in the twin to cause hardening able to faithfully capture anisotropy upon any loading orientation and any initial texture.

Key words: crystal plasticity, deformation twinning, magnesium, texture, ebsd

DEDICATION

I dedicate this work to my family, who endured many sacrifices without complaint and supported me in countless ways to make this possible.

ACKNOWLEDGMENTS

I would like to express my sincere gratitude to my co-advisors Mark Horstemeyer and Haitham El Kadiri for the generous and patient gift of their time and insight in helping me navigate through the sometimes arduous path of finishing this thesis and the entire graduate program.

My special thanks go foremost to Carlos Tomé for introducing me to the world of crystal plasticity and the fundamentals of twinning, the opportunity to complete experimental work at Los Alamos National Laboratory under his mentorship, the use of the Visco-Plastic Self-Consistent (VPSC) code, as well as the many interactions since.

I am honored to have been supervised by these three great researchers in the field of plasticity and whose impact will felt for my scientific career.

I am also thankful to my other graduate committee members, including Esteban Marin, Douglas Bammann, John Berry, and Philip Gullett for the many deeply appreciated discussions.

Other people assisted me as well, and at the Center for Vehicular Systems (CAVS), the list includes: Arsalan Adil, Crawford Baird, Ibrahim Gaber, Stephen Horstemeyer, Quancang Ma and Wilburn Whittington for their assistance with some of the experimental work; Ricolindo Cariño and Bohumir Jelenik with some of the numerical simulations work and guidance with GNU/Linux; and the camaraderie of fellow gradu-

ate students Mei Qiang Chandler, Brian Jordon, Matthew Tucker, Kiran Solanki, Neil Williams and others, many of whom have completed their programs of study and are now scientists in their own right.

During a summer at Los Alamos National Laboratory, where some of the experimental work was done, I am grateful for the contributions of Laurent Capolungo for discussions on VPSC modeling, George Kaschner for discussions on mechanical testing, Ricardo Lebensohn for discussions on the VPSC code, Manuel Lovato for performing some mechanical testing, Rodney McCabe for discussions on SEM, EBSD and TEM, Carlos Tomé and Sven Vogel for performing neutron diffraction texture analysis on samples.

The financial support of the Center for Advanced Vehicular Studies, the Hearin Foundation, Department of Energy Southern Regional Center for Lightweight Innovative Design, the U.S. Army Tank Automotive Research, Development and Engineering Center (TARDEC) and Department of Energy Basic Energy Science funded this work.

TABLE OF CONTENTS

LIST OF TABLES

LIST OF FIGURES

LIST OF SYMBOLS, ABBREVIATIONS, AND NOMENCLATURE

| | |
|---|---|
| $\rho$ | Dislocation density |
| $V$ | Volume fraction of twin in a grain |
| $\alpha$ | Transmutation matrix |
| $C$ | Correspondence matrix |
| $R$ | Rotation Matrix |
| $S$ | Characteristic Shear Matrix |
| $\xi$ | Accommodation effect parameter |
| $k_1$ | Constant for dislocation generation |
| $k_2(\dot{\varepsilon}, T)$ | Constant for dislocation removal |
| $D$ | Drag stress |
| $g$ | Activation energy |
| $s$ | Characteristic twin shear |
| $\otimes$ | Tensor product |
| $\overline{\otimes}$ | Contracted tensor product |
| $\overline{\overline{\otimes}}$ | Double contracted tensor product |
| $\tau$ | Shear stress |

| | |
|---|---|
| $\gamma$ | Shear strain |
| $\dot{\gamma}$ | Shear strain rate |
| $m$ | Schmid Factor |
| $D$ | Drag Stress |

CHAPTER 1

# INTRODUCTION

## 1.1 Summary

The goal of this thesis is to develop a mesoscale model capable of simultaneously predicting the stress-strain behavior, twin volume fraction evolution, and texture evolution in hexagonal close packed (HCP) metals that can profusely twin. The research objectives of this thesis are to expand and assess with numerical and experimental investigations an existing mesoscale dislocation-based model [Beyerlein and Tomé, 2008] that captures (i) hardening by dislocation transmutation upon their incorporation in the twinned regions, (ii) twin accommodation effects, and (iii) dislocation-dislocation latent hardening. The theoretical expansion in each of these three research objectives will be achieved through researching a set of mathematical equations in ascending capabilities based on the physics and appropriate kinematics/kinetics gaging the effects of energetics and driving forces acting on the evolving topology of dislocations and twin disconnections. The success measure of the theories will be based upon validation and assessment by consecutive numerical and experimental investigations. The numerical investigations will consist of modifications to the hardening models in the Visco-Plastic Self-Consistent VPSC code originally developed by Lebensohn and Tomé [1993]. The VPSC framework provides a robust stress estimation scheme in the grains using the

self-consistent method based on Eshelby's inclusion theory [Eshelby, 1957]. Second, using pure magnesium and an extruded AM30-graded magnesium as testbeds for the theories, the code will simulate the stress-strain behaviors, intermediate textures, and volume fraction of twins under various loading orientations. The simulation results will be evaluated by experimental results obtained through mechanical testing under simple compression, macrotexture analyses through Neutron Diffraction and X-Ray diffraction (XRD), and microtexture analyses through Electron Backscatter Diffraction (EBSD). The existing dislocation-based model shows an exciting long-term prospect since the formulation allows the underlying physics of hardening to be mathematically captured if the effects of stress, texture, strain rate, prestrain and temperature on dislocation nature and topology are understood at the atomic and microscopic scale levels.

## 1.2 Intellectual Merit

This project will enable the science of polycrystal plasticity to give for the first time a physics-based rationalization of the increasing strain hardening rate of Regime II [El Kadiri and Oppedal, 2010] encountered only under profuse twinning. Regime II was indeed satisfactorily predicted in previous literature, with a noticeable offset from either or both of the observed intermediate twin volume fractions and intermediate textures, and sometimes from the location and amplitude of the inflection point separating Regime II and Regime III (e.g. Proust et al. [2009]). Regime II is viewed and researched in this project as to be primarily underlain by the high magnitude of slip-slip latent hardening in the twin upon transmutation of incorporated dislocations.

Even in materials where twinning is not preceded by substantial easy slip, the twin accommodation effects in polycrystals is expected in this project to generate enough slip dislocations for the transmutation to be effective at the early stages of Regime II. This project will make a substantial push in the science of multiscale modeling approaches that have a tremendous difficulty to encompass HCP structures.

## 1.3 Broader Impacts

The automotive and aircraft industries will be the primary beneficiary of this project. As lightweighting vehicles became one of the main concerns of the nation under the constraints of foreign oil dependence, magnesium and titanium are researched to be massively integrated in large mechanical structures. This project will enable to overcome the economical barriers against their integration in automotive and aircraft structures.

## 1.4 Background

Magnesium alloys have attractive properties in applications that favor lower weight [Mordike and Ebert, 2001], [Roberts, 1960]. However, magnesium alloys exhibit an HCP (hexagonal close packed) crystalline structure that leads to low ductility and strong anisotropy compared to other FCC (face centered cubic) and BCC (body centered cubic) metals. In fact, magnesium can undergo profuse recrystallization twinning and glide twinning during their manufacturing and performance which leads to a marked anisotropy. Figure 1.2 illustrates this anisotropy in a rolled polycrystal pure

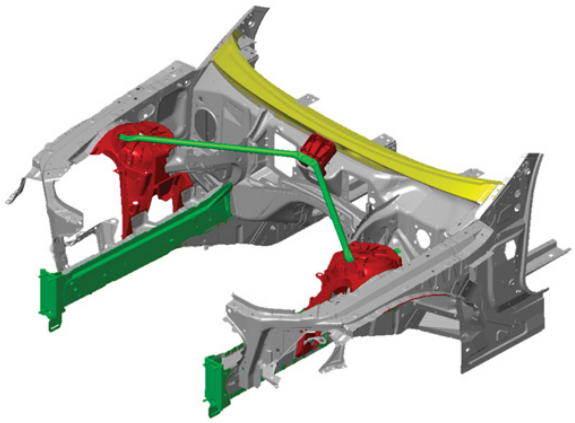

Figure 1.1 DOE-USCAR Front End Magnesium Project.

Potential magnesium front-end components that will be redesigned for the DOE-USCAR Front End Magnesium Project. [USAMP AMD 604, 2006]

magnesium sheet when loaded along the ND (normal direction - the parabolic $\sigma - \epsilon$ curve) and along the RD (rolling direction - the "sigmoidal" $\sigma - \epsilon$ curve). Particularly, recrystallization and glide twinning induce a substantial development of sharp textures, which is problematic against meeting design specifications at acceptable manufacturing rates. For performance, glide twinning promotes faster propagation of fatigue cracks under cyclic loading. This project will enable the industry to reliably improve the controllability of the manufacturing conditions, which is essential to cost-effectively improving the durability of lightweight materials. If the ductility and anisotropy could be controlled, magnesium alloys could be developed and formed to fill an increasing market as lighter weight, more fuel efficient vehicles become important. Figure 1.1 shows potential front-end components for magnesium research under the umbrella of the DOE-USCAR Front-End Magnesium Project.

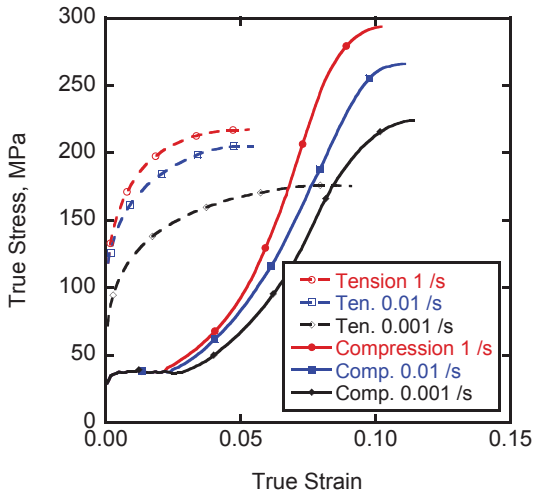


Figure 1.2 Magnesium mechanical anisotropy.

Polycrystalline pure textured Magnesium stress-strain plot shows anisotropic behavior. Rolled sheet material, in-plane direction shows a "parabolic" curve for tension, "sigmoidal" for tension. The "sigmoidal" shape is caused by deformation twinning. [Reed-Hill, 1973]

In order for magnesium to be used in a ubiquitous design mode, the notion of the structure-property relations is key. In the context of this research, the focus will be mechanisms of strain hardening by glide twinning. In particular, a crystal plasticity model that comprehensively captures the effect of twinning will be researched and validated. Experiments from the literature and performed in this effort will be performed to provide information regarding the evolution of twins for pure magnesium.

## 1.5 Dissertation Structure

Chapter I describes the motivation for the dissertation and introduces the concepts of the thesis. Chapter II describes in detail the fundamental details of twinning, strain path anisotropy, a background to the implementation of twinning into mesoscale

crystal plasticity modeling, and the proposed mechanisms that cause anisotropy in magnesium, and a proposed method to implement the dislocation transmutation and twin accommodation mechanisms in the existing VPSC model. Chapter III is an application of this dislocation transmutation concept to basal textured pure magnesium comparing VPSC simulations to experimental behavior and macro- and micro texture analysis. Chapter IV is an application to a rod textured, extruded AM30 Magnesium comparing simulations from VPSC using two different hardening rules and mechanical behavior of samples with four different loading paths. Chapter V is a summary of the work and recommendations for future work.

# CHAPTER 2

# A CRYSTAL PLASTICITY THEORY FOR LATENT HARDENING BY GLIDE TWINNING THROUGH DISLOCATION TRANSMUTATION AND TWIN ACCOMMODATION EFFECTS

## 2.1 Summary

Imagine a residual glide twin interface advancing in a grain under the action of a monotonic stress. Close to the grain boundary, the shape change caused by the twin is partly accommodated by kinks and partly by slip emissions in the parent; the process is known as accommodation effects. When reached by the twin interface, slip dislocations in the parent undergo twinning shear. The twinning shear extracts from the parent dislocation a twinning disconnection, and thereby releases a transmuted dislocation in the twin. Transmutation populates the twin with dislocations of diverse modes. If the twin deforms by double twinning, double-transmutation occurs even if the twin retwins by the same mode or detwins by a stress reversal. If the twin deforms only by slip, transmutation is single. Whether single or double, dislocation transmutation is irreversible. The multiplicity of dislocation modes increases upon strain, since the twin finds more dislocations to transmute upon further slip of the parent and further growth of the twin. Thus, the process induces an increasing latent hardening rate in the twin. Under profuse twinning conditions, typical of double-lattice structures, this

rate-increasing latent hardening combined with crystal rotation to hard orientations by twinning is consistent with a regime of increasing hardening rate, known as Regime II or Regime B. In this chapter, we formulate governing equation of the above transmutation and accommodation effects in a crystal plasticity framework. We use the dislocation density based model originally proposed by Beyerlein and Tomé [2008] to derive the effect of latent hardening in a transmuting twin. The theory is expected to contribute to surmounting the difficulty that current models have to *simultaneously* predict under profuse twinning, the stress-strain curves, intermediate deformation textures, and intermediate twin volume fractions.

## 2.2 Introduction

In hexagonal metallic double-lattice structures, the possible slip modes accommodating deformation along the $c$-axis require the creation and glide of dislocations with large Burgers vector on planes atomically rough leaving high-energy stacking faults. For instance, a perfect $\langle c+a \rangle$ dislocation lying on a pyramidal plane may require 12 atomic bonds to break, compared to only five needed to break for the nucleation of a glissile dislocation lying on a close packed basal plane [Rosenbaum, 1964]. Glide twinning thus occurs as an easier homogeneous simple shear to mediate $c$-axis deformation. The twin can easily form and grow from glide activities of liberated partial twinning dislocations that spread a stable twin fault. In double-lattice structures, the shear is mostly accompanied by necessary atomic shuffles.[1] Atomic shuffles do

[1] $\{11\bar{2}1\}$ are the only twins in metallic HCP structures not requiring atomic shuffles.

not induce deformation, but cost energy. The mechanisms underlying production of twinning dislocations and atomic shuffles during the nucleation and growth regimes are still not well understood with the rigor needed to capture them in a numerical crystal plasticity model.[2]

Glide twinning (a kind of deformation twinning) exhibits the dual macroscopic complication over slip of being polar and discontinuously reorienting a region of the parent grain. The polarity brings about the necessity of at least two frequent twin modes to accommodate both tension and compression. The $\{10\bar{1}2\}$ twins in metals such as Mg, Ti, Zr and Be can present a relatively low characteristic shear and simple atomic shuffle mechanisms, making them the most frequent twins in these metals. They are tensile twins[3] for most commercialized[4] HCP metals, as the shear reversal from tensile to compressive for these twins operates at $c/a$ ratio equal to $\sqrt{3}$. In fact, apart from Zn and Cd, the rest of most of the other commercialized HCP metals such as Ti, Re, Be, Zr and Mg have a $c/a$ ratio falling in a narrow subgroup band just below the perfect $\sqrt{8/3}$ ratio. Although $\{10\bar{1}3\}$ twins offer a low characteristic shear for tension in this band, they are usually associated with double-twinning by $\{10\bar{1}2\}$, so propagation is rendered difficult. On the other hand, the most frequent twins offering compression in this $c/a$ band are $\{10\bar{1}1\}$ and $\{11\bar{2}2\}$. The first is, however, usually affected by double-twinning with $\{10\bar{1}2\}$, while the second has a higher characteristic

[2]The problems of twin nucleation and twin growth are, however, beyond the scope of this work.

[3]Tensile or compressive refer to the sign of deformation with respect to the $c$-axis.

[4]Apart from Helium, there is a total of 22 discovered HCP metals with different $c/a$ ratios

shear, so propagation and nucleation are more difficult, respectively. For both types of these twins, the propagation is further mitigated by the more complex shuffles lowering the mobility of twinning dislocations. A dislocation with a Burgers vector having a component along the *c*-axis may then be favored over compressive twinning under appropriate temperature and stress regimes. Other possible twin systems predicted by the non-shuffling shear minimization approach [Jaswon and Dove, 1956, 1957, 1960] involve either, complex shuffles, double-twinning or otherwise, a higher characteristic shear. Low temperature always favors glide twinning over slip regardless of the twin mode and polarity.

The crystallographic reorientation caused by twinning is a regional volume (proportional to the characteristic twin shear deformation), but it can spread upon deformation at a rate that dramatically changes the type and activity of operative deformation modes. A sigmoidal stress-strain behavior with an inflection point is thus systemic with profuse twinning. Profuse twinning can be favored or inhibited in sharp textured materials by changing the loading orientation. This results in strong mechanical anisotropy, which is problematic for forming and performance of HCP metals.

Casting has been regarded as a possible manufacturing solution to generate random textures. However, at high temperature, some commercialized metals such as Mg and Ti are excessively reactive — they entrap excessive amounts of pores and atmospheric elements which impair fatigue resistance. Furthermore, recrystallization

twinning can be systemic in solidification textures relative to some important materials such as Mg.

Accordingly, the past two decades have seen intensive research into predicting anisotropy of formed HCP metals through polycrystal plasticity simulations. An important focus was dedicated to develop polycrystal plasticity codes that can capture deformation for both single and double-lattice structures. Pioneering works by Molinari et al. [1987] and Lebensohn and Tomé [1993] led to the Visco-Plastic Self-Consistent (VPSC) code. The micromechanical self-consistent method precludes the need of finite elements (FE) and provides more realistic stress estimation than in Taylor's [Taylor, 1938] and Sachs' [Sachs, 1928] assumptions. As such, faster runs could be performed by reasonably reducing the total number of orientations. The constitutive laws used in the VPSC model, however, corresponded to models originally developed to suit slip deformation mechanisms, and as such were unable to capture mechanisms unique to glide twinning. A recent attempt was made by Beyerlein and Tomé [2008] for a dislocation density based constitutive law for Zr using equations from Mecking and Kocks [1981]. The dislocation density based formulation is a suitable framework for incorporation of microscopic deformation mechanisms related to interaction between slip and glide twinning.

In this chapter, we review some important elements of these mechanisms and formulate governing equations, without extreme mathematical complexity, within the dislocation density based framework. We particularly introduce the hardening effect

of dislocation "transmutation"[5] upon their incorporation in the twinned regions. This allows us to suggest an additional basis to interpreting the sigmoidal curve associated with profuse twinning that was classically attributed to the combined effect of Hall-Petch mechanism and the triggering of high stacking fault slip modes and/or high-shear twins in the twinned regions.

### 2.3 Current correlation approaches to hardening in HCP

Annealed, textured Zr and Mg with a $c$-axis fiber along the normal direction (ND) were the main processed material testbeds used to study the effect of twinning and multimode slip on anisotropy of polycrystalline HCP structures. For their simplicity, extended Voce formulations represented the hardening models most extensively utilized in polycrystal VPSC simulations to fit the macroscopic stress-strain curves. In the model correlations motivated by experimental evidence, authors primarily considered $\langle a \rangle$ slip dislocations lying on the basal and prismatic planes, $\langle c + a \rangle$ slip dislocations lying on the first/second order pyramidal planes, tensile twinning and compression twinning. For Zr, $\langle a \rangle$ slip dislocations were only lying on the prismatic planes.

For $c$-fiber textures, a simple compression perpendicular to ND (IPC) gave rise to profuse tensile twinning ($\{10\bar{1}2\}$ for Mg and Zr) (Figure 2.1). The stress-strain behavior is sigmoidal; that is, it shows an initial plateau (noted here Regime I), followed by a regime of increasing hardening rate (Regime II), and then an inflection to a regime of

[5]The change of plane and Burgers vector of a dislocation upon incorporation in the twin is referred to in the recent literature by transformation. This term was avoided by Christian and other authors to prevent confusion with transformation twins and martensitic transformation. Here we suitably adopt the nomenclature "transmutation."

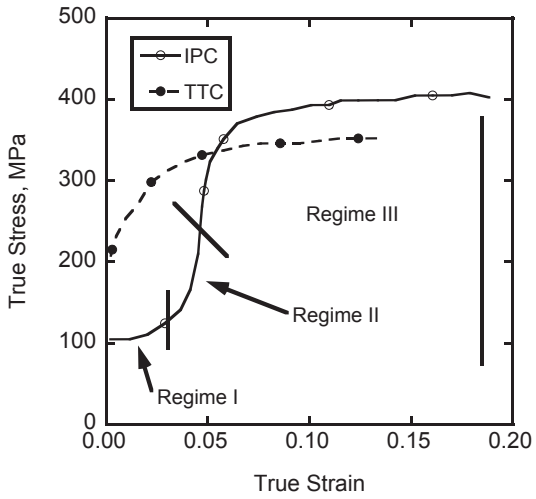


Figure 2.1 Stress-strain curves of a $c$-axis basal textured Mg AZ31.

Stress-strain curves of a $c$-axis basal textured Mg AZ31 showing a concave curve upon through thickness simple compression (TTC) and a sigmoidal shaped curve upon in-plane simple compression (IPC) with three subsequent regimes: Regime I, with constant hardening rate; Regime II with important increase in hardening rate; and Regime III with decreasing hardening rate to an asymptotic plateau. [Proust et al., 2009]

decreasing hardening rate (Regime III). (Figure 2.1). Simple compression along ND (TTC) produces a higher yield stress, and an monotonic decrease in hardening rate from a very high initial slope. This behavior in TTC is characteristic of deformation dominated by slip. However, for low temperatures, e.g. Liquid Nitrogen (LN) temperature, Zr could show an inflection point under TTC, which is associated with an important contribution of $\{10\bar{1}1\}$ compressive twinning [McCabe et al., 2006]. Unarguably, the higher yield stress and initial slope under TTC is attributed to an important contribution of the hard pyramidal $\langle c+a \rangle$ slip needed to accommodate deformation along the $c$-axis. To be consistent, this hard slip mode would also be responsible for the sharp increase of stress after the initial plateau associated with the profuse tensile twinning in IPC loading.

Tensile twinning, in fact, tends to rotate the $c$-axis fiber in the range of 90° (depending on the $c/a$ ratio), so to align it with the IPC axis; that is, a similar loading orientation as in TTC is retrieved.

Clearly, only increasing the hardness of pyramidal $\langle c+a \rangle$ slip did not provide acceptable fit to both stress-strain curves. Specifically, Voce parameters of pyramidal $\langle c+a \rangle$ slip providing good fit to the TTC curve were unable to match up the increase in hardening rate associated with Regime II under IPC. A good fit to this regime provides an overestimation of the TTC curve. Authors had then to consider modifying parameters that do not act in loading orientations where twinning is prohibited, i.e. twinning related parameters.

A slight increase of twinning self-hardening parameters caused an increase in the reference threshold stress sufficient to noticeably overestimate the initial plateau of first twin proliferation. Otherwise, the threshold stress for easy slip modes had to be unreasonably reduced, and upset the yield stresses and TTC predictions. The increased rate of twinning reference threshold stress was then kept relatively low or strictly neutralized. However, to bring the necessary hardening for Regime II, authors assumed a latent hardening of twinning on slip in the parent. This latent hardening could also harden the slip in the twinned regions if secondary twinning is allowed.

The use of slip-twin latent hardening parameters was generally successful in predicting the curve under profuse twinning conditions [Agnew and Duygulu, 2005, Parisot et al., 2004, Proust et al., 2007, Tomé et al., 1991]. However, the necessary slip-twin latent hardening capable of good fit to IPC Regime II without altering the fit

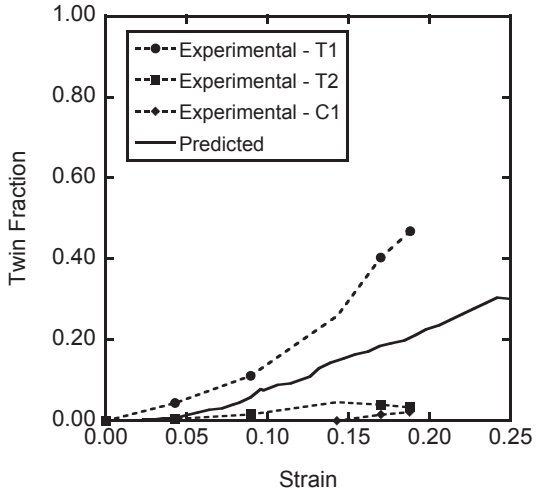


Figure 2.2 Twin volume fraction evolution of Zr.

Twin volume fraction evolution of Zr under In-Plane Compression (IPC) at 76 K of clock-rolled Zr according to experimental data from McCabe et al. [2009], and predicted data from Tomé et al. [2001]. T1 is $\{10\bar{1}2\}\langle 10\bar{1}\bar{1}\rangle$ tensile twin, T2 is $\{11\bar{2}1\}\langle 11\bar{2}\bar{6}\rangle$ tensile twin, and C1 is $\{11\bar{2}2\}\langle 11\bar{2}\bar{3}\rangle$ compressive twin.

of TTC curve ranged from 400% [Agnew and Duygulu, 2005, Jain and Agnew, 2007, Proust et al., 2007, Tomé et al., 1991] to 3500% [Proust et al., 2009] higher than a slip-slip self hardening, depending on the material and model integration. Here, it is worthwhile recalling that for FCC single lattice structures, a slip-slip latent hardening is only 20% to 40% higher than slip-slip self hardening [Kocks, 1970]. Although the twinning hardening parameters led to a good reproduction of the experimental stress-strain curve, in most cases it failed to reproduce the experimental twin volume fraction evolution. Regardless of the scheme used to evolve regions reoriented by twinning, the twin volume fraction was mostly not well predicted (Figure 2.2).

Another discrepancy unexplained by current approaches is the higher saturation stress under IPC than TTC even though pyramidal $\langle c+a \rangle$ dominates in the saturation regime for both orientations. A higher saturation in IPC reflects that the grains store more dislocations if they align their $c$-axis with the loading axis during the course of deformation by twinning, than if they were initially oriented as so. This "apparent" higher storage rate under IPC will be discussed in section 2.5.

## 2.4 The physics premises of twin -self and -latent hardenings

The latent hardening of twin on slip in the parent could not be physically supportable unless a twin boundary can act as a barrier against slip dislocations. That is, a sort of pile-up could be asserted occurring ahead of the twin interface. The grain refinement caused by twinning could thus increase the Hall-Petch effect, which would draw a physics-premise for the correlation approach based on slip-twin latent hardening. Mechanisms related to the effect of dislocation pile ups ahead of a growing glide twin on hardening constitute an intricate problem. There is indeed formal evidence of pile-ups against twin interfaces, but the twins were mostly annealing twins [Rémy, 1981] or very slow growing twins prevented from further growth in BCC materials where twinning and fracture are usually associated [Mahajan, 1971, 1975, 1981]. Otherwise, a possible pile-up of dislocations arising stress concentration ahead of a growing twin is to penetrate the twin. However, as pointed out by Christian and Mahajan [1995], successive pile-up dislocations penetrating the twin must cause the induced twinning dislocations to rapidly move away along the interface. The acceleration of

the glide of these twinning disconnections will cause a faster twin growth. As such, the twin will tend to rapidly consume the pile-up and thus, substantially mitigating a tendency of hardening by the Hall-Petch effect. So pile-ups will tend to act against the hardening they would produce. Otherwise, if dissociation could not occur at the interface to ensure appropriate penetration of the pile-up in the twin, the twin interface will avoid the overworked slip band causing twin fragmentation. To our knowledge, islands of untwinned regions are indeed frequent in BCC twins but not in HCP twins. However, Sleeswyk [1962b] proposed that twin fragmentation might be rather the result of emissary dislocations bypassing obstacles. Glide of emissary dislocations is characteristic of the catastrophic lengthwise thickening of the twin. Stacking faults were recently observed in Zr tensile twins [Bhattacharyya et al., 2009] but to a very limited extent, not likely to point out to any significant effect related to Hall-Petch.

Moreover, a Hall-Petch correlated to grain refinement by *profuse* glide twinning would have an effect on hardening that should be rather higher at low fractions of twins and then critically decrease as twin lamellae start to coalesce. In fact, an average grain size or mean free path of mobile dislocations would increase as twin volume fraction increases in the coalescence regime. If Hall-Petch hardening is operational, the material would then softens as the twins grow. This tendency is inconsistent with the increasing hardening rate in Regime II. This conclusion is substantiated by Figure 2.5 revealing that twinning in an extruded AM30 alloy actually consumed the entire initial texture before strains falling closely within the upper-bound of Regime II [Oppedal et al., 2010]. The initial state before deformation is presented in Figure 2.4. An important

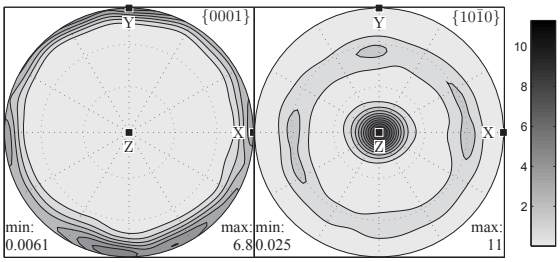


Figure 2.3 Pole figures of initial texture of AM30 Magnesium.

Complete {0001} and {10$\bar{1}$0} pole figures obtained by neutron diffraction of initial texture of AM30 Magnesium revealing an almost axisymmetric rod texture from extrusion process of a cylindrical billet. The z-axis corresponds to the extrusion direction.

point from Figure 2.5 is that the coalescence regime of twin lamellae took place before the initiation of Regime II. Therefore, any assumed Hall-Petch mechanism based on twin segmentation would have actually induced a decrease in hardening rate starting from the upper-bound of Regime I, and strictly before Regime II takes place. The fact that Regime II initiates a hardening of increasing rate clearly eliminates the assumption of Hall-Petch by grain refinements through profuse twinning.

The initial texture corresponded to an almost axisymmetric rod-texture measured by Neutron Diffraction (ND) as shown by Figure 2.3. The complete experimental method for mechanical testing and texture analyses is reported in a different paper [Oppedal et al., 2010].

Another possible hardening mechanism in the parent due to twinning could actually be attributed to the dislocations repelled by the twin, which would increase the dislocation density in the parent. In fact, Yoo [1981] demonstrated using anisotropic elasticity theory substantiated with TEM reports that some of the non-screw basal

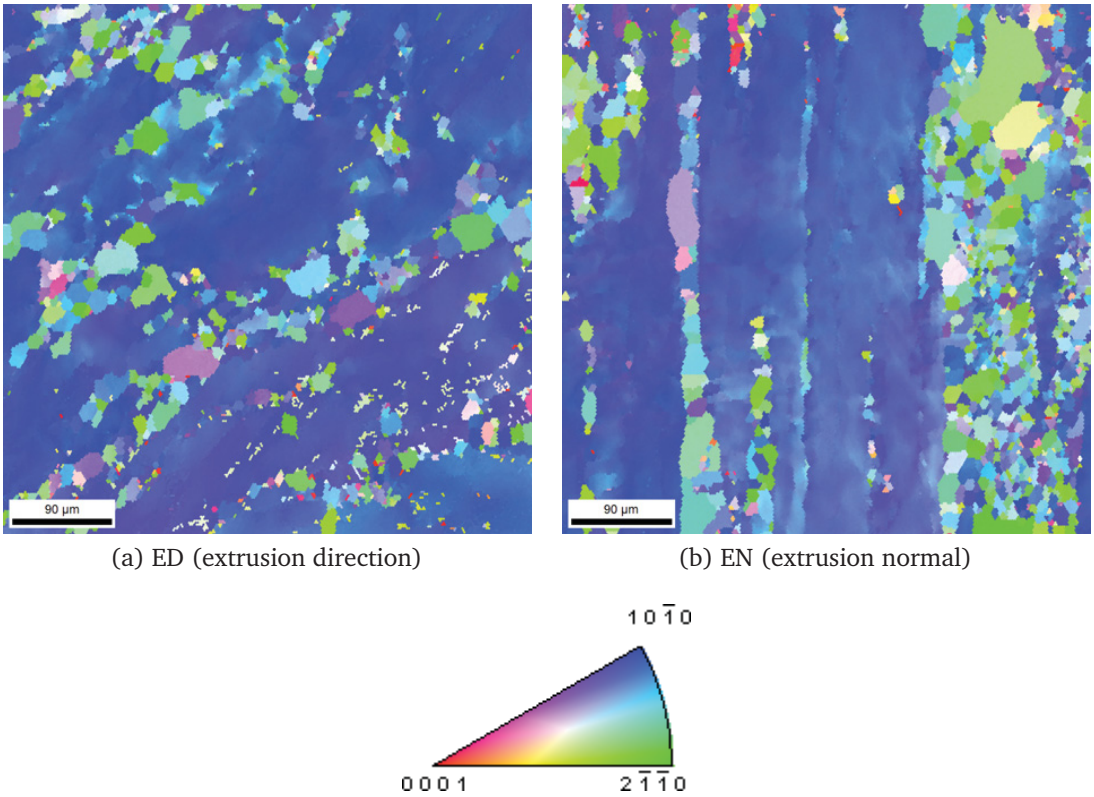


(a) ED (extrusion direction)

(b) EN (extrusion normal)

(c)

Figure 2.4 EBSD inverse pole figure map of initial AM30 Magnesium.

EBSD inverse pole figure maps of AM30 Magnesium showing microtexture on (a) a section normal to the extrusion direction (ED) and (b) section normal to the extrusion radial (ER). The grain microstructure is dual, the elongated grains having the prismatic direction aligned with the ED and small recrystallized grains rendering the parent grain prismatic texture more axisymmetric.

dislocations could be pushed back into the parent as their incorporation, in the absence of appropriate dissociation, requires the creation of faults with high energy in the twin interface. This is the case of parent dislocations having a corresponding twin vector as an integral fraction of the lattice vector. However, it is possible for a pair or a group of such dislocations to penetrate the twin as a single dislocation without leaving a fault at the interface, which is an effect similar to the passing stress problem in the pole

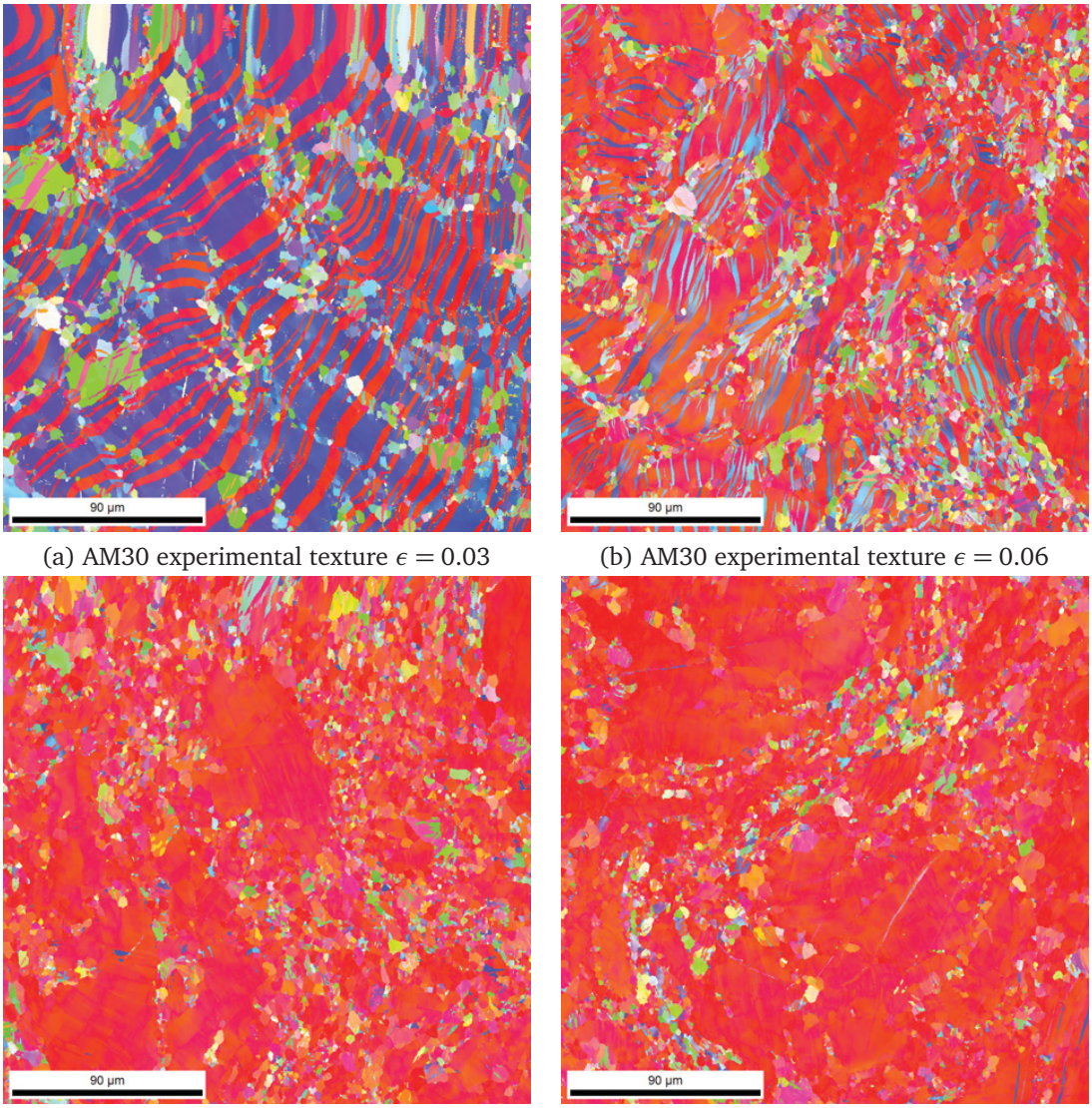


(a) AM30 experimental texture $\epsilon = 0.03$

(b) AM30 experimental texture $\epsilon = 0.06$

(c) AM30 experimental texture $\epsilon = 0.08$

(d) Predicted texture $\epsilon = 0.11$ (rupture)

Figure 2.5 EBSD inverse pole figure map of deformed AM30 Magnesium.

EBSD inverse pole figure map for AM30 Magnesium, deformed along the extrusion direction (ED) up to four strain levels, namely (a) 3%, (b) 6%, (c) 9%, and (d) 18% (rupture). At 3% plastic strain the twins are separated lamellae rotating 33% of the parent prismatic grain to a sharp basal pole. At 6% plastic strain, coalescence has already reached an advanced stage where the twins have invaded approximately 70% of the whole structure. At 9% plastic strain twinning invaded the entire elongated grains and approximately 50% of the recrystallized grains. At rupture, substantial double twinning by $\{10\bar{1}1\}$ compression twinning took place when almost the entire matrix is twinned by tensile twinning.

mechanism. In contrast, the other non-screw basal dislocations should be attracted to the twin boundary and cause a reversed softening effect [Yoo and Wei, 1966].

In sum, a latent hardening slip-twin whether based or not on a Hall-Petch mechanism seems not to be experimentally substantiated for *profuse twinning*, and it is unlikely to have substantial effect given the mobility of the twin interface under stress.

Of considerable importance, is that this conclusion is consistent with that of Cáceres et al. [2008] and that of Salem et al. [2003] made on the hardening properties of HCP Ti based materials. More interestingly, Cáceres et al. [2008] demonstrated that the quasi-Hall Petch hardening associated with grain segmentation by the tensile twin $\{10\bar{1}2\}$ in Mg has a relatively small effect on hardening. For textured polycrystals, the authors demonstrate through analyses using Kocks-Mecking equations that this was due to the small value of the Hall-Petch constant, while for random oriented grains the fraction of grains undergoing twinning is small, despite the larger Hall-Petch constant. As such, under profuse twinning Hall-Petch has a minor contribution to hardening.

Other experimental works that substantiate our conclusions correspond to the microhardness results on Cu – 8 at. % Al [Basinski et al., 1997], Hadfield steel [Karaman et al., 2000] and Ti [Kalidindi et al., 2003], revealing that twinned lamellae are harder than the adjacent parent. This also excludes the possibility of Hall-Petch because the Hall-Petch mechanisms would provide similar microhardness values on both sides of a coherent twin boundary. However, these results should be carefully taken since the twin and parent have different crystallographic orientations.

Under the above facts, an additional mechanism should be most responsible for the increasing hardening rate in Regime II and the smooth transition between Regime I and Regime II. This mechanism should act in combination with the effect of twinning on deformation texture to explain the anisotropy retrieved under any given level of twinning contribution. In the following, we suggest a coupling effect between dislocation transmutation and latent hardening within the twin. We formulate phenomenological equations for this mechanism operating under simplified assumptions, but are expected to provide a pragmatic rationale for the observed hardening anisotropy.

### 2.5 Dislocation "transmutation" effect on slip-slip latent hardening

Upon edgewise[6] thickening of a twin, parent dislocation segments in the new twinned region must presumably be incorporated in the twin if no fragmentation mechanism is asserted. As such, their interaction with the twinning shear must be considered. A generating node, in the sense defined by Bilby and Christian [1956], is formed if the transmutation of the dislocation segments obeys the rule of the correspondence matrix approach. The node joins the incorporated dislocation line, the parent dislocation line and a twinning disconnection running from the two crossing points between the dislocation segment and the composition plane. The kinematics and crystallographic properties related to the formation of the twinning disconnection is beyond the scope

[6]The problem of dislocation incorporation upon the catastrophic lengthwise thickening of the twin may be more appropriately treated under the nucleation event, which is beyond the scope of the current work.

of this work. Here, we rather focus on the properties of the incorporated dislocation which is more relevant to hardening caused by twinning.

For FCC metallic structures, Niewczas [2007], provided an exhaustive description, with substantiation from TEM studies on copper, of dislocation products supporting the matrix correspondence transformation upon a pure generating node. The author classified events of matrix dislocation transmutation upon the passage of a twin front into five categories: i) glissile-to-sessile, ii) sessile-to-glissile, iii) glissile-to-glissile, iv) sessile-to-sessile, and v) formation of three-dimensional structures in the twin including dislocation loops, jogs and refined debris. Earlier work on incorporation of slip dislocations into twins included Saxl [1968], Yoo [1969] and Basinski et al. [1997].

Based on the correspondence matrix method, Bhattacharyya et al. [2009] recently reported incorporated systems in Zr tensile and compression twins from matrix dislocations with Burgers vector $\langle a \rangle$ lying on prismatic planes. The details of derivation were not reported, but the method is similar to that described by Niewczas [2007] for FCC. Only two incorporated systems corresponded to usual slip modes in Zr, namely, systems of pyramidal $\langle c+a \rangle$ mode. Otherwise, tensile and compressive twins transmute dislocations to high index systems.

An important consideration is the ramification on slip transfer from the correspondence matrix assumption — the matrix slip will be crystallographically equivalently to the incorporated system *only* if $K_2$ or $\eta_2$ constitute a slip plane or a slip direction, respectively. For HCP metals, this condition seems to be only fulfilled for $\{22\bar{4}1\}$, $\{20\bar{2}1\}$ and $\{11\bar{2}1\}$ twins, which are not common twin systems considered in polycrys-

tal simulations. Thus, when incorporated under a generating node assumption, HCP glide twins will see a high latent hardening since dislocations from different modes will interact inside the twin volume. This defines an attribute unique to twinning hardening especially for low symmetry structures having to deform under multiple slip modes. Thus, latent hardening and dislocation transmutation should play, in combination, a vital role in the hardening correlated to profuse twinning. The multiplicity of dislocation types inherited by the twin from the parent was probably the motif that stimulated certain authors [Capolungo et al., 2009] to suggest that the twin stores more rapidly dislocations than the parent. Here, it is important to understand, in contrast to some other suggestions in the literature, that latent hardening serves only as a stress rising agent rather than a multiplier of dislocations [Beyerlein and Tomé, 2008]. As such, the typical higher saturation stress in IPC than in TTC is a systemic cause of the higher latent hardening in the twin induced by transmutation effects.

Consider a parent grain containing a volume fraction $V^T$ of a single lamellar twin in a grain of unit volume (Figure 2.6). Assume that upon a small deformation increment $\mathrm{d}\varepsilon$, the twin thickens uniformly edgewise by fraction $\mathrm{d}V/2$ on each of its sides. After slip, the dislocation densities for a given dislocation type $i$ in the twin and in the parent are $\rho^{iT}$ and $\rho^{iP}$, respectively. Here, an $i$ dislocation may be sessile or glissile, but, obviously, only those which have been considered to provide deformation could be directly affected by slip deformation. However, if within the new twinned volume, a $j$ dislocation from a given deformation mode in the parent prior to twinning

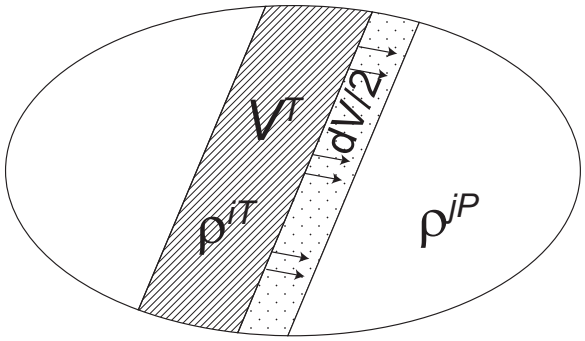


Figure 2.6 A schematic illustration of a twin lamella growing by d$V/2$.

is transmuted to an $i$ dislocation upon twinning, the final density of $i$ dislocations in the twin, $\rho^{iTF}$ should increase according to the following equation:

$$\rho^{iTF} = \frac{V^T \rho^{iT} + \mathrm{d}V \sum_j \alpha_{ij} \rho^{jP}}{V^T + \mathrm{d}V} \tag{2.1}$$

Here, we introduced a phenomenological second order transmutation matrix $\boldsymbol{\alpha}$ to which we associate an application defined from the affine space $D^P$ of dislocation densities in the parent to the affine space $D^T$ of dislocation densities in the twin. The respective dimensions $p$ and $t$ of $D^P$ and $D^T$ correspond to the number of dislocation types defined in each of the parent and the twin, which are not necessary identical. For the correspondence matrix approach, the dimension of $D^T$ will be always greater than that of $D^P$ upon twinning, and vice-versa upon detwinning. The number of components in the matrix associated to $\boldsymbol{\alpha}$ is $[\sup(p,t)]^2$.

The $\boldsymbol{\alpha}$ parameter is a non-dimensional measure of the fraction of $j$ dislocations transmuted to several types of $i$ dislocations. The partition is governed by the dislocation character and the type of dissociation upon incorporation. Thus, the alpha-parameter

partitions in a dimensionless fashion the new formed dislocation types in the twin (upon twinning or in the parent upon detwinning) from a single kind of parent dislocations intersecting a coherent twin boundary. The sum of a line values in the alpha matrix is strictly less than unity. The correspondence matrix approach will, at most, double the number of initially activated slip modes for each twin.

The effect of alpha is rather primarily sensed by the increase of the densities of dislocation types (slip modes) that do not correspond to the primary dislocation types generated in the twin (upon twinning or in the parent upon detwinning) by the deformation of the twin itself according to the rule of the highest Schmid factor.

If the interface contains the Burgers vector of the incident dislocation, then the incorporation is achieved in screw orientation. In this case, a transmutation may not occur if a twin slip meeting the intersection line has an appropriate lattice vector to incorporate the dislocation. Also, there would be no twinning dislocation. This case can be exemplified by the incorporation mechanism of a basal dislocation in a Ti $\{10\bar{1}2\}$ twin suggested by Yoo and Wei [1966]. In the absence of shuffles, the one to one correspondence matrix $C_{ij}$ upon the generating node assertion for centrosymmetric structures is:

$$C = X^{-1}\overline{\otimes}R\overline{\otimes}X\overline{\otimes}S \tag{2.2}$$

where $X_{mn}$ is the transformation matrix from the parent basis to the twin interface-related orthonormal basis constructed by axes $x_k$ parallel to $\eta_1$, perpendicular to the plane of the shear and perpendicular to $K_1$, respectively, $R_{mn}$; is the proper rotation

matrix from $x_k$ to the twin basis; and $S_{mn}$ is the characteristic glide twinning shear matrix.

The new slip modes in the twin could be formally considered to provide deformation along their slip systems. However, it would be simpler as a first approximation to only consider their effect on latent hardening, since their critical resolved shear stress in the parent was tacitly considered to be too high to be reached during the test.

When a portion of a parent grain twins in a polycrystalline material, the deformation by the twin is usually accommodated by slip. Even for single crystals, whereupon stopped twins spread across the entire sample cross section, the shape change is partly accommodated by kinking and partly by slip [Holden, 1952, Pratt and Pugh, 1952]. The slip could be concentrated on one side of the crystal and induce a zigzag markings that could in some cases destroy coherency and not allow detwinning upon stress reversal. The twinning induced slip is usually referred to in the literature as accommodation effects. In polycrystalline materials, there are primary kinks and secondary kinks [Gilman, 1954, Rosenbaum, 1961]. The dislocation sources could be activated at the grain boundary segments where the twin edge ends, but a more systemic mechanism could be correlated to the combinations and accumulations of twinning dislocations at these segments. This is commonly believed to be so for the emissary dislocation correlated to the first lengthwise thickening of the twin [Sleeswyk, 1962b]. In any case, the dislocation densities in the parent should be partly increased by the contribution of twinning-induced slip dislocations. Primary kinks were observed to be essentially formed by easy slip dislocations, while secondary kinks are a result of non-easy slip

dislocations. The partition may be affected by cross slip and the resolved shear stress in the parent regions neighboring the twin boundaries. That is, the density $\rho^{iP}$ of each slip dislocations in the parent will be partly increased due to accommodation effects through a parameter, $\xi^i$, acting on the Mecking and Kocks equations as:

$$\rho^{iPF} = \rho^{iP} + \mathrm{d}\rho^{i_{\mathrm{acc}}} = \rho^{iP} + \xi^i \left[ k_1^i \sqrt{\rho^{iP}} - k_2^i(\dot{\varepsilon}, T)\rho^{iP} \right] \left( s\mathrm{d}V - \mathrm{d}\gamma_{\mathrm{kink}} \right) \tag{2.3}$$

where the sum of the constants $\xi^i$ over all modes must meet $\sum_i \xi^i \leq 1$.

In this formula, $\mathrm{d}\rho^{i_{\mathrm{acc}}}$ represents the increment of $i$ dislocation density induced by the twin accommodation effects, $\rho^{iP}$ the density of $i$ dislocation before the twin grows by $\mathrm{d}V/2$, $k_1^i$ the constant for $i$ dislocation generation, $k_2^i$ the rate sensitive constant for $i$ dislocation removal, $s$ the characteristic twin shear, and $\mathrm{d}\gamma_{\mathrm{kink}}$ the part of twin deformation accommodated by kinking, that may supposed to be proportional to $s\mathrm{d}V$. As first approximation, it may be convenient to consider only dislocations from the easy slip mode, so only one accommodation parameter is left to be adjusted.

The density of dislocation debris $\rho^P_{\mathrm{deb}}$ in the parent should be updated including debris from the accommodation effects, that is, using Beyerlein and Tomé [2008] equations we have:

$$\mathrm{d}\rho^P_{\mathrm{deb}} = q \sum_i 2A_i^2 b_i^2 \rho^{iP} \left\{ \left[ k_1^i \sqrt{\rho^{iP}} - k_2^i(\dot{\varepsilon}, T)\rho^{iP} \right] \mathrm{d}\gamma_i \right.$$
$$\left. + \xi^i \left[ k_1^i \sqrt{\rho^{iP}} - k_2^i(\dot{\varepsilon}, T)\rho^{iP} \right] \left( s\mathrm{d}V - \mathrm{d}\gamma_{\mathrm{kink}} \right) \right\} \tag{2.4}$$

Here, $A_i$ and $q$ are phenomenological parameters reflecting the production rate of debris from each type of dislocations, and $b_i$ is the corresponding Burgers vector.

The effect of dislocation transmutation on hardening of twinned regions will be sensed primarily through extensive latent hardening and secondarily through the extra debris created. The latent hardening could be termed following Lavrentev and Pokhil [1975b], and the debris following Madec et al. [2002] as,

$$\tau_c^{mi} = \tau_0^i + \sum_j \chi_{ij}\mu_j b^j \sqrt{\rho^j} + k_{\text{deb}}\mu_i b^i \sqrt{\rho_{\text{deb}}} \log\left[\frac{1}{b^i\sqrt{\rho_{\text{deb}}}}\right] \tag{2.5}$$

where, for each orientation $\tau_c^{mi}$ is the critical resolved shear stress of the slip system $m$ belonging to the considered deformation mode $i$ evolving from an initial value $\tau_0^i$, $\chi_{ij}$ the latent hardening parameters reflecting the effect of $j$ dislocation on $i$ dislocation whereupon for a twinned region (resp. detwinned region) $j$ runs upon twinning (resp. for parent upon detwinning) through all dislocation types including those transmuted from the parent (resp. from the twin upon detwinning) even if there are sessile or glissile not considered as providing deformation, $\mu_j$ is the shear modulus correlated to a slip system of $j$ dislocation, $\rho_{\text{deb}}$ is the sum of debris densities over all dislocation types including the transmuted ones, and $\rho^j$ is the density of $j$ dislocations.

Here, it is of considerable importance to recall that experimental evidence in magnesium showed that the latent hardening of pyramidal on basal exceeded a range of 400% higher than the self-hardening basal on basal [Lavrentev, 1975, Lavrentev and

Pokhil, 1975a,b, Lavrentev et al., 1978, Lavrentev and Vladimirova, 1970, Michel and Champier, 1975, 1976, Vladimirova and Lavrentev, 1973].

## 2.6 Discussions

The correspondence matrix method might represent the most obvious assumption for dislocation transmutation that could be systemically violated. To be consistent with Bilby and Christian [1956] notation, the situation that does not favor a generating node will be called here a non generating node. Non-generating node phenomena were substantially evidenced in BCC structures [Mahajan, 1971] and even in FCC [Mahajan and Chin, 1973a, Rémy, 1977] and HCP structures [Tomsett and Bevis, 1969, Yoo and Wei, 1966].

Actually, the problem of dislocation incorporation in the twin is better to be considered, as it was frequently done in eminent literature [Christian and Mahajan, 1995], under the inverse process of the penetration of the twin by slip dislocations in the matrix, so slip transfer is of a concern. Here, the role of the stress would become important in the mechanisms controlling the selection of the incorporation plane and the Burgers vector transmutation. In the correspondence matrix approach, the action of stress is tacitly ignored as if the twin was considered as a form of an obstacle that may engulf dislocations; that is, annealing, growth or mechanical twins bear no differences. Particularly, observe that according to the correspondence matrix method used by Niewczas [2007], glissile-to-glissile transmutations are limited to dislocations with Burgers vectors parallel to $K_1$ or $K_2$. As pointed out by Christian and Mahajan [1995],

the inverse process is better suited for transmutations performed by glide twinning and even for fast growing glide twins, because the stress that is responsible for the twin formation and growth should be responsible for the slip near the twin interface. As such, the twin interface will tend to endure appropriate reactions to allow transfer of matrix slip on systems admitting equal signs of the resolved shear stresses in the twin and the matrix.

As a consequence, if the dislocation is to glide in the twin, it must dissociate in a way to generate a Burgers vector in the twin that is a lattice vector of the incorporation plane, which is not, as aforementioned, a usual case offered by the generating node assumption. Accordingly, authors such as Mahajan and Chin [1973b] and Rémy [1981] suggested and demonstrated, e.g. FCC, the systemic occurrence of dislocation dissociations at the twin interface permitting slip transfer even if they violate the Frank rule. Mahajan and Chin [1973b] declared that the defect structure close to the interface always induces a stress concentration that would overshadow the imbalance of energy dictated by the Frank rule on the dissociations permitting slip penetration.

These dissociations do not cancel the possibility of generation of sessile dislocations observed in TEM studies on both single Niewczas [2007] and double-lattice metallic structures [Bhattacharyya et al., 2009]. Most of the dissociations suggested for slip transfer involve the extra creation of sessile dislocations or glissile dislocations not necessary belonging to a usual slip system. For instance, the unexplained $\langle c \rangle$ dislocation in the twin by the correspondence matrix method in Zr [Bhattacharyya et al., 2009], could be a mere result of a dissociation suggested by Yoo and Wei [1966] for $\langle a \rangle$ slip

dislocations transferring in pairs through an HCP tensile twin interface without leaving a stacking fault.

An assumption supporting the non-generating node case presents the advantage of reducing the number of dislocation types considered in a polycrystal simulation, and as such will lead to a reduction in the number of latent hardening parameters.

For FCC, Mahajan and Chin [1973a,b] proposed a series of dissociations permitting slip transfer that do not obey the correspondence matrix method. Rémy [1977, 1981], Mori and Fujita [1980], and Robertson [1986] not only confirmed these dissociations by TEM observations, but strikingly revealed pile-ups as playing the role of stress raiser agents responsible for upsetting the Frank rule. There is also the possibility that shuffling upsets the incorporation to the corresponding plane if the atomic movement required by shuffles affects the dislocation core in such away to not favor the generation of a Burgers vector appropriate for the corresponding plane. An analysis of this effect requires revisiting the assumption of Jaswon and Dove [1957] made on the kinematics of the composition plane in double-lattice structures. These authors assumed that the $K_1$ plane is situated half-way between the corrugations, which is in fact equivalent to a $Y/2$ type shuffling between the opposite corrugations. A striking example demonstrating the breakdown of the correspondence matrix method is the dissociation of an $\langle a \rangle$ dislocation in Ti at 60° to a $\{10\bar{1}2\}$ twin interface into only interfacial defects [Serra and Bacon, 1996]. The atomic simulations performed by these authors evidenced no corresponding dislocation in the twin, and neither a slip transfer.

Apart from fragmentation, the last category of three-dimensional defect structures observed by Niewczas [2007] in Cu twin could be actually attributed to the high level of interactions between dislocations specific to the deformation within the growing twin. Under these interactions, generation of sessile dislocations, in particular the observed $\langle c \rangle$ type dislocation in HCP twins, will be possible upon dissociations of superjogs formed at the intersection between glissile dislocations of different modes. Also, pinched-off loops could result from the degeneration of dislocation dipoles expected to substantially form in the twin. Partridge and Roberts [1964] observed similar three-dimensional structures in a polycrystalline magnesium $\{10\bar{1}2\}\langle\bar{1}011\rangle$ twin including jogs, dislocation dipoles, and dislocation loops lying on non-basal planes. An observation of considerable importance in hardening induced by twinning made by this author is the high amount of dislocation debris produced at the boundary of intersection between two coalescing twins. Similar structures were observed by Niewczas [2007] in FCC copper and Bhattacharyya et al. [2009] in HCP Zr but were arguably attributed to dissociations during twin nucleation. The formation of debris during twin coalescence could be a distinguishing hardening mechanism in the regime of twin coalescence.

## 2.7 Conclusions

The increasing rate of parent dislocation transmutation in the twin is consistent the increasing rate of hardening in Regime II which is the main characteristic of the sigmoidal curve when profuse twinning occurs in double-lattice structures. As the parent slips and the twin grows, the twin finds an increasing density of dislocations

to incorporate and transmute. The process multiplies the types of dislocations in the twin. As such, transmutation results in the presence of a greater number and a higher fraction of dislocation types within the twinned regions than in the parent, forcing them to interact and induce an increasing latent hardening unique for twinning. The alleged twin-induced Hall-Petch effect that was widely used to predict the behavior of HCP metals does not find a good physical basis and turns out to conflict with eminent literature and important recent experimental evidences. Of important consideration is its inconsistency with the observed peculiar hardening rate increase of Regime II correlated to profuse twinning. In this writing, we suggest an alternative way to account for hardening in Regime II based upon the mechanisms correlated to twinning transmutation. Polycrystalline plasticity models were also found to have overlooked the accommodation effects, and a model was suggested accordingly. Accommodation effects are important for transmutation to take place early on upon strain. Considerable analyses are further required to shed light on dissociation mechanisms at the twin interfaces as they dominate hardening when the twin volume fraction approaches the asymptotic regime. A physics-based expression of the alpha-parameters needs these mechanisms to be mathematically appreciated.

CHAPTER 3

# HARDENING MECHANISMS UPON PROFUSE TWINNING IN PURE MAGNESIUM

## 3.1 Summary

Textured hexagonal close packed double-lattice structures show stronger anisotropy than textured single-lattice structures. The reason lies behind the necessity to activate glide twinning and hard slip dislocation modes. Although the mechanisms behind activation of dislocations with non-basal Burgers vectors are still not fundamentally understood, the effect of twinning on hardening presents the most substantial challenge to polycrystal plasticity modelers. The origin of the increasing strain hardening rate regime (Regime II) upon profuse twinning is still not fundamentally clear. Previous successful attempts to fit the stress-strain behaviors based on a Hall-Petch effect by twin segmentation had systemically led to discrepancies in predicting intermediate textures and/or twin volume fraction evolutions. A recent dislocation-based hardening rule incorporated into the Visco-Plastic Self-Consistent (VPSC) model allows slip and twinning to be physically coupled in the simulations. In this chapter, we investigate hardening mechanisms in pure magnesium and apply a dislocation based formalism to model anisotropy. In contrast to magnesium alloys, we show that pure magnesium under large strains develops substantial multivariant twinning and multifold twinning. These twinning phenomena are accompanied by a marked grain

refinement and blunting of former twin boundaries. This blunting suggests severe accommodation effects in the soft matrix that caused the twin boundary to lose coherency. Thus, multivariant and multifold twinning take place to accommodate further deformation, but the subsequent twin-twin interactions arise to contribute in material hardening. The strain path anisotropy related to the saturation stresses revealed major missing links for comprehending hardening by twinning and substantiated dislocation transmutation effect by twinning shear.

## 3.2 Introduction

As lightweight metals, magnesium and titanium are intensively sought for the possibility of integration in large thermomechanical structures. Magnesium and titanium present a hexagonal closed-packed (HCP) structure that is of significant low crystal symmetry compared to the crystal structures of base materials commonly used in automotive and aircraft components. The dislocation glide activities needed to mediate plasticity in HCP structures involve defect dynamics of complex crystallography. Modern industrial goals in achieving more energy savings are now reviving wide attention to the complex fundamentals of transformations upon plasticity in metallic double-lattice structures.

The basic problem with HCP structures is that the closed-packed directions are all normal to the *c*-axis. In fact, in real structures, interatomic distances along a direction that has a component along the *c*-axis deviate from the ideal case and do not belong to an easy-glide plane. As such, deformation along the *c*-axis, necessary to

satisfy arbitrary deformation, is a matter of complex dislocation dynamics. There are two most common patterns of these dislocation dynamics: (1) an apparent pyramidal-$\langle c+a \rangle$ dislocation and (2) glide twinning; glide twinning being the most extensively studied since the 1950s. The mechanisms involved in the triggering of both of these dislocation patterns are still widely debated. The threshold stresses for glide twinning activation seems to be athermal and can be substantially different from that of easy slip depending on the state of pre-existing defects. The threshold stresses for activation of the apparent pyramidal-$\langle c+a \rangle$ depends strongly on temperature and can exceed that of easy slip by up to three to four time below room temperature. That is, a strong anisotropy characterizes HCP structures.

Strain path anisotropy is most striking when glide twinning is profuse. Compression normal to $c$-axis fibers induces the universally-observed $\{10\bar{1}2\}\langle 10\bar{1}1 \rangle$ twin mode to be profuse, while it can be nearly totally prohibited upon compression parallel to the fiber [Tomé et al., 2001]. Here, for materials having prisms as the easiest slip planes, the yield stress is remarkably the highest when twinning is precluded. Whether basal or prismatic slip is the easiest slip plane, when twinning is profuse, there is an unusual change of concavity with a merging of a regime characterized by an increasing hardening rate, known as Regime II [Kelley and Hosford, 1968, Reed-Hill, 1973, Wonsiewicz and Backofen, 1967]. Most remarkably, although not addressed in the literature, for $c$-axis fibers, when basal slip is the easiest, the saturation stress reached upon profuse twinning is noticeably higher than that reached when slip dominates strain accommodation.

Previous approaches to hardening upon profuse twinning failed to satisfactorily capture texture evolution and the twin fraction evolution when stress-strain behaviors of slip dominated and profuse twinning dominated were acceptably correlated to the experimental data. This spurred the need to analyze the major mechanisms relevant to hardening in HCP metals. El Kadiri and Oppedal [2010] have recently reviewed major advances in the literature in understanding and modeling of hardening by twinning, and attempted to identify main missing links for reliable predictions of plasticity upon profuse twinning. They invoked the dislocation transmutation by the twins at the $K_1$ plane (first invariant plane by the homogenous shear) as a major potential mechanism that leads to Regime II, in combination with accommodation effects and rotation of the matrix to hard orientation by twinning. The authors suggested a model that phenomenologically incorporates dislocation transmutation and twin accommodation effects. However, no formal experimental evidences were put forward.

In this work, we experimentally and numerically demonstrate the essential role that the transmutation mechanisms may have in unlocking the high extent of rapid hardening in Regime II upon profuse twinning. We use pure magnesium as a material test-bed and apply the dislocation-based hardening rule recently incorporated in the Visco-Plastic Self-Consistent (VPSC) model and validated for Zr by Beyerlein and Tomé [2008]. The twinning contribution to deformation was modeled with the composite grain scheme developed and incorporated within VPSC by Proust et al. [2007]. We show that when not using the Hall-Petch [Hall, 1951, Petch, 1953] effect by twin segmentation or apparent latent hardening twin-slip, it is necessary to increase

the dislocation storage capability within the twins over that of the parent to provide a good correlation of both of Regime II and the anisotropy related to the saturation stress. Pure magnesium poses further challenges since it exhibits severe accommodation effects that lead to complex multifold, multivariant twinning, twin-twin interactions, marked grain refinement, and twin boundary blunting. The pure magnesium was tested under different orientations, and the deformation texture was characterized by neutron diffraction and Electron-Backscattered Diffraction.

### 3.3 Materials and Experiments

The chemical composition of the magnesium employed in this study is presented in Table 3.1 and corresponded to the pure magnesium studied by Livescu et al. [2006]. The material was extruded to a thick plate by Timminco. However, to be compatible with prior studies that used VPSC for polycrystal plasticity simulations, we examined a basal texture rather than a rod-texture typical of extrusion. Hence, the material was subsequently rolled down to a 12 mm thick sheet. Even after rolling, the formation of the $c$-axis fiber did not saturate throughout the sheet. Some remaining components along the transverse direction (TD) (0001) || TD persisted from the rod-texture. To increase the reliability of the hardening rule correlation reliability, we tested two slightly different textures representing samples extracted from the center and the edge of the rolled sheet. Subsequent to rolling, cuboidal samples were used for uniaxial compression (7 mm x 8 mm x 9 mm) testing that were extracted by electrical discharge machining (EDM) and then isolated in vacuum for a heat treatment of 30 minutes at

Table 3.1 Composition of pure Magnesium, ppm.

| Al | Ca | Mn | Zr | Zn | Sn | Si | Pb | Mg |
|---|---|---|---|---|---|---|---|---|
| 30 | 10 | 40 | 10 | 130 | 10 | 40 | 10 | balance |

200 °C. The heat treatment was intended to obtain equiaxed grains and eliminate the dislocation structures introduced by the previous forming processes. The annealing led to a more uniform distribution of dislocation densities suitable for the modeling purposes. The temperature and soaking period were chosen so that the texture was not affected by recrystallization. The initial and deformation textures were analyzed through EBSD and neutron diffraction.

The neutron diffraction texture analyses were performed on the High-Pressure Preferred Orientation (HIPPO) diffractometer at the Los Alamos Neutron Science Center (LANSCE) in Los Alamos National Laboratory. Wenk et al. [2003] and Von Dreele [1997] describe the facilities and techniques for the neutron diffraction analyses. Figure 3.1 presents pole figures obtained by neutron diffraction that were used to generate initial texture data for VPSC simulations. Figure 3.1a and Figure 3.1b correspond to textures near the center of the sheet and the edge of the sheet, respectively. The central regions of the sheet developed more enhanced $c$-axis fibers than those near the edge and would be harder upon a through-thickness loading. The EBSD texture analyses presented in Figure 3.2 are compatible with those obtained by neutron diffraction and show a grain size of approximately 120 $\mu$m in diameter. There is a substantial fluctuation of grain size that is typical of advanced stages of abnormal grain growth events due to

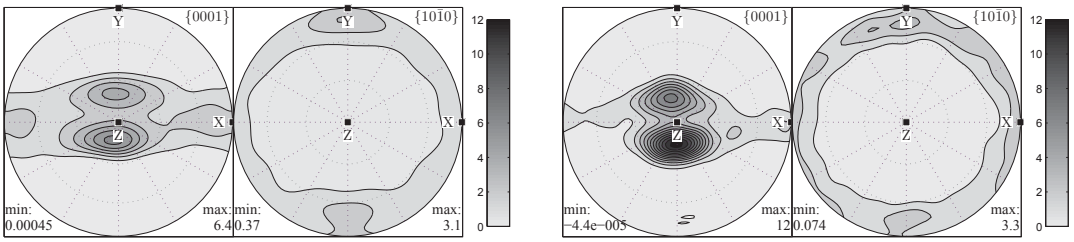


(a) (b)

Figure 3.1 Pole figures of pure untested magnesium.

{0002} and {10$\bar{1}$0} pole figures obtained by neutron diffraction on two different annealed, untested pure magnesium specimens. Sample (a) was tested and labeled TTC-1, and sample (b) labeled TTC-2 in the text and subsequent figures. X, Y, and Z axes stands for TD (transverse direction), RD (rolling direction) and ND (normal direction), respectively.

annealing. Uniaxial compression tests were performed at room temperature and at a strain rate of 0.001 $s^{-1}$. Additional samples were tested up to 3%, 6%, 9% and 12% plastic strain levels to analyze intermediate deformation textures and twin volume fractions necessary to optimize the hardening parameters.

Results of compression tests along TD, termed in-plane compression (IPC), and along the normal direction, termed through-thickness direction (TTC), are depicted in Figure 3.3 together with the modeling results. The modeling comprised simulation results with, and without, $\{10\bar{1}1\}\langle 10\bar{1}2\rangle$ compression twins for four different cases of a higher dislocation generation in the twin over that in the parent by means of a twin storage factor (TSF). In Figure 3.3, when compression twins were included, three additional simulations were performed corresponding to different values of the TSF, namely two, three, and four. The softer and harder TTC curves are denoted here TTC-1 (Figure 3.1a) and TTC-2 (Figure 3.1b), respectively. The IPC stress-strain curve

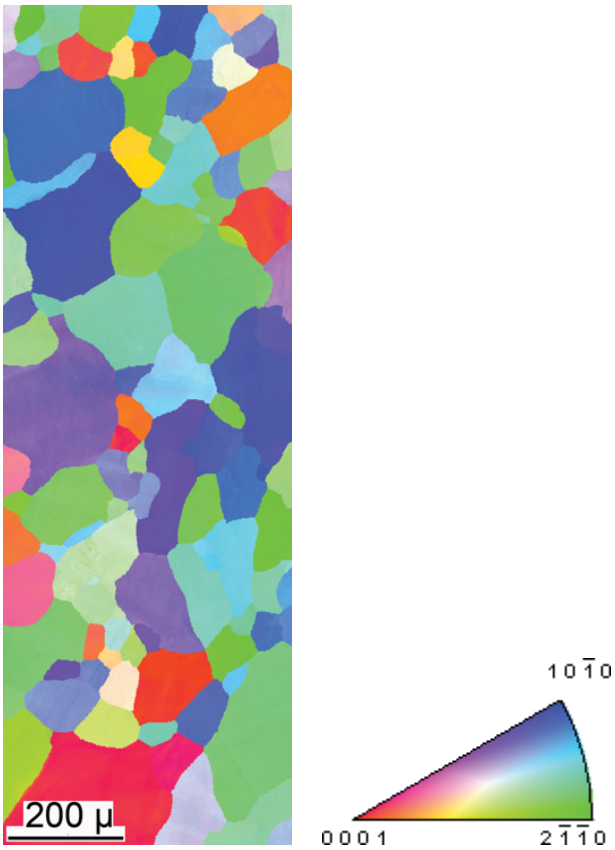


(a) (b)

Figure 3.2 EBSD texture analysis of initial state of pure Magnesium.

EBSD (electron backscattered diffraction) texture analysis of the initial state of pure magnesium before compression testing showing an inverse pole figure (IPF) map with TD (transverse direction) out of the plane of the paper. Note the equiaxed grains and abnormal growth phenomena from annealing, which correspond to large grains consuming their small neighbors. Some orientations along the TD may correspond to recrystallized grains or a previously extruded rod-texture.

presents a sigmoidal shape signature of profuse twinning. The sigmoidal shape is better illustrated in Figure 3.4 by the strain hardening rate - effective stress curve (theta-sigma) [Mecking and Kocks, 1981], which reveals the exact location of the inflection point, and the extent of Regime II. In Figure 3.4, we also included the theta-sigma curves from

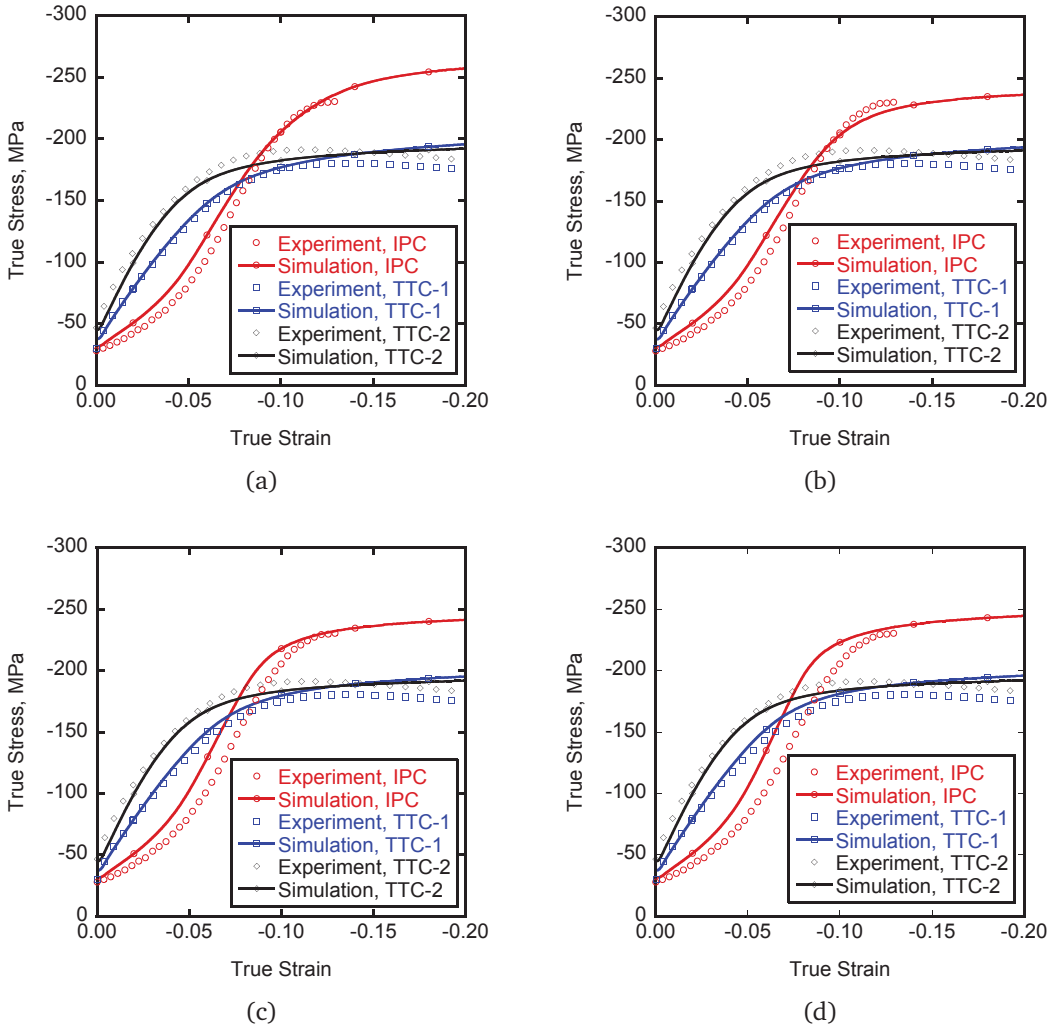


Figure 3.3 Results of compression tests and simulations for pure magnesium.

Results of compression tests and simulations for pure magnesium tested along the through-thickness direction (TTC) that corresponds to the normal direction of the sheet, and along the in-plane (IPC) direction that corresponds to the transverse direction of the sheet. In (a) $\{10\bar{1}1\}$ compression twins were excluded in the simulation and a twin storage factor (TSF) of two was adopted, while in (b), (c) and (d) the $\{10\bar{1}1\}$ compression twins were included in three simulations corresponding to a twin storage factor equal to two, three and four, respectively. The parameter that is varied in the figure (twin storage factor) modify the twinning response, which is more pronounced in the IPC case.

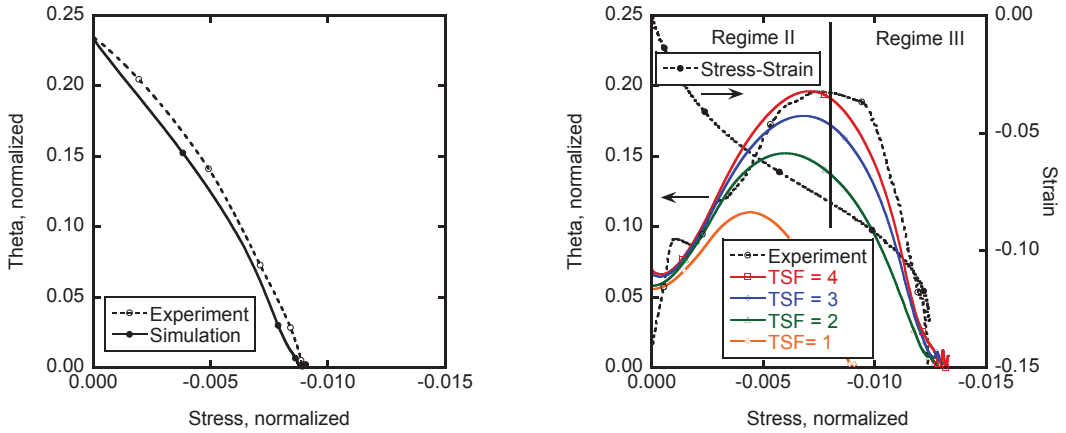


(a) TTC (b) IPC

Figure 3.4 Strain hardening rate versus stress plots.

Strain hardening rate versus stress plots $\left(\theta = \frac{\mathrm{d}\theta}{\mathrm{d}\varepsilon}, \theta \text{ vs. } \sigma\right)$ plots from compression tests and simulation results with compression twins and four values of the twin storage factor, namely unity, two, three and four on a pure magnesium tested (a) along the through-thickness direction (TTC) that corresponds to the normal direction of the sheet, and (b) along the in-plane direction (IPC) that corresponds to the transverse direction of the sheet. Stress values were normalized by $\sigma_{\text{normalized}} = (\sigma - \sigma_y)/\mu$ where $\sigma_y$ is yield stress and $\mu$ is shear modulus.

the simulation results with the four values of the twin storage factor, namely unity, two, three, and four. An important point from Figure 3.3 is the relative insensitivity of the initial yield stress to the loading orientation compared to the striking difference found in pure Zr [Beyerlein and Tomé, 2008] and magnesium alloys textured with similar $c$-axis fibers. Another point of considerable importance is the substantial difference in the saturation stress between TTC and IPC, namely 170 MPa and 240 MPa, respectively, although pyramidal-$\langle c + a \rangle$ slip Agnew et al. [2001] dominates strain in conjunction with easy slip in the saturation regime of both TTC and IPC. Thus, the material hardens more substantially under IPC than under TTC.

After the saturation regime, both TTC-1 and TTC-2 stress-strain curves show a peculiar stress decrease that may correspond to shear localization.

### 3.4 The polycrystal model and hardening rule

For modeling mechanical anisotropy of pure magnesium, we used mesoscale simulations where the macroscopic behavior was computed through the behavior of discrete grains in a polycrystal aggregate material that follows single-crystal constitutive rules. Stress, $\sigma$, is estimated following the VPSC scheme adapted by Molinari et al. [1987] to polycrystal plasticity and implemented by Lebensohn and Tomé [1993]. Hardening is based on updating the critical resolved shear stress $\tau^{\alpha}$ following the constitutive power law that provides the shear strain rate $\dot{\gamma}^{\alpha}$ in each slip mode $\alpha$ based on the Schmid factor $m^{\alpha}$ and a constant $\dot{\gamma}_0$ reflecting the macroscopic strain rate:

$$\dot{\gamma}^{\alpha} = \dot{\gamma}_0 \left| \frac{m^{\alpha} \overline{\overline{\otimes}} \sigma}{\tau^{\alpha}} \right|^{n} \operatorname{sign}\left( m^{\alpha} \overline{\overline{\otimes}} \sigma \right) \tag{3.1}$$

The hardening model is a dislocation density based model, fully described in the paper by Beyerlein and Tomé [2008], which incorporates slip and glide twinning under the "composite grain" twin scheme put forward by Proust et al. [2007]. This hardening rule is a temperature and strain rate dependent formulation that assumes the effects of a dislocation forest, dislocation debris (or substructure), a Hall-Petch effect on slip propagation, and the effects of slip and Hall-Petch on twin propagation. If $\alpha$ denotes

a slip mode having $s$ as a slip system, and $\beta$ denotes a twin mode having $t$ as a twin system, both of these effects are given by the following:

$$\tau_c^\alpha = \tau_0^\alpha + \tau_{\text{forest}}^\alpha + \tau_{\text{sub}} + \tau_{\text{HP}}^s \tag{3.2}$$

$$\tau_c^t = \tau_0^\beta + \tau_{\text{HP}}^t + \tau_{\text{slip}}^\beta \tag{3.3}$$

The critical resolved shear stresses for the slip resistance equation take the following forms for each of the forest, substructure, and Hall-Petch effects, respectively:

$$\tau_{\text{forest}}^\alpha = b^\alpha \chi \mu \sqrt{\rho^\alpha} \tag{3.4}$$

$$\tau_{\text{sub}}^\alpha = k_{\text{sub}} \mu b^\alpha \sqrt{\rho_{\text{sub}}} \log\left(\frac{1}{b^\alpha \sqrt{\rho_{\text{sub}}}}\right) \tag{3.5}$$

$$\tau_{\text{HP}}^s = \mu \text{HP}^\alpha \sqrt{\frac{b^\alpha}{d_g}} \text{ for } s \in \alpha \text{ without twins} \tag{3.6}$$

Here, $b$ is the Burgers vector, $\chi$ is the dislocation interaction coefficient smaller that unity, $\mu$ is the shear modulus, and $d$ is the spacing between twin lamellae.

The rate of dislocation density is modeled through Mecking and Kocks [Kocks and Mecking, 2003, Mecking and Kocks, 1981] equations who primarily used a $f(x) = \sqrt{x} - x$ type equation that has a decreasing rate for $0 < x < 1$ and allows for hardening and recovery to be incorporated as phenomenological parameters $k_1$ and $k_2$. Here we introduced a fitting parameter, twin storage factor (TSF), that allows the possibility that twins harden more than the parent. This is the same parameter used by Capolungo

et al. [2009] but finds a good physical premise in the transmutation theory developed by El Kadiri and Oppedal [2010]. In the transmutation theory, the twins harden more than the parent through a higher latent hardening in the twin by a rapid increase in the dislocation multiplicity in the twin. Here the twin storage factor captures the extra hardening in the twins, not by latent hardening, but instead by a constant that increases the dislocation densities only in the twin. Thus, the mechanism tacitly assumed by TSF may not be physical. However, it provides a similar effect on hardening compared to the effect provided by the latent hardening through dislocation transmutation across the twins.

$$\frac{\partial \rho^{\alpha}}{\partial \gamma^{\alpha}} = \frac{\partial \rho_{\text{generation}}}{\partial \gamma^{\alpha}} - \frac{\partial \rho_{\text{removal}}}{\partial \gamma^{\alpha}} = \text{TSF} k_1^{\alpha} \sqrt{\rho^{\alpha}} - k_2^{\alpha}(\dot{\varepsilon}, T)\rho^{\alpha} \tag{3.7}$$

Thus, the temperature and rate dependence are introduced in $k_2$ following a pure thermodynamic approach to describe how dislocations overcome barriers when the strain rate is lowered or when the temperature is increased:

$$\frac{k_2^{\alpha}(\dot{\varepsilon}, T)}{k_1^{\alpha}} = \frac{\chi b^{\alpha}}{g^{\alpha}} \left(1 - \frac{kT}{D^{\alpha}(b^{\alpha})^3} \log\left(\frac{\dot{\varepsilon}}{\dot{\varepsilon}_0}\right)\right) \tag{3.8}$$

Here $D$ is termed as the drag stress, and $g$ is the activation energy in an Arrhenius type rule for the strain rate dependence. The two critical resolved shear

stresses for resistance to twin propagation relate to the Hall-Petch effect and slip and take the following forms, respectively:

$$\tau^t_{HP} = \frac{HP^\beta}{\sqrt{d_g}} \text{ with no twins or when } t \in \beta$$

and $t$ is the predominant twin system (PTS) (3.9)

$$\tau^t_{\text{HP}} = \frac{HP^{\beta\beta'}}{\sqrt{d^s_{\text{mfp}}}} \text{ when } t \in \beta \text{ and } t \text{ is not the PTS, with PTS } \in \beta' \tag{3.10}$$

$$\tau^\beta_{\text{slip}} = \mu \sum_\alpha C^{\beta\alpha} b^\beta b^\alpha \rho^\alpha \tag{3.11}$$

Here, $C^{\beta\alpha}$ reflects the interaction between twin and slip, which may be negative or positive depending on whether slip hinders or promotes twin growth. In our simulations, we did not consider these two barriers for twin propagation for reasons that will be developed further in this chapter.

## 3.5 Results of simulations and deformation texture analyses

### 3.5.1 Synopsis of parameter fit

Following TEM observations from Lavrentev [1980], Lavrentev and Pokhil [1975a,b], Lavrentev and Vladimirova [1970] the slip systems considered in all simulations were restricted to the easy close-packed slip mode $\{0001\}\frac{1}{3}\langle 2\bar{1}\bar{1}0\rangle$ termed as basal-$\langle a\rangle$, two slip modes including non close-packed planes, namely $\{10\bar{1}0\}\frac{1}{3}\langle\bar{1}2\bar{1}0\rangle$ termed as prismatic-$\langle a\rangle$ and $\{11\bar{2}2\}\frac{1}{3}\langle\bar{1}\bar{1}23\rangle$ termed as pyramidal-$\langle c+a\rangle$. For twinning,

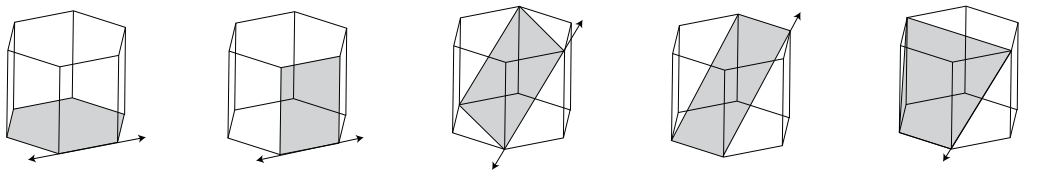

(a) basal $\langle a \rangle$ $\{0001\}\langle 11\bar{2}0\rangle$ (b) prismatic $\langle a \rangle$ $\{10\bar{1}0\}\langle 11\bar{2}0\rangle$ (c) pyramidal $2^{nd}$ $\{11\bar{2}2\}\langle 11\bar{2}3\rangle$ (d) tension twin $\{10\bar{1}2\}\langle 10\bar{1}1\rangle$ (e) compression twin $\{10\bar{1}1\}\langle 10\bar{1}2\rangle$

Figure 3.5 Deformation modes considered in the numerical simulations

we included the $\{10\bar{1}2\}\langle 10\bar{1}1\rangle$ "tension" twin mode providing extension along the $c$-axis and the $\{10\bar{1}1\}\langle 10\bar{1}2\rangle$ "compression" twin mode providing contraction along the $c$-axis.

The best fit of the two TTC curves and the IPC curve in Figure 3.3b corresponded to the hardening model parameters for slip, tensile twin, and compression twin that are listed in Table 3.3 and Table 3.4, respectively. It is important to note that the parameters were fit comparing the experimental and simulation stress-strain curves, and endeavored to simultaneously fit the TTC (through thickness compression) and IPC (in-plane compression) curves. The resulting simulations were used to predict the resultant textures in Figures 3.6 and 3.7, and the twin volume fraction evolution in Figure 3.8, but they were not themselves used to fit the parameters.

The parameters related to the generation of debris ($A^{\alpha}$ and $q$), twin hardening by slip ($C^{\beta\alpha}$), and Hall-Petch for both twin on slip and twin on twin hardenings were not needed and, therefore, could not be evaluated.

Following El Kadiri and Oppedal [2010], we did not find a strong physical premise for $\mathrm{HP}^{\alpha\beta}$ reflecting the effect of twin segmentation on slip. The twin boundary

Table 3.2 Slip and Twinning Modes used in these simulations for Mg

| Symbol | Mode | Crystallography | S | No. of Systems | b (nm) |
|---|---|---|---|---|---|
| $\alpha = 1$ | Prismatic $\langle a \rangle$ | $\{10\bar{1}0\}\frac{1}{3}\langle\bar{1}2\bar{1}0\rangle$ | | 3 | 3.21E-01 |
| $\alpha = 2$ | Basal $\langle a \rangle$ | $\{0001\}\frac{1}{3}\langle 2\bar{1}\bar{1}0\rangle$ | | 3 | 3.21E-01 |
| $\alpha = 3$ | Pyramidal $\langle c + a \rangle$ | $\{11\bar{2}2\}\frac{1}{3}\langle\bar{1}\bar{1}23\rangle$ | | 6 | 6.12E-01 |
| $\beta = 1$ | Tensile Twin | $\{10\bar{1}2\}\langle 10\bar{1}1\rangle$ | 0.13 | 6 | 4.92E-02 |
| $\beta = 2$ | Compression Twin | $\{10\bar{1}1\}\langle 10\bar{1}2\rangle$ | 0.1367 | 6 | 1.09E-01 |

Table 3.3 Hardening parameters for slip

| | Prismatic ($\alpha = 1$) | Basal ($\alpha = 2$) | Pyramidal ($\alpha = 3$) |
|---|---|---|---|
| $k_1$ $1/m$ | 2.00E+09 | 0.25E+09 | 2.00E+09 |
| $\dot{\epsilon}_0$ $s^{-1}$ | 1.00E+07 | 1.00E+07 | 1.00E+07 |
| $g^\alpha$ | 0.0035 | 0.0035 | 0.003 |
| $D_0^\alpha$ MPa | 3.40E+03 | 10.0E+03 | 0.08E+03 |
| $A^\alpha$ | 0 | 0 | 0 |
| $\tau_0^\alpha$ MPa | 30 | 11 | 50 |
| $\chi$ | 0.9 | 0.9 | 0.9 |
| $q$ | 0 | 0 | 0 |
| $HP^\alpha$ | 0 | 0 | 0 |
| $HP^{\alpha\beta}$ | 0 | 0 | 0 |

Table 3.4 Hardening parameters for twinning

| Parameters / Modes | Tensile Twin ($\beta = 1$) | Compression Twin ($\beta = 2$) |
|---|---|---|
| $\tau_0^\beta$ MPa | $\tau_{crit} = 15$, $\tau_{prop} = 10$ | $\tau_{crit} = 185$, $\tau_{pro} = 185$ |
| HP | 0 | 0 |
| $C^{\beta 1}$ | 0 | 0 |
| $C^{\beta 2}$ | 0 | 0 |
| $C^{\beta 3}$ | 0 | 0 |
| Twin Storage Factor | 2 | 2 |

is a coherent moving interface able to consume any possible dislocation pile-ups at their early stage of nucleation. In fact, dislocation pile-ups would promote interfacial glide of twinning disconnections by intensifying the stress they locally produce ahead of the leading dislocation.

For the effect of slip on twin propagation, El Kadiri and Oppedal [2010] demonstrated that a substantially pre-strained AM30 Mg alloy led to a fast and a total invasion of the matrix by the $\{10\bar{1}2\}\langle 10\bar{1}1\rangle$ tensile twins. The twins punched easier through the dislocation substructures before Regime II was completed. Thus, prescribing positive values of $C^{\beta\alpha}$ is difficult to justify for magnesium. Furthermore, we did not need negative values for $C^{\beta\alpha}$ since a null value has already been accompanied by an overestimation of the twin volume fraction.

However, the fit was only possible by assuming that twin hardens at least twice as much as the parent. Otherwise, the misprediction is highlighted in Figure 3.8. This extra hardening of the twins was reflected by a twin storage factor of dislocations that acts on dislocation multiplication in the twin independently of that in the parent.

Debris generation was disregarded since stage IV of both TTC and IPC is characterized by an apparent decrease in the stress. Thus hardening by dislocation debris would cause more fitting difficulties.

### 3.5.2 Deformation texture analyses

Measured and calculated pole figures after 3%, 6%, 9% and 12% plastic strain are given in Figures 3.6 and 3.7 for TTC and IPC, respectively.

For IPC, most of the {0002} || ND components were reoriented by tensile twinning to the {0002} || TD fiber before 6% plastic strain. Complete reorientation appears to have occurred before 9%, that is, before, or at, the inflection into Regime III. The evolution of tensile twin volume fraction could be estimated through integration of intensities around the basal pole within several upper-bounds of the radial angle $\alpha$ [Bunge, 1982, Clausen et al., 2008]. The pre-existing intensities at the initial state were subtracted from these integrals and reported in Figure 3.8. After approximately $\alpha = 47°$, the intensities start to decrease, since the subtracted fraction increased upon incorporation of components close to the initial *c*-axis fiber. We then kept the angle for subtraction approximately equal to 38°. Therefore the best estimation of the extent of tensile twinning upon strain corresponds to intensity integrals with a tolerance approximately equal to $\alpha = 47°$. It is important to note that these integrals would underestimate the extent of twinning if double twinning or retwinning are operational. As shown in next section, retwinning and double twinning was found to exceed the extent of actual primary twinning. The simulated volume fraction of twins slightly overestimated the intensity integral based estimation in the saturation regime of twinning, which occurred in the vicinity of the inflection point of the stress-strain behavior.

In Figure 3.7, the experimental neutron diffraction {0002} pole figures at 6% of plastic strain show noticeably more important departure from the {0002} || TD fiber than the simulated one. This departure reduces dramatically at 9% until 12% plastic strains when the simulated and experimental pole figures are back in good agreement.

To identify mechanisms behind these prediction discrepancies, EBSD analyses with 0.2 $\mu$m step size were carried out on specimens deformed to the four plastic strain levels. The corresponding IPF maps are presented in Figure 3.9 with TD (parallel to loading direction) being normal to the plane of the paper.

At 3% plastic strain, one twinning sequence, SQ1, could be identified (Figure 3.10) while at 6% plastic strain two twinning sequences, SQ1 and SQ2 coexist (Figures 3.11 and 3.12). Twin identification was based on the combined recognition of the misorientation and the common $K_1$ plane between the parent and the twin, both of which give sufficient characteristics for a given twin mode. The pole figures of the misorientation axis $\langle 10\bar{1}2\rangle$ were not reported here but gave excellent corroborations between the parent and the relevant twins.

SQ1 refers to $\{10\bar{1}2\}$–$\{10\bar{1}1\}$ double twinning, where a primary $\{10\bar{1}2\}$ tensile twin variant (PTt) retwins by $\{10\bar{1}1\}$ compression twins forming a double compression twin (DCt). SQ2 consists of two variants of $\{10\bar{1}2\}$ tensile twins that simultaneously twin the matrix, but one is largely retwinned by another $\{10\bar{1}2\}$ tensile twin variant. SQ1 and SQ2 were found to reach their peak activities at 6% plastic strain. From the pole figures in Figures 3.10, 3.11, and 3.12, both SQ1 and SQ2 alters an isomorphic transformation of the initial fiber by causing a substantial scatter around TD. This relates to the higher spread of texture components around TD at 6% identified by neutron diffraction and not captured by any simulation.

At 9% and 12% plastic strains, there is a profuse twinning sequence SQ3 that affects nearly all the matrix (Figure 3.13). SQ3 is either SQ1 augmented by a pure

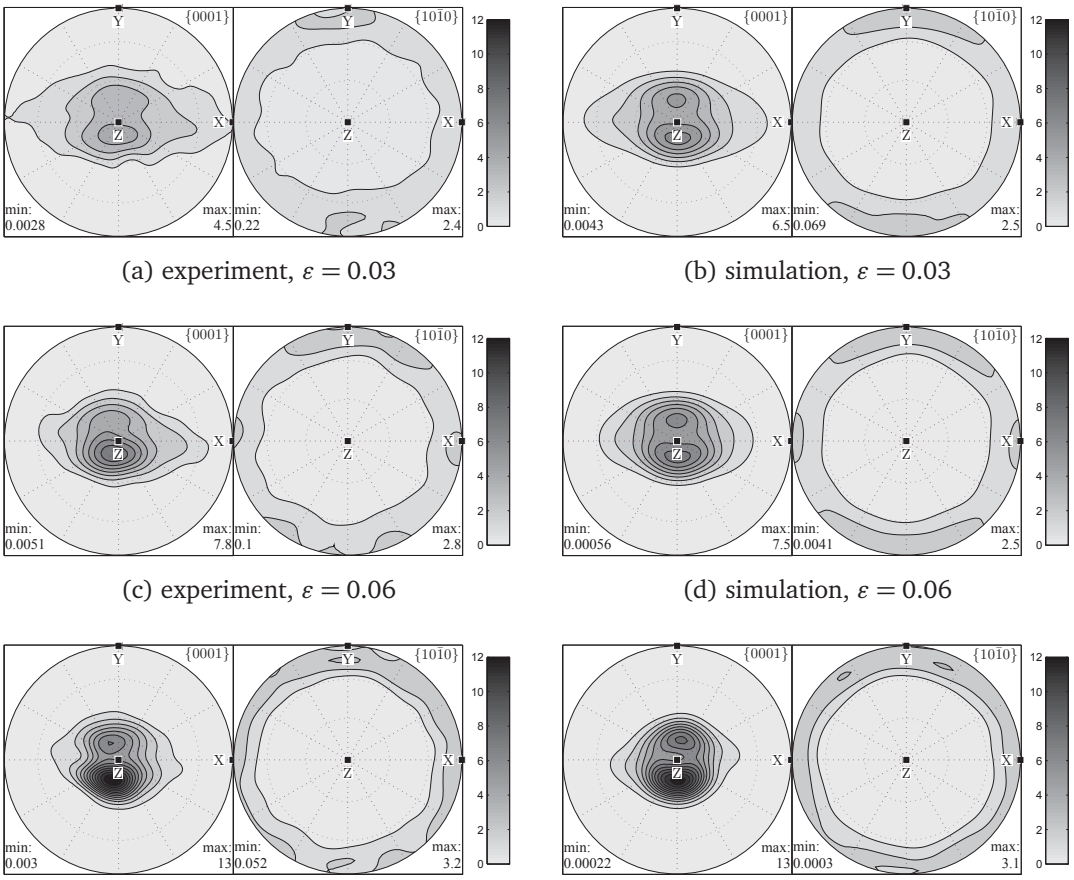


(a) experiment, $\varepsilon = 0.03$

(b) simulation, $\varepsilon = 0.03$

(c) experiment, $\varepsilon = 0.06$

(d) simulation, $\varepsilon = 0.06$

(e) experiment, $\varepsilon = 0.09$

(f) simulation, $\varepsilon = 0.09$

Figure 3.6 Comparison of polefigures.

Comparison of {0002} and {10$\bar{1}$0} pole figures obtained by neutron diffraction on deformed TTC (through thickness compression) samples and simulations up to 3%, 6%, and 9% plastic strains including {10$\bar{1}$1} compression twins. The TSF (twin storage factor) had no effect on texture. X, Y, and Z axes stands for TD, RD and ND, respectively. Note that TTC 9% corresponds to TTC-2 initial texture while TTC 6% and TTC 3% correspond to the TTC-1 initial texture.

twofold double tensile twinning {10$\bar{1}$2}–{10$\bar{1}$2} (Figure 3.13) or SQ2 augmented by a single instance of double tensile twinning {10$\bar{1}$2}.

SQ1 and SQ2 ultimately lead to quadruple tensile twinning QTt, through triple tensile twinning TTt, QTt being reoriented so the {0002} is closer to the loading axis.

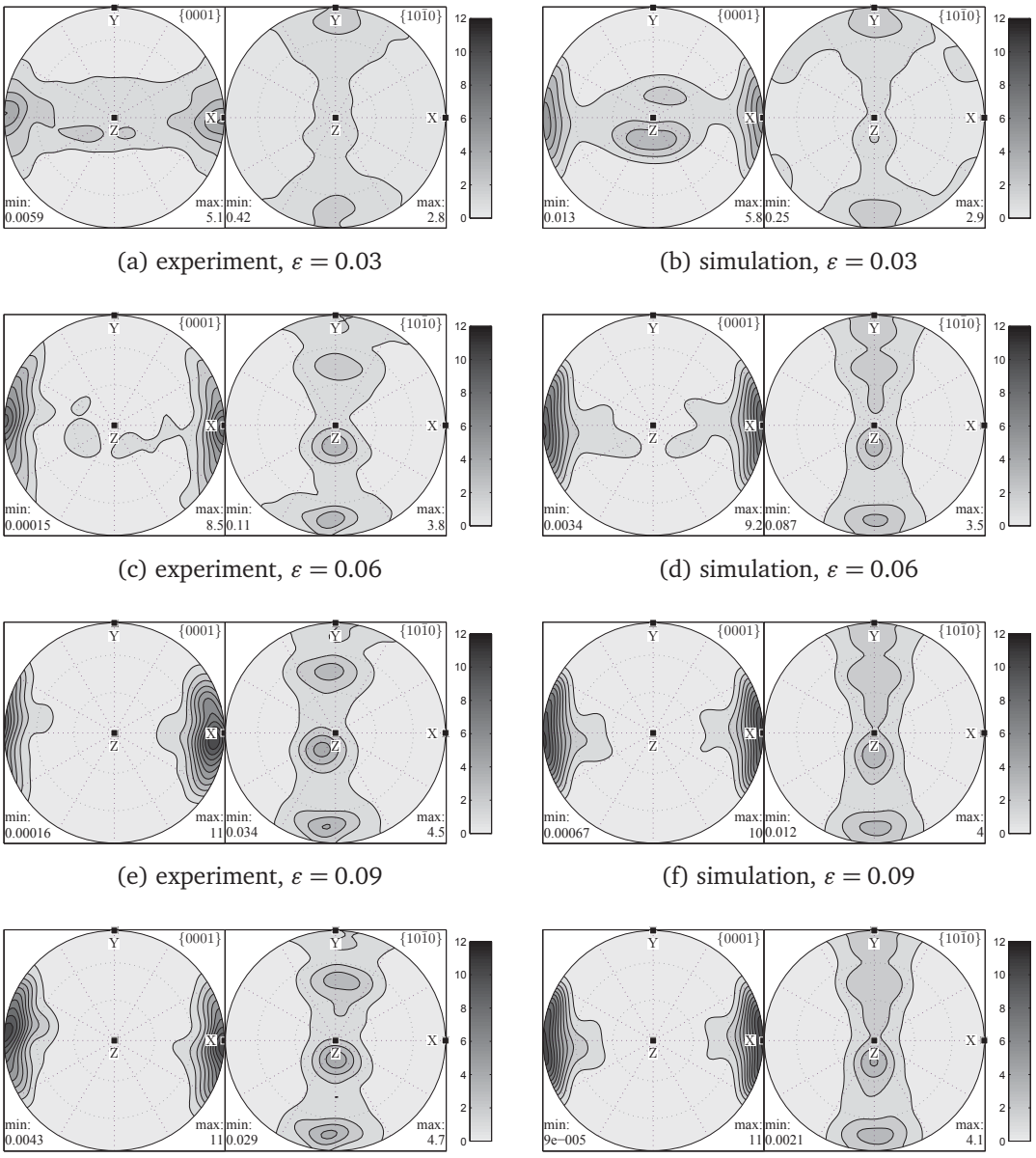


(a) experiment, $\varepsilon = 0.03$

(b) simulation, $\varepsilon = 0.03$

(c) experiment, $\varepsilon = 0.06$

(d) simulation, $\varepsilon = 0.06$

(e) experiment, $\varepsilon = 0.09$

(f) simulation, $\varepsilon = 0.09$

(g) experiment, $\varepsilon = 0.12$

(h) simulation, $\varepsilon = 0.12$

Figure 3.7 Comparison of pole figures on deformed IPC samples.

Comparison of {0002} and {10$\bar{1}$0} pole figures of textures obtained by neutron diffraction on deformed IPC (in-plane compression) samples and predicted by simulations up to 3%, 6%, 9%, and 12% plastic strains including {10$\bar{1}$1} compression twins. The TSF (twin storage factor) had no effect on texture. X, Y, and Z axes stands for TD (transverse direction), RD (rolling direction) and ND (normal direction), respectively.

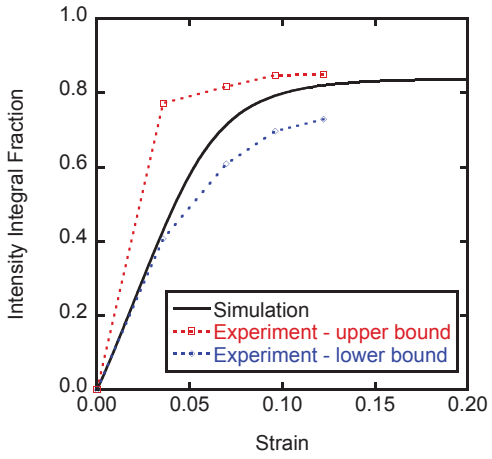


Figure 3.8 Twin volume fraction evolution.

Simulated twin volume fraction evolution as a function of strain (solid line) compared to the fraction of intensity integrals at different tolerances of neutron diffraction data used to estimate the amount of tensile twinning. The saturation at around an angle of 38° indicates a lower-bound estimation while around an angle of 75° provides an upper-bound estimation. These measurements disregard any multifold twinning. The simulation uses the parameters in Tables 3.3 and 3.4.

As such, the substantial activity of SQ3 in Regime III leads to direct sharpening of the transformed fiber, which was apparently captured by the simulations.

All through SQ1, SQ2 and SQ3, the grains are substantially refined by natural growth of multifold twins within their relative matrices. The average grain diameter dropped from approximately 137 $\mu$m to 28 $\mu$m (Figure 3.18). It is of considerable importance to note that all the multifold twin boundaries blunted relatively fast upon their early stages of growth, which may give the appearance of grain refinement solely by polygonization. The blunting strongly suggests that the twins lost coherency at a given growth level, which prohibited their further growth. This phenomenon explains the substantial extent of multifold twinning since accommodation of strain by twin

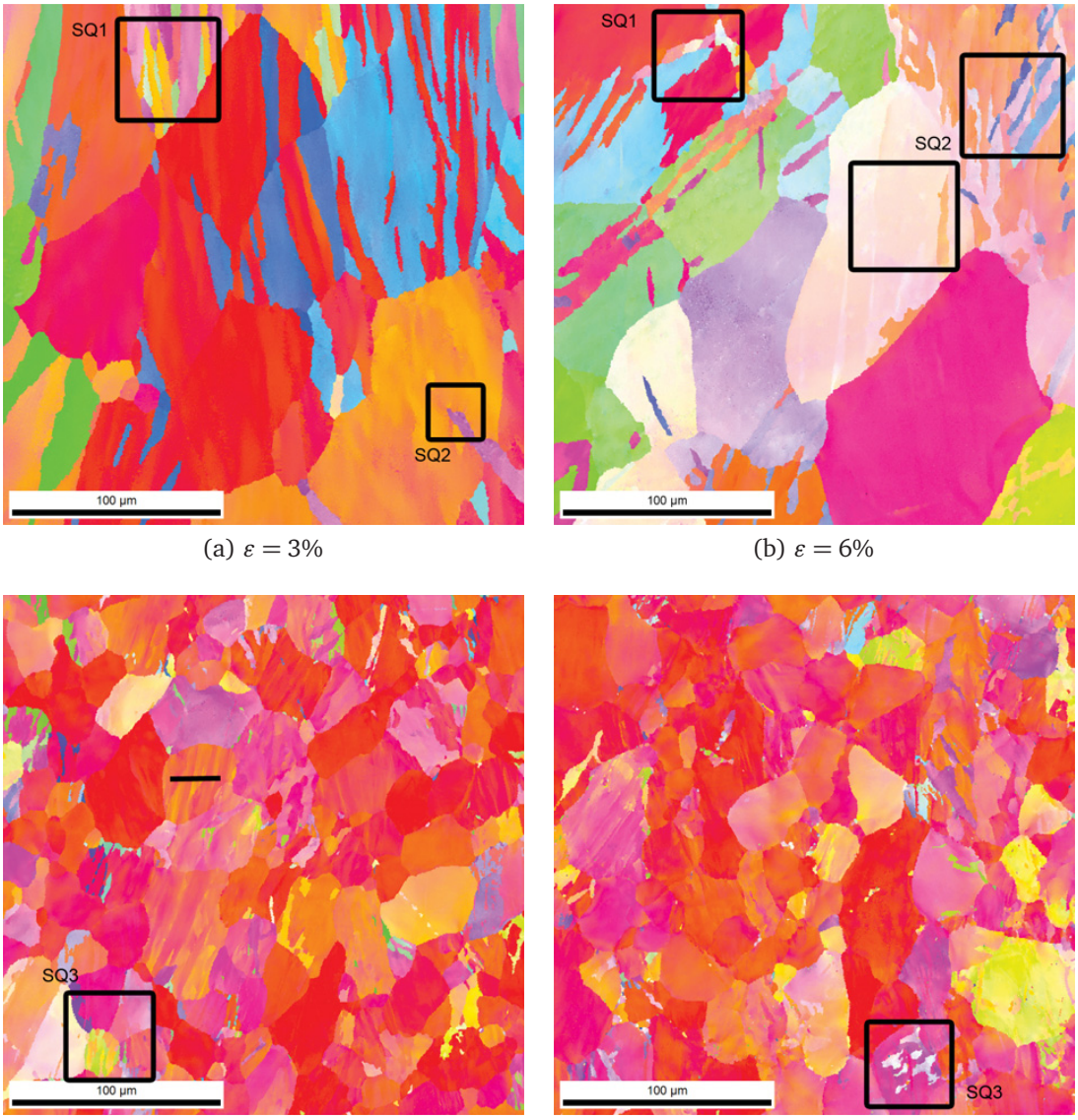


(a) $\varepsilon = 3\%$ (b) $\varepsilon = 6\%$

(c) $\varepsilon = 9\%$ (d) $\varepsilon = 12\%$

Figure 3.9 EBSD inverse pole figure maps of pure magnesium deformed along IPC.

Electron backscattered diffraction (EBSD) inverse pole figure maps of pure magnesium deformed along the transverse direction (IPC) up to four strain levels: (a) 3%, (b) 6%, (c) 9%, and (d) 12%. Note the substantial change in texture and grain refinement that occurs at 6% and after 9% plastic strain, respectively. The highlighted regions indicate example of locations where the twinning sequences SQ1, SQ2 and SQ3 occurred, which will be identified in the subsequent figures.

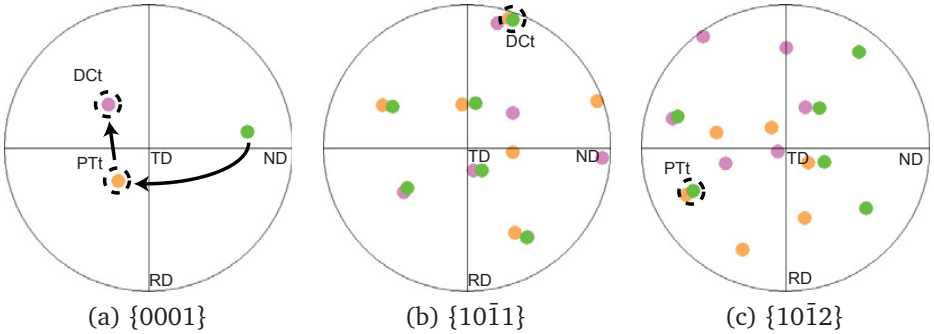


(a) {0001} (b) {10$\bar{1}$1} (c) {10$\bar{1}$2}

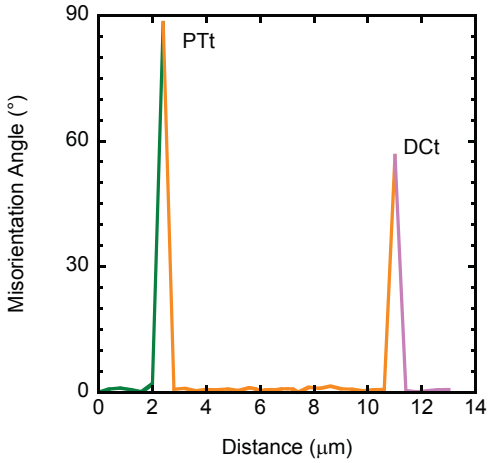


(d)

Figure 3.10 EBSD analysis of an IPC sample deformed to 3% plastic strain.

Texture analyses using EBSD (electron backscattered diffraction) of an IPC (in-plane compression) sample deformed to 3% plastic strain revealing Sequence 1 (SQ1) type twinning that consists of double twinning {10$\bar{1}$2}–{10$\bar{1}$1} that is a parent tensile twin (PTt) that twinned with a compression twin (DCt). The colors used here correspond to the colors of the IPF map in Figure 3.9a. The occurrence in Figures (3.9a, 3.9b) of SQ1 {10$\bar{1}$2}–{10$\bar{1}$1} double twinning is confirmed (a) by the common $K_1$ plane (first invariant plane by the homogenous shear) between the parent and daughter for each twin mode, and (b) by the peak misorientation of the $c$-axis between the parent and daughter around $\langle 1\bar{2}10\rangle$, which is approximately around 87° for the {10$\bar{1}$2} tensile twin and approximately 56° for the {10$\bar{1}$1} compression twin.

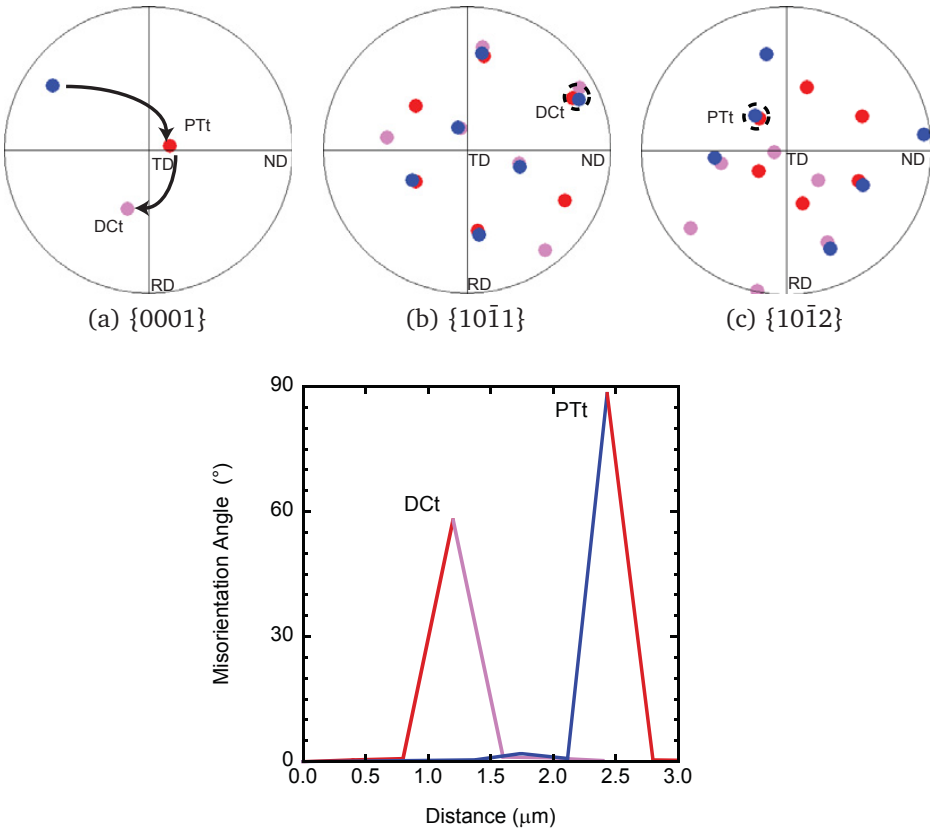


Figure 3.11 EBSD analysis of an IPC sample deformed to 6% plastic strain.

Texture analyses using EBSD (electron backscattered diffraction) of an IPC (in-plane compression) sample deformed to 6% plastic strain revealing Sequence 1 (SQ1) type twinning that consists of double twinning {10$\bar{1}$2}–{10$\bar{1}$1} (PTt and DCt) and encountered at 3% plastic strain in Figure 3.10. Here, however, the extent of double twinning and the growth of compression twins are much higher than that at 3% plastic strain. The double twinning contributes to the substantial deviation of the texture components around the loading axis.

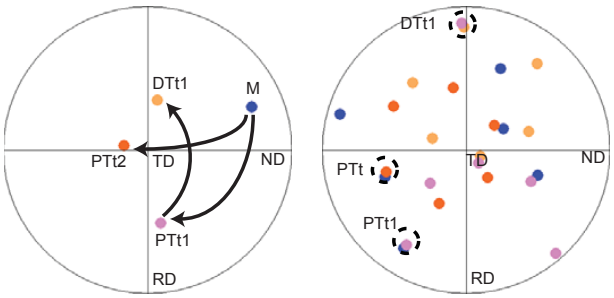


(a) {0001} (b) {10$\bar{1}$2}

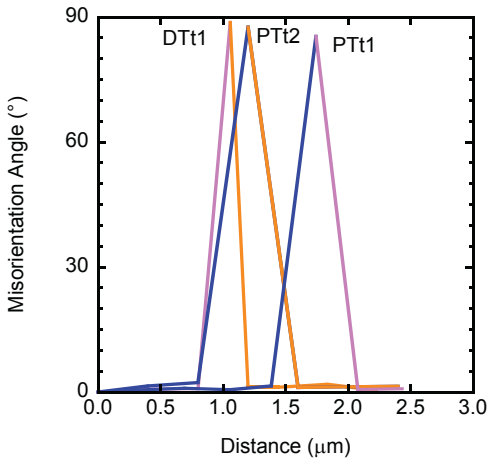


(c)

Figure 3.12 EBSD analysis of an IPC sample deformed to 9% plastic strain.

Texture analyses using EBSD (electron backscattered diffraction) of an IPC (in-plane compression) sample deformed up to 6% plastic strain revealing Sequence 2 (SQ2) type twinning that consists of a {10$\bar{1}$2}–{10$\bar{1}$2} retwinning (PTt1 and DTt1), and multi-variant {10$\bar{1}$2} twinning within the same grain (PTt1 and PTt2). The colors used here correspond to the colors of the IPF map in Figure 3.9b. Both multi-twinning and double twinning cause scatter of the texture components around the loading axis which peaked at 6% plastic strain as revealed by neutron diffraction. Retwinning and multi-twinning cause grain refinement starting at 6% plastic strain.

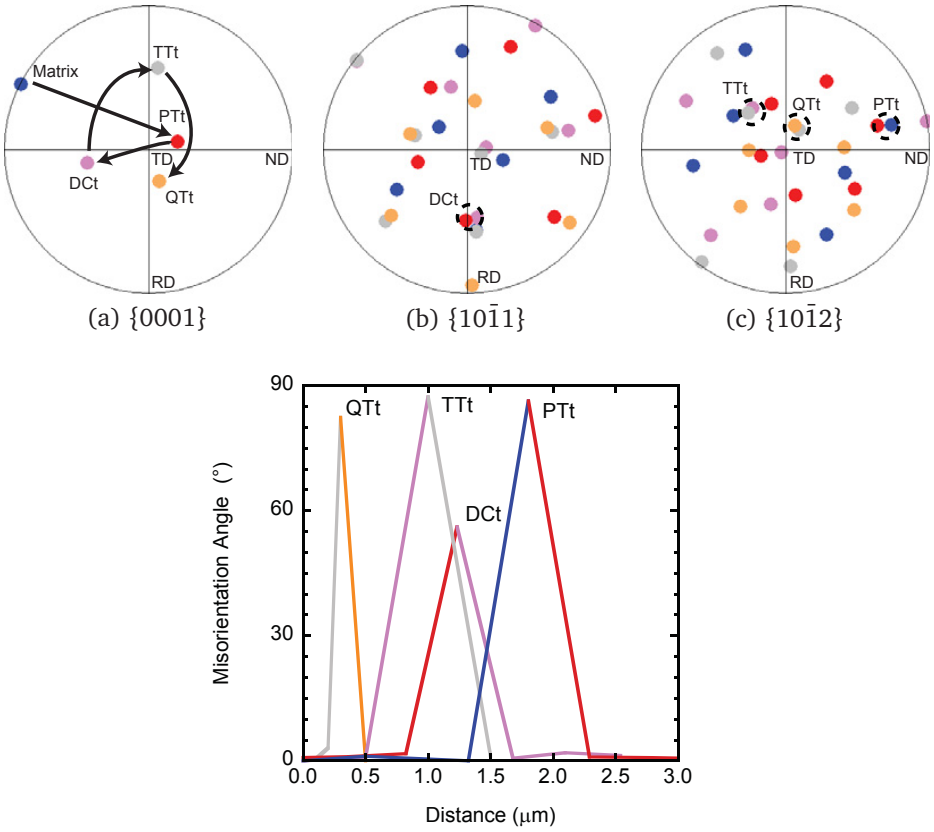


(a) {0001} (b) {10$\bar{1}$1} (c) {10$\bar{1}$2}

(d)

Figure 3.13 EBSD analysis of an IPC sample deformed to 12% plastic strain.

Texture analyses using EBSD (electron backscattered diffraction) of an IPC (in-plane compression) sample deformed up to 12% plastic strain revealing Sequence 3 (SQ3) type twinning that consists of a quadruple twinning phenomena, which is a combination of {10$\bar{1}$2}–{10$\bar{1}$1} double twinning (DCt), and multi-variant retwinning by {10$\bar{1}$2} twins within {10$\bar{1}$1} compression twins (TTt and QTt). The colors used here correspond to the colors of the IPF map in Figure 3.10. Both multi-twinning and double twinning cause scatter of texture components around the loading axis that peaks at 6% plastic strain as revealed by neutron diffraction. Also, retwinning and multi-twinning cause grain refinement starting at 6% plastic strain.

growth is brought to an end when the twin/parent interface has lost coherency. The loss of coherency is explained by the twin accommodation effects enhanced by the soft pure magnesium matrix compared to commercial magnesium alloys widely studied in the literature. Grain boundary blunting is itself enhanced by the high density of twin disconnections created upon dislocation incorporation within the twin and the accommodation effect inducing slip dislocations in the parent [Armstrong and Zerilli, 1999].

## 3.6 Discussion

### 3.6.1 Mechanisms in IPC Regime I

In contrast to Zr [Beyerlein and Tomé, 2008], which is the most studied HCP structure in pure state, pure magnesium shows only a slight increase in initial yield under TTC compared to IPC. This reduction in anisotropy of initial yield stems from the relatively lower Schmid factor of the easiest slip mode in Zr prismatic $\langle a \rangle$ compared to that in Mg (basal $\langle a \rangle$) for a similar $c$-axis fiber loaded under TTC. Thus, substantially less activity of pyramidal slip or/and compression twinning takes place when the basal $\langle a \rangle$ is actually the easiest slip mode. For Zr, the simulations by Tomé et al. [2001] predict even a higher activity of the pyramidal slip than the easy slip compared to that by Beyerlein and Tomé [2008] although the same material was used. Figure 3.14 presents the deformation mode activities for all three samples: TTC-1, TTC-2, and IPC.

The threshold stress of tensile twins was found to be almost identical to that of the closed-pack slip mode. These predictions were found to be reliable since they accurately captured both TTC-1 and TTC-2, although TTC-1 shows a slightly higher contribution of tensile twinning. This value of tensile twin threshold stress in relation to basal slip is in disagreement with most of simulations performed on magnesium alloys [Agnew et al., 2001, Proust et al., 2009] and pure zirconium [Tomé et al., 2001]. In fact, for these materials, most authors ascribed substantially larger threshold stresses to twinning compared to those ascribed to easy slip. This phenomenon reveals the significant sensitivity of twin nucleation to alloying elements and prior slip activity in the crystal, which could be affected by the initial grain size [Armstrong and Horne, 1963, Armstrong and Zerilli, 1999]. A slight increase in early activity of the easy slip mode by having a softer material promotes a more noticeable effect on twin nucleation.

This increasing effect of solute concentration reduction on twinning stress was not found to be the same for the non-basal slip systems. The pyramidal and prismatic threshold stresses decreased to keep almost the same ratios with respect to the basal slip. For example, in an AZ31B alloy Jain and Agnew [2007] found the threshold stress ratios of prismatic and pyramidal scaled over that of basal to be equal to 3.2 and 5, respectively. These ratios are almost identical to those found by our simulations for the pure magnesium.

In contrast to the alloy state, the extent of IPC Regime I, characterized by a constant hardening rate, was limited in the pure state. This can be explained by the higher contribution of easy slip in the pure state within the same range of deformation.

The relative basal slip activity exceeded 40% at the onset of plasticity and only dropped to 35% within Regime I to increase quickly back in Regime II. This argument may not be sufficient since even with an almost vanishing activity of basal slip for a total dominance of tensile twinning in Regime I for anAZ31B material, the experimental plateau was not satisfactorily captured by the simulations put forward by Proust et al. [2009].

The fastest onset of Regime II correlated to this higher activity of basal slip is in agreement with the theory put forward by El Kadiri and Oppedal [2010]. In fact, higher slip contributions would allow more transmutation and as such a more intense latent hardening in the twin, so Regime II takes place rapidly and at the expense of Regime I. Hence, transmutation operates significantly earlier in strain.

### 3.7 Mechanisms in IPC Regime II

An important point is that by not including Hall-Petch by twin segmentation, fitting the IPC curve was impossible without upsetting initial fits to the TTC curves. The TTC-1 curve was more sensitive to this phenomenon since it reflects more twinning than TTC-2. The fit was only possible by assuming that the twin hardens at least more than the parent by a factor of TSF=2. That is, the hardening in IPC has to be partially decoupled from that in TTC. The necessity of decoupling seems to be the reason that motivated other authors to consider Hall-Petch by twin segmentation which is not operational under TTC. The simulated stress-strain curves using the parameters listed in Tables 3.3 and 3.4, except for keeping the TSF equal to one, are presented

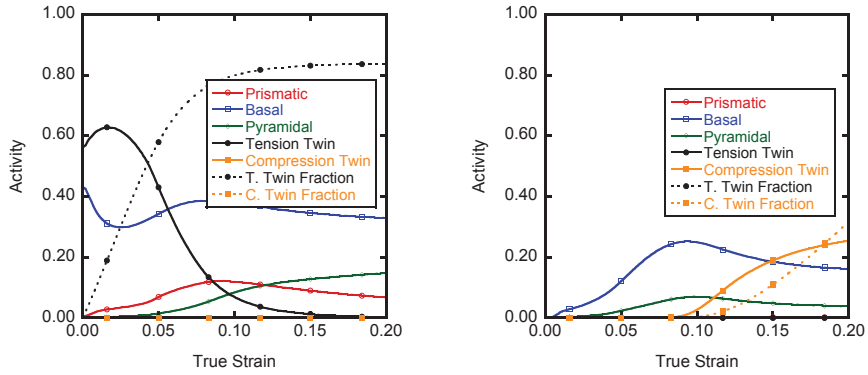


(a) IPC Activity, Parent




(b) IPC Activity, Twin

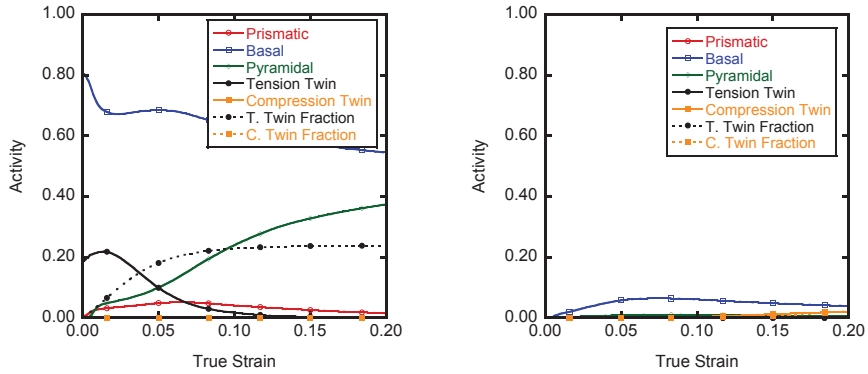


(c) TTC–1 Activity, Parent




(d) TTC–1 Activity, Twin

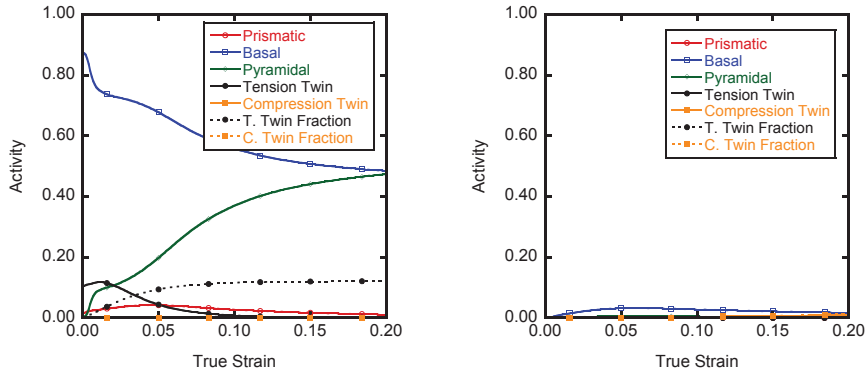


(e) TTC–2 Activity, Parent




(f) TTC–2 Activity, Twin

Figure 3.14 Simulations showing relative activities of slip and twinning.

Simulation results with the Twin Storage Factor equal to two showing the relative activities of slip and twinning within the parent and the twin for (a-b) in-plane compression (IPC), (c-d) through-thickness (TTC-1), and (e-f) through-thickness (TTC-2), respectively.

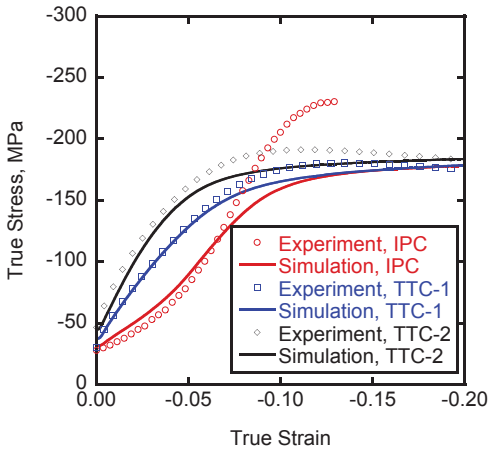


Figure 3.15 Simulations using twin storage factor = 1.

Comparison of simulation and experimental results when considering the parent and twinned regions having the same dislocation storage capabilities with the other material constants being the same as listed in Tables 3.3 and 3.4. Note the substantial discrepancies in predicting the extent of Regime II and the saturation stress in Regime III upon IPC (in-plane compression). Naturally, the same dislocation storage leads to the same saturation stress for all curves.

in Figure 3.15. Here the extent of Regime II and saturation stress was substantially mispredicted. Figure 3.4a shows that the existence of Regime II was indeed produced by the sole contribution of rotation to hard orientation by twinning. However, the predicted extent of Regime II was far from matching the experimental results.

A striking point to be emphasized is the inability of avoiding a noticeable overestimation of TTC-1 and TTC-2 curves by increasing the hardening rate of the pyramidal slip although pyramidal slip mainly affects the twins in IPC. This clearly indicates that twin induced reorientation does not account alone for the increasing hardening in Regime II.

The higher dislocation storage in the twin than in the parent was assumed to reflect in a pragmatic manner the effect of the higher latent hardening within the twin than in the parent following dislocation transmutation mechanisms. It is clear that this approach provides more flexibility to reproduce Regime II as observed in the strain hardening rate - effective stress curve (theta-sigma) in Figure 3.4. The best model correlation to the theta-sigma curve was achieved by a TSF equal to four. Both Regime II and Regime III in the theta-sigma curve were remarkably reproduced while still matching the saturation stress. Earlier attempts substantially underestimated the theta-sigma curve for magnesium alloys [Proust et al., 2009]. In most cases, the authors did not compare results of experiments and simulations in terms of theta-sigma curves, even if the stress-strain curve showed an inflection point.

Figure 3.17 here, and Proust et al. [2009], showed that the experimental strain hardening rate - effective stress curve (theta-sigma) curve has a Regime II of increasing rate in magnesium alloys, while in pure magnesium the curve was nearly linear. This probably pertains to the erratic transmutation by the multivariant twinning situation where the twins were unable to build quickly enough a complex structure of various dislocation modes. The predictions of the theta-sigma curves in the literature not only did not correlate well the overall extent of Regime II experimental data, but the rate of theta-sigma curve was of opposite sign [Proust et al., 2009]. Our simulations show a good agreement with the tendency of Regime II in the theta-sigma curve.

In Regime II, the experimental IPC strain hardening rate - effective stress curve (theta-sigma) curve shows several kinks that corresponded to load drops characteristic

of the catastrophic lengthwise thickening of the twins. These kinks persisted up to 4% plastic strain, which falls well within Regime II. For the pure magnesium studied in this work, the profuse sequences SQ1 and SQ2 are consistent with these observed load drops in Regime II.

The multivariant twinning is inconsistent with the Tomé et al. [1991] predominant twin reorientation (PTR) approach used for the twinning models in the VPSC [Tomé et al., 1991]. The Composite Grain method [Proust et al., 2007] used in these simulations, adopts a similar philosophy to track the accumulated shear of each twin system and designates the system with the maximum grain volume fraction as the predominant twin system (PTS). The PTS approach assumes that in each parent grain, only a single twin variant predominates, that is, nucleation by lengthwise thickening stops within Regime I and only growth by edgewise thickening takes place thereafter. As the twinning model used the predominant twin reorientation (PTS) scheme, multivariant twinning was not captured in the simulations. Multifold twinning was allowed for both tensile and compression twinning. However, the simulations did not lead to retwinning by tensile twinning of the tensile twins and the double twins. This is probably due to a non-Schmid effect related to tensile twin nucleation within the twins. In fact, the Schmid factor for retwinning by tensile twinning may be too low, but because of the severe accommodation effects, nucleation of tensile twins is promoted to accommodate further strain. As accommodation effects were not captured in the model, allowing multifold twinning in the simulations is not sufficient alone to capture the observed twinning sequences. This effect is somehow similar to the “non-Schmid effect” observed

in a rod -textured AM30 Mg alloy by Ma et al. [2010]. In fact, in grains with a high "Schmid factor" for tensile twinning, only decreasing and increasing the Schmid factor for tensile twinning of the neighboring grains led to limited twinning by "stopped elastic twins" and profuse twinning by residual twins, respectively.

Multivariant and multifold twinning are not documented for magnesium in the alloyed state, so the PTS scheme is probably accurate for magnesium alloys. For instance, Figure 3.16 shows IPF maps of a rod-textured AM30 Mg alloy deformed up to 3% and 9% plastic strains where a single twin variant clearly predominates in each grain. Figure 3.17 shows the corresponding strain hardening rate - effective stress curve (theta-sigma) curve of an inflecting stress-strain curve, but with no load drops in Regime II.

The development of profuse multifold and multivariant twinning in the pure magnesium could be interpreted by severe accommodation effects that occurred in the adjacent matrix to the twins. Since pure magnesium does not allow sufficient solid solution hardening, slip emission at the twin interface is facilitated. The slip could be materialized by kink boundaries lateral to the primary twins as indicated by Armstrong and Zerilli [1999]. These accommodation effects could easily induce the twin/parent interface to lose coherency as pointed out by Christian and Mahajan [1995]. The primary ongoing twins are thus prohibited from growing. Other twin variants or multifold twins are then necessary to accommodate deformation by twinning, so kinks emerge in Regime II. The nucleation of these other twin variants could be facilitated by the kink boundaries suggested by Armstrong and Zerilli [1999]. The

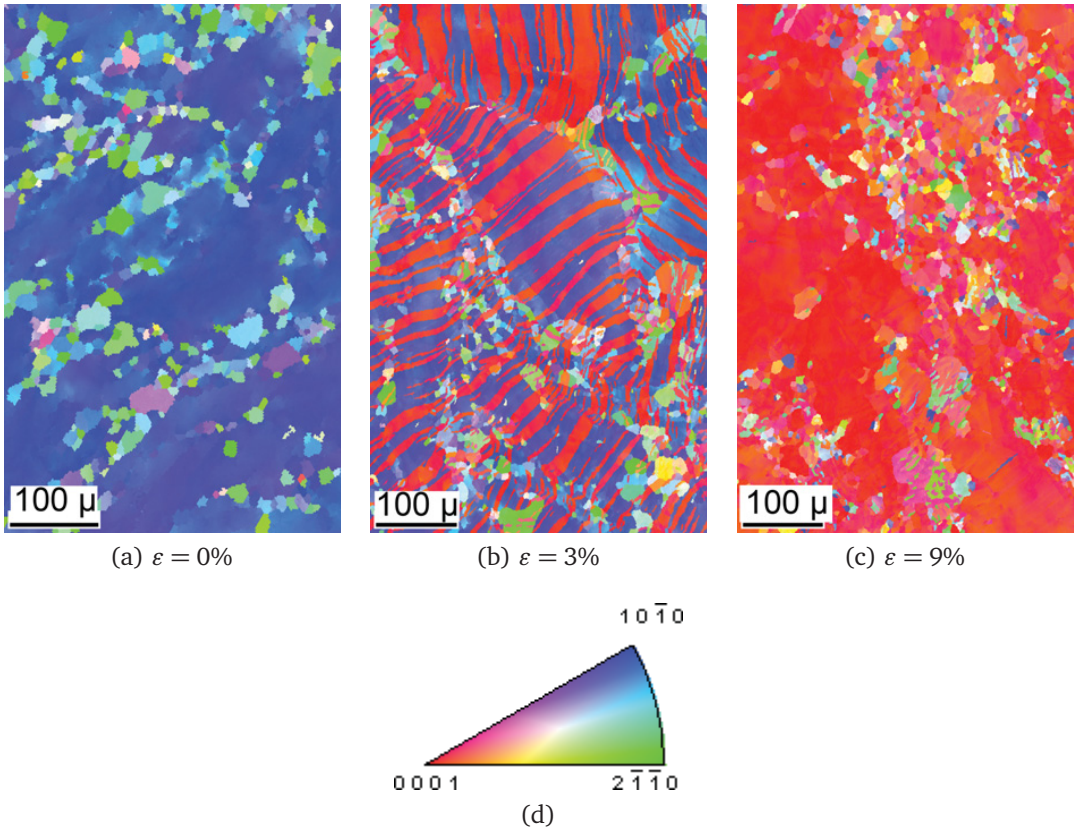


(a) $\varepsilon = 0\%$ (b) $\varepsilon = 3\%$ (c) $\varepsilon = 9\%$

(d)

Figure 3.16 EBSD inverse pole figure maps of deformed AM30.

EBSD inverse pole figure maps of an AM30 alloy deformed upon profuse twinning from (a) the initial state up to (b) 3% and (c) 9% plastic strains. Note the absence of multivariant and multifold twinning to the benefit of a predominant twin reorientation situation.

multifold and multivariant twins grow now in harder matrices that would mitigate the accommodation effects. In fact the multifold twins grow in twins that experienced transmutation-induced latent hardening, while the multivariant twins grow in a parent that incurred more slip.

A common fundamental outcome of multivariant twinning is twin-twin type hardening. However, since "stopped elastic twins," i.e. an elastic twin unable to detwin upon unloading due to plastic accommodation [30], were not observed, this type of

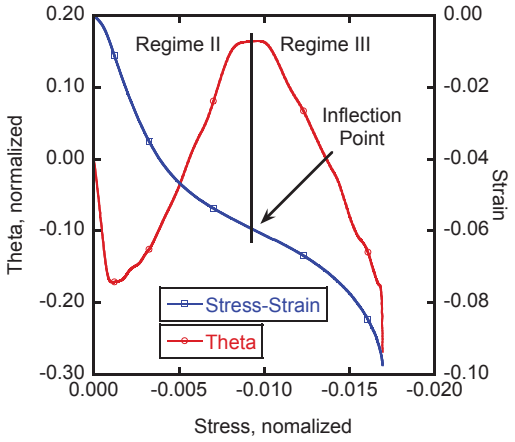


Figure 3.17 Hardening rate versus stress for AM30.

Hardening rate (theta) versus effective stress (in red) garnered from compression stress-strain curves (in blue) of an AM30 Mg alloy with a rod texture deformed along a direction giving profuse twinning. Note the absence of load drops in Regime II. Stress values were normalized by $\sigma_{\text{normalized}} = (\sigma - \sigma_y)/\mu$ where $\sigma_y$ is yield stress and $\mu$ is shear modulus.

hardening should have had a limited extent. The limited extent of "stopped elastic twin" formation may arise from the absence of small precipitates and solid solution that could upset the glide of early twinning dislocations during the lengthwise thickening stage. As such, the emissary dislocations suggested by Sleeswyk [31] did not form.

SQ1 and SQ2 both induce substantial orientation refinement and scatter so at 6%, the PTS scheme could not capture the slight orientation broadening around the {0001} || TD fiber.

### 3.7.1 Mechanisms in IPC Regime III

In Regime III, the orientation refinement peaked upon profuse SQ3, which is a multifold tensile twinning sequence affecting SQ1 and SQ2. Of substantial importance

is the blunting of most twinning boundaries refined by the SQ2 and SQ3 sequences. The blunting gave the appearance of polygonized subgrains typical of recovery mechanisms. However, orientation profiles confirmed that misorientations along boundaries ranged between 30° and 88°, typical of the three identified sequences. Furthermore, it is helpful to note that coalesced twins of the same variants left only straight boundaries with approximately 2° to 10° misorientations typical of high angle subgrain boundaries (Figure 3.19). As put forward by Partridge and Roberts [1964], the high angle boundaries merged as a result of the high density of twin disconnections being converted to dislocations in the matrix aligned in parallel patterns upon twin coalescence. As such, the dislocation density was not high enough to cause blunting of these coalesced boundaries. Therefore, the blunting of former twin boundaries that impinged into other twins of different variants was driven by a substantially higher dislocation density. These higher dislocation densities were most likely the result of the accommodation effects that caused a loss of coherency with the parent matrix. Dissociation mechanisms of the twin partials similar to that mentioned by Sleeswyk [1962a] could have occurred to promote dislocation cross slip in the matrix so accommodation effects are favored.

Mapping of grain area upon deformation reveals that the grains were refined by a factor of four up to 12% of plastic strain (Figure 3.18). An important outcome of the lower difference in yielding between TTC and IPC compared to that for Zr is that the difference in the saturation stress between TTC and IPC is revealed for pure magnesium. As mentioned previously, this poses a serious problem for a good model correlation without increasing the dislocation storage capability of the twins (TSF)

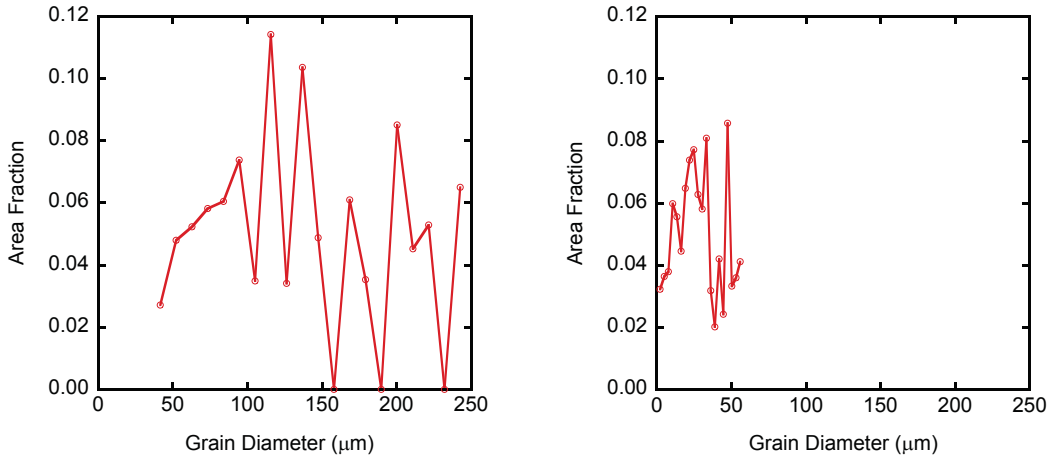


(a) Initial state (b) IPC $\varepsilon = 12\%$

Figure 3.18 Grain size of initial state.

Grain size diameter histogram plot corresponding to (a) the initial state before compression garnered from data in Figure 3.2, and (b) after 12% plastic strain upon IPC garnered from data in Figure 3.9d. The average grain size diameter in the initial state is 137 $\mu$m compared to 28 $\mu$m when strained to = 12% in IPC.

compared to that of the parent. If hardening within the twin and within the parent are of the same magnitude, the model incorrectly predicts IPC and TTC to equally saturate (Figure 3.15). Since the twin deforms primarily by pyramidal or/and compression twins, increasing the hardening of this mode(s) would appear to be the best way to capture the higher saturation stress and the higher extent of Regime II. However, this increase leads to a direct overestimation of the TTC curves. This reveals, in fact, that an extraordinary hardening operates under the IPC mechanism, not just the increase in the amount of necessary hard slip modes by twinning. We found that transmutation inducing a preferential increase of latent hardening in the twin upon IPC is the extra

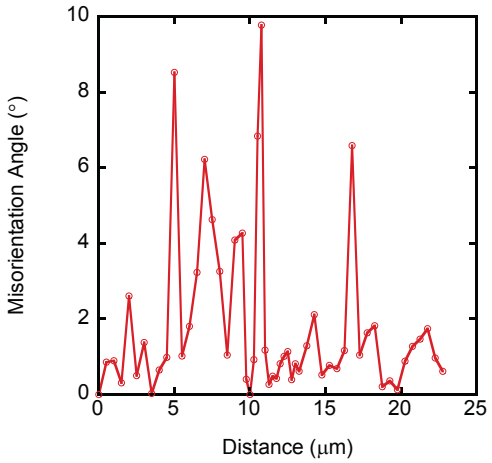


Figure 3.19 Misorientation profile.

The misorientation profile along the highlighted line in Figure 3.9c that corresponds to 9% plastic strain upon IPC. The line crosses multiple subboundaries arising from coalescence of twin lamellae of the same twin variant.

hardening mechanisms with justifiable physical premises, which could explain the high rates of Regime II.

### 3.7.2 Mechanisms in TTC

Under TTC loading, basal and pyramidal slip predominate strain accommodation (Figure 3.14). Basal slip marked the highest activity at the yield point and monotonically decreased thereafter to the benefit of pyramidal slip. Interaction between basal and pyramidal slip is then expected to have an important effect on hardening, but no latent hardening was considered in the present simulations. The softer TTC-1 underwent a strengthening of the basal peak since the minor orientations in the vicinity of the {0001} || TD component rotated toward the load axis by the limited tensile twinning. No grain refinement was observed for TTC deformed samples analyzed by

EBSD, which were not reported in this work. This substantiates the primary role of profuse multivariant and multifold twinning through accommodation effects in refining grains and blunting of former twin boundaries which were observed under IPC.

Despite the predominance of pyramidal slip in the saturation regimes for both TTC and IPC, TTC saturated under lower stress compared to IPC. This underlines the considerable effect of transmutation of incorporated parent dislocations in the twinned regions. It is noteworthy to observe the nearly similar saturation stress of the TTC-1 and TTC-2 although TTC-1 was softer. This greatly substantiates the effect of dislocation transmutation on the saturation stress, since TTC-1 twins slightly more than TTC-2.

The decrease in stress in the saturation regime of the TTC curves could be explained by shear localization and not by dynamic recrystallization. Despite that pure magnesium is able to dynamically recrystallize at room temperature via transmutation effects [Kaibyshev and Sitdikov, 1994, Sleeswyk, 1962a], we did not observe any recrystallized grains. In fact, the dynamic recrystallization in pure magnesium was reported to start therein after 50% of plastic strain which was not investigated in the present work. The shear localization in magnesium was also reported by Klimanek and Pötzsch [2002].

### 3.8 Conclusions

Anisotropy in pure magnesium is characterized by a more complex twinning phenomena compared to magnesium alloys. Substantial multivariant and multifold twinning arose in the matrix and was consistent with severe accommodation effects

that could have potentially occurred in the relatively soft matrix. The accommodation effects seemed to have been so severe that the primary twin boundaries lost coherency and triggered other twin variants and modes throughout the matrix so further strain could be accommodated. As a consequence, several load drops appeared in the strain hardening rate - effective stress curves (theta-sigma) characteristic of the lengthwise thickening of the twins. The accommodation effects ultimately led to multivariant and multifold twinning and in turn substantial grain refinement and blunting of former twin boundaries as they lost coherency with the matrix. This radical change in the microstructure and texture of pure magnesium upon profuse twinning was not captured in the crystal plasticity simulations although it could have a noticeable effect on hardening. The grain refinement was found to not be induced by dynamic recrystallization at room temperature as previously observed in the literature for pure magnesium [Kaibyshev and Sitdikov, 1994].

Choosing not to utilize the Hall-Petch effect by twin segmentation allowed us to realize that rotation to hard orientation by twinning is sufficient to cause a Regime II of increasing hardening rate. However, the extent of the hardening rate was substantially underestimated by the model unless a higher hardening rate in the twins was used when compared to the parent. In this case, the other loading orientations where twinning was limited, such as TTC in basal textures, were still satisfactorily predicted. A fitting parameter called the twin storage factor had a dominant effect on comparing the model to the experimental stress-strain behavior when extra hardening in the twins was considered. This is consistent with the transmutation theory put forward by El Kadiri

and Oppedal [2010]. However, it is emphasized that according to the transmutation theory, the higher hardening in the twins over that in the parent is not due to an increase in the dislocation generation in the twin over that in the parent. Rather, it is due to an increase of latent hardening in the twins by a rapid increase in dislocation multiplicity within the twins.

When considering that the twin regions harden more than the parent, not only were the stress-strain behaviors well predicted but the strain hardening rate - effective stress curve (theta-sigma) was as well. This kind of model correlation to experimental data was not previously reported in the literature. A hardening level within the twin higher than four times than that in the parent was necessary to satisfactorily capture the theta-sigma curve.

CHAPTER 4

# LIMITATION OF CURRENT HARDENING MODELS IN PREDICTING ANISOTROPY BY TWINNING IN HCP METALS: APPLICATION TO A ROD-TEXTURED AM30 MAGNESIUM ALLOY

## 4.1 Summary

When a strongly textured hexagonal close packed (HCP) metal is loaded under an orientation causing profuse twinning or detwinning, the stress-strain curve is sigmoidal in shape and inflects at some threshold. Authors have largely attributed the dramatic stress increase in the lower-bound vicinity of the inflection point to a combined effect of a Hall-Petch mechanism correlated to grain refinement by twinning, and twinning-induced reorientation requiring activation of hard slip modes. These two mechanisms drove the correlation approaches of crystal plasticity hardening models to the macroscopic mechanical response. In this work, we experimentally and numerically demonstrate that these two mechanisms alone are unable to consistently reproduce the stress-strain behaviors obtained under intermediate loading orientations correlated to in-between profuse twinning and nominal twinning. We argue based on adopting various mechanistic approaches in hardening model correlations from the literature. We used both a physics dislocation based model and a phenomenological Voce hardening model. The HCP material is exemplified by an extruded AM30 magnesium alloy

with a $\langle 10\bar{1}0\rangle$-fiber parallel to the extrusion direction. The intermediate loading orientations corresponded to obtuse angles with the extrusion direction and gave rise to curve inflections progressively vanishing toward the extrusion radial direction. We demonstrate that this behavior could only be captured when Hall-Petch is disregarded and the twin is considered to harden by slip at least three times more than the parent. This consideration was stimulated by the dislocation transmutation effects by the interfacial twinning shear.

## 4.2 Introduction

Sharply textured HCP metals can exhibit pronounced deformation anisotropy because twinning [Cáceres et al., 2008] becomes profuse under a suitable loading orientation, and nominal or prohibited under other loading orientations. This anisotropy promotes complex distortions in wrought metals, notably Mg and Ti, when formed at the conventional velocity ranges used for cubic structures. Until this day, high strength magnesium alloys could not be formed with velocities allowing reasonable costs.

The $\{10\bar{1}2\}\langle 10\bar{1}1\rangle$ twins are the most frequent twins in these two metals [Christian and Mahajan, 1995], due to their relatively low characteristic shear and easy shuffle mechanisms. However, due to twinning polarity, this twinning mode can only accommodate extension along the $c$-axis for these metals and other HCP metals having a $c/a$ ratio less than $\sqrt{3}$. Other twin modes, or difficult to activate $\langle c+a\rangle$ pyramidal slip systems, are necessary to accommodate contraction along the $c$-axis. For Mg, Zr and Ti, the most frequent compression twins are $\{10\bar{1}1\}$ and $\{10\bar{2}2\}$ twins Christian and

Mahajan [1995] despite their relatively high characteristic shear. Other less frequent twinning modes with higher characteristic shear or complex shuffling requirements could occur under high stress or complex loading, temperature and alloying conditions. Double twinning could also occur as a successive or simultaneous combination of multiple twinning modes affecting the same region. However, the growth and as such the deformation accommodated by these less frequent twin modes are usually sufficiently small to be disregarded in polycrystal plasticity simulations.

A *c*-axis fiber, or basal, texture is typical of clock rolled sheets, has been widely utilized in "benchmarking" the visco-plastic self-consistent (VPSC) model developed by Molinari et al. [1987] based on the Eshelby inclusion theory Eshelby [1957], and later implemented by Lebensohn and Tomé [1993] for polycrystal plasticity simulations. Simple compression at room temperature along the normal direction (Through Thickness Compression; TTC) results in a concave stress-strain curve typical of slip predominance through dislocations with Burgers vectors having a component along the *c*-axis. At temperatures close to liquid nitrogen (LN) temperature (76 K), however, compression twins can accommodate an important part of the deformation for HCP metals for which prismatic slip is most readily activated, such as Zr and Ti [Tomé et al., 2001]. The stress-strain curve is inflecting with an initial plateau (Regime I), a saturation regime (Regime III) and intermediate regime with increasing hardening rate (Regime II). If the *c*-axis fiber is loaded along the in-plane rolling or transverse direction (In-Plane Compression; IPC), a sharp sigmoidal stress-strain behavior is obtained at temperatures up to 573 K due to the occurrence of tensile twinning [Reed-Hill, 1973]. The initial

plateau corresponds to dramatic twin growth characterized by an important "parabolic" increase of the twin volume fraction. The twinning occurs as residual lamella from an initial complete lengthwise thickening. The residual twin usually reaches both sides of the grain, and the strain is accommodated partly by kinking and partly by slip dislocation activities in the twin or in the parent, called accommodation effects. The partition between kinking and slip is dictated by the compatibility restrictions at the grain boundary and the strength of the material. The number density of lamella is characteristic of the twin mode and the alloy but not the initial grain size. The twins continue growing edgewise by glide of interfacial partial twinning dislocations that induce the parent/twin interface to advance forward toward the parent. Spontaneous nucleation of twin islands at the twin/parent interface is possible, but it is unlikely to be important, for the high rates of edgewise growth observed experimentally.

The twin lamellae are crystallographically new orientations conserving the parent lattice structure - for example, upon IPC of Mg c-axis fiber textures, $\{10\bar{1}2\}$ tensile twinning reorients the twinned lamellae approximately 87° from the parent toward the compression axis. The tensile twin lamellae must thus deform by compression twinning or slip along the $c$-axis under the same stress that controls their ongoing growth. Motivated by TEM observations [Stohr and Poirier, 1972], second order pyramidal $\langle c+a \rangle$ dislocations are considered in most polycrystal simulations as the only slip mode accommodating $c$-axis compression. Because of its relatively high Peierl's stress, large Burgers vector and rough atomic planes, this slip mode is harder to activate than the tensile twin, and $\langle a \rangle$-type dislocations. Agnew et al. [2001] showed through

VPSC simulations that the double-peak phenomena experimentally observed after TTC loading of basal texture could only be attributed to pyramidal dislocation activities with a Burgers vector having a component along the $c$-axis.

Some authors have questioned the presence of glissile pyramidal $\langle c+a \rangle$ dislocations even as dissociated partials. Recent atomistic simulations by Li and Ma [2009] suggested that the independent glide of two partials: $\frac{1}{2} \cdot \frac{1}{2}[01\bar{1}2]$ and $\frac{1}{3} \cdot \frac{1}{2}[2\bar{1}\bar{1}0]$, which when combined at the free surface gave rise to a perfect dislocation lying on the second order pyramidal plane with $\langle c+a \rangle$ as net Burgers vector. These authors observed no pyramidal $\langle c+a \rangle$-dislocations within the crystal bulk. If this hypothesis is correct, the Schmid factor should be adjusted for slip along the $c$-axis and this may question current stress-strain behavior correlations in polycrystal plasticity simulations.

As the twin volume fraction increases, i.e. the fraction of grains with $c$-axis close to the loading axis increases, the texture becomes harder. The critical resolved shear stress and hardening parameters of $\langle c+a \rangle$-pyramidal slip found to reproduce the inflecting curve upon profuse twinning were, however, to cause an overestimation of the stress-strain behavior in the TTC direction. That is, the hardening involved with an activity of pyramidal $\langle c+a \rangle$-dislocations would be higher if the grains progressively align their $c$-axis with the loading axis through twinning, than if they were initially oriented as such. This reflects a discrepancy in the dislocation storage capability between the two orientations, which will be discussed in the core of this chapter.

In an effort to simultaneously reproduce both TTC and IPC stress-strain behaviors with the same set of parameters, part of the large hardening induced by twinning

was asserted to originate from a Hall-Petch Hall [1951], Petch [1953] effect induced by the creation of twin interfaces. This Hall-Petch effect could be naturally correlated to grain refinement resulting from twinning. For the Voce type hardening model, this Hall-Petch effect was portrayed through the latent hardening slip-twin parameters. In the literature, an acceptable correlation for Mg and Zr stress-strain behaviors under both TTC and IPC loading orientations compelled the latent hardening slip-twin to range for all slip systems from 400% to 3500% higher than the slip-slip self hardening Proust et al. [2009].

In this work, by using a $\langle 10\bar{1}1 \rangle$ fiber texture and adopting the same correlations approaches used in the literature, we derive an important discrepancy in the prediction of the stress-strain behaviors measured under loading orientations with intermediate volume fractions of twins. Only the stress-strain behaviors under orientations completely prohibiting twinning and maximizing twinning could be acceptably reproduced. In between, the models do not provide enough precision to capture the hardening trend.

We demonstrate that the reason lies behind a misunderstanding of the nature of twin-slip interactions.

A first misunderstanding comes from the Hall-Petch effect. In fact, on one hand we show that the measured twin volume fraction evolution is incompatible with the evolution of the Hall-Petch effect needed to capture the increasing hardening rate in Regime II of the stress-strain behavior. The dislocation based model is more sensitive to this effect, since no good correlations could even be achieved for the two classical

limiting loading orientations. In fact, in contrast to Zr, the curves from profuse twinning and nominal twinning do not saturate at the same level in Mg, and this could not be captured by any simulation with Hall-Petch terms. On the other hand, the Hall-Petch effect accounted for by a sort of slip-twin latent hardening in the Voce type hardening model was not able to inflect the simulated curves with loading at an obtuse angle from ED.

A second misunderstanding comes from disregarding the dislocation transmutation effects upon twin incorporation El Kadiri and Oppedal [2010]. The Voce model is unable to capture this effect, but the dislocation model Beyerlein and Tomé [2008] is. A pragmatic factor distinctly increasing the stored dislocations in the twin over that of the parent had an encouraging effect on modeling anisotropy in HCP metals using the transmutation effects.

We use an extruded, rod-textured, AM30 magnesium alloy obtained by relatively fast extrusion with high ratio at high temperature. Neutron diffraction, x-ray diffraction (XRD) and electron backscatter diffraction (EBSD) analyses were used to measure the deformation texture and evolution of volume fractions of twins. The VPSC code is used for the polycrystalline plasticity simulations with the dislocation-based model and an extended Voce hardening model.

## 4.3 Materials and testing

Table 4.1 Chemical composition of Mg AM30 used in the extrusion process.

| Al | Mn | Zn | Fe | Si | Cu | Ce | Ni | Mg |
|---|---|---|---|---|---|---|---|---|
| 2.54 | 0.4 | 0.018 | 0.003 | 0.008 | 0.011 | 0.025 | 0.005 | balance |

### 4.3.1 Material initial state

The material is an AM30 Magnesium alloy received from Timminco in the form of a 200 mm diameter billet extruded from a 450 mm diameter as-cast ingot. The extrusion operated at 570 °C and at a 0.3 m/s extrusion speed. The chemical composition of the alloy is given in Table 4.1.

Samples for uniaxial mechanical testing were prepared using EDM (electrical discharge machining) to extract right cylinders 10 mm dia. x 10 mm length. The materials in this study were tested in the "as received" state. The tests were conducted at room temperature and a strain rate of 0.001 $s^{-1}$. Uniaxial compression tests were conducted to several different strain levels so that the experimental macro- and micro-texture analysis could be conducted on the samples. Samples used for comparison to numerical simulation results were not tested to failure.

Samples were prepared for testing along four different loading paths (see Figure 4.1). Conventionally, previous investigators chose orthogonal loading paths to maximize and minimize the effect of twinning on the mechanical behavior. In this study, additional intermediate loading paths were desired, and were obtained by extracting samples at intermediate orientations. Samples were prepared allowing loading along the Extrusion Direction (ED), 30 degrees from the extrusion direction

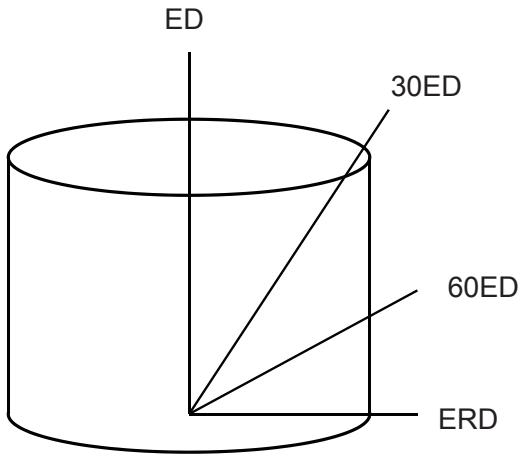


Figure 4.1 Schematic illustration of sample orientations from billet.

(ED30), 60 degrees from the extrusion direction (ED60), and perpendicular to the extrusion direction, i.e. extrusion radial direction (ERD).

EBSD analyses showed large elongated grains in the extrusion direction, and small equiaxed grains preferentially located at the grain boundaries of the large elongated grains (Figures 4.2a and 4.2b). Some of the large grains, however, seemed to be completely consumed by the equiaxed grains. The grain orientation spread reveals the large elongated grains to be parent grains that underwent substantial deformation and equiaxed grains that were recrystallized with an average misorientation spread less than $1^\circ$ (Figures 4.3). The parent grains show a sharp rod texture with the pole ED $\parallel \{10\bar{1}0\}$, while the recrystallized grains show a mixed texture between ED $\parallel \langle 2\bar{1}\bar{1}0\rangle$ and ED $\parallel \{10\bar{1}0\}$. Here we adopted ED, ERD, and ETD as the sample basis, where ETD is the Extrusion Tangent Direction.

The pole ED $\parallel \langle 2\bar{1}\bar{1}0\rangle$ is more predominant in the recrystallization texture as the corresponding grains exhibit a higher tendency for primary grain growth than those

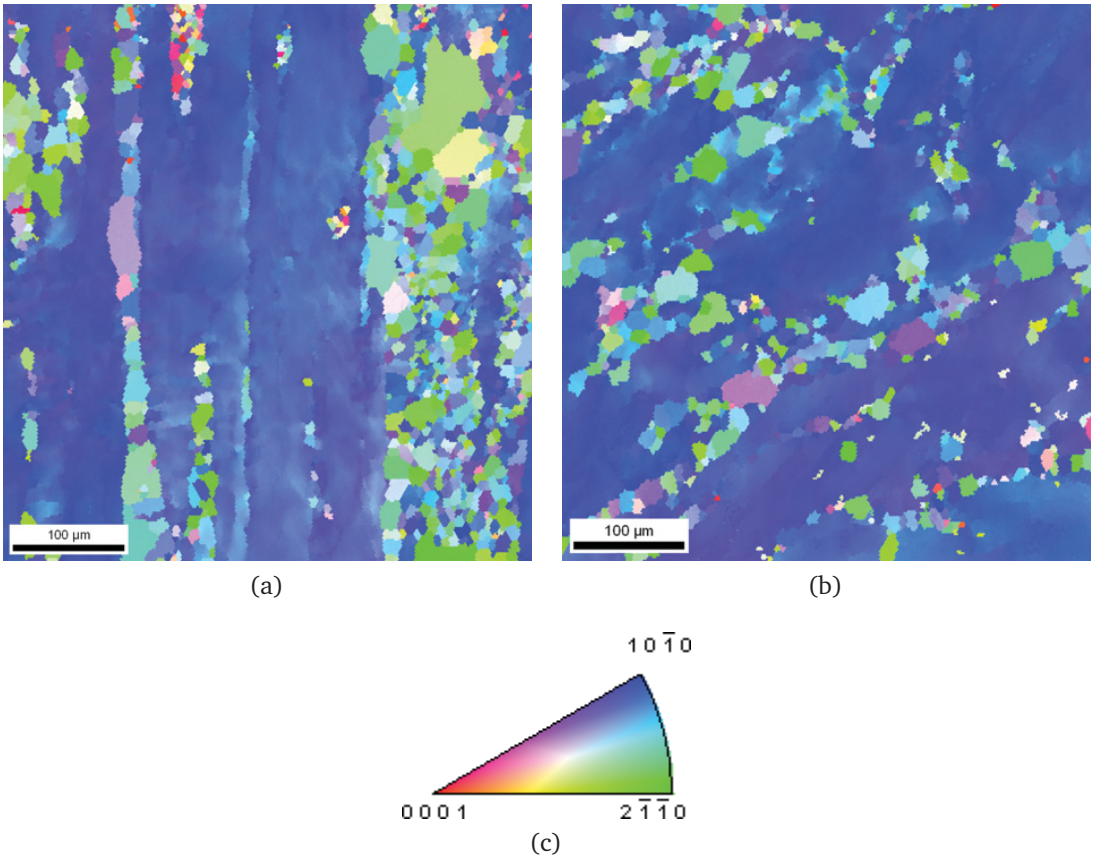


Figure 4.2 AM30 initial state EBSD IPF maps.

Inverse pole figure maps obtained by EBSD analyses (a) on a section normal to Extrusion Radial (ERD), and (b) on a section normal to Extrusion Direction (ED). For the color key of these two maps, however, the texture in (a) was rotated 90° around ERD so to coincide with sample axes in (b) and provide the same textural visualization.

associated to the recrystallized ED || $\{10\bar{1}0\}$ component (Figure 4.3). The recrystallized portion of the grains reached 33% surface fraction as revealed in Figure 4.3.

The macrotexture information in this study was collected by x-ray diffraction (XRD) and neutron diffraction (ND) using a Rigaku Smartlab X-Ray Diffractometer and also by neutron diffraction using the facilities of LANSCE (Los Alamos Neutron Science) at Los Alamos National Laboratory. Details of the LANSCE facility can be found in

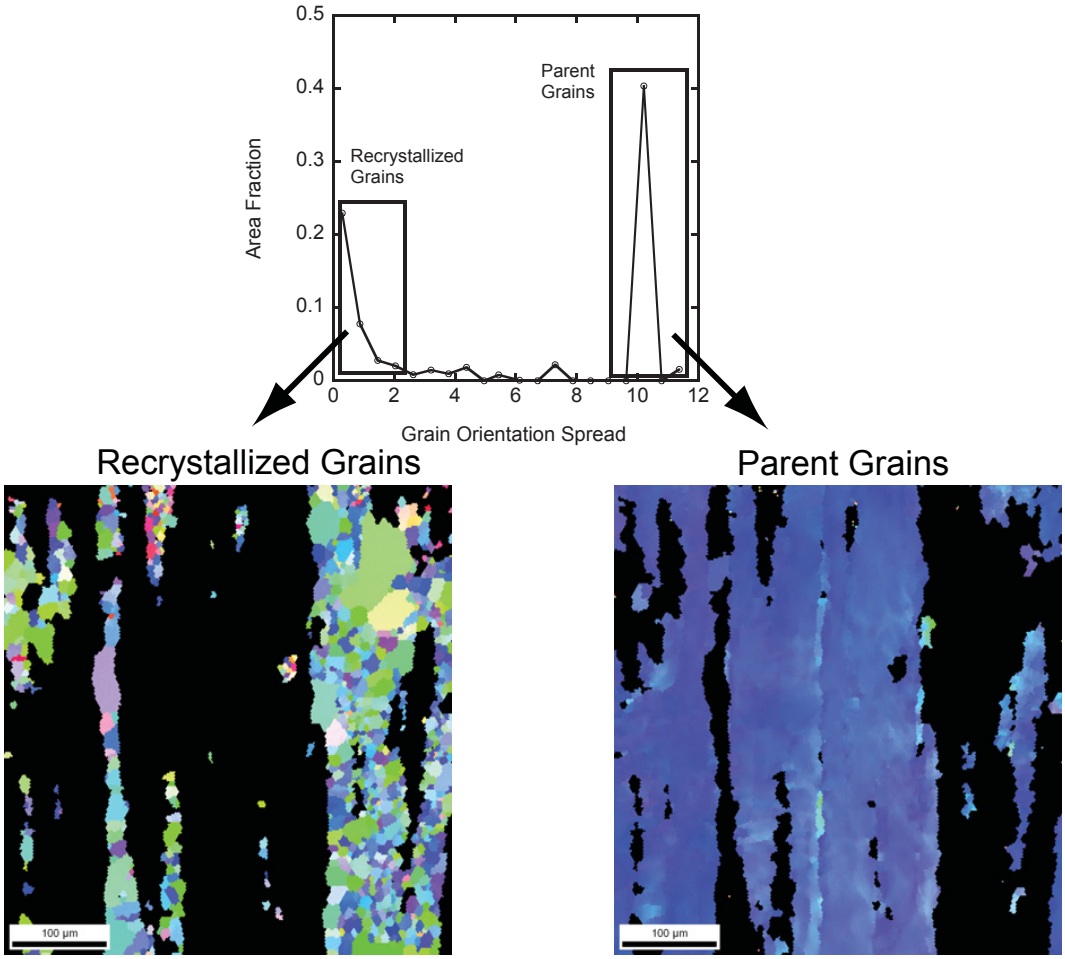


Figure 4.3 AM30 EBSD grain orientation spread.

Electron Backscatter Diffraction (EBSD) analyses showing a plot of grain orientation spread versus area fraction exhibiting two peaks highlighted with the tolerance showed with the dashed rectangles to generate Inverse Pole Figure (IPF) maps of the corresponding grains; that is, the microstructure in Figure 4.2a is formed by fine recrystallized grains as a combinations of two poles Extrusion Direction (ED) $\parallel \langle 2\bar{1}\bar{1}0\rangle$ and ED $\parallel \langle 10\bar{1}0\rangle$, and large non-recrystallized, elongated grains showing a single sharp ED $\parallel \langle 10\bar{1}0\rangle$.

Von Dreele [1997] and Wenk et al. [2003]. Texture analyses and pole figure plots of XRD and ND were done using the popLA [Kocks et al., 1995] and pole8 [Tomé, 2008]

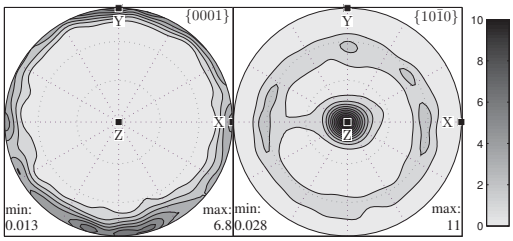


Figure 4.4 AM30 initial pole figures.

{0001} and {10$\bar{1}$0} pole figures obtained by neutron diffraction on an untested specimen. Z corresponds to extrusion direction; X and Y correspond to the extrusion tangent and extrusion radial directions, respectively. A pronounced ED || {10$\bar{1}$0} fiber from the extrusion process is evident.

software from Los Alamos National Laboratory, and MTEX [Hielscher and Schaeben, 2008].

### 4.3.2 Mechanical testing

The mechanical tests corresponded to uniaxial compression at room temperature and at a rate of 0.001 $s^{-1}$. The intermediate loading directions (30ED and 60ED) were performed in an effort to tests the hardening models and correlation approaches used in the literature to fit the entire yield surface domain corresponding to various levels of twin activity. This is of great importance to metal forming modeling since real world conditions correspond exactly to intermediate twin activities in between profuse and nominal.

The specimens all yielded at approximately 100 MPa, but the strain hardening behavior was markedly different. This difference is not monotonic upon angle deviation from ED toward ERD. The ED curve is pronouncedly inflecting as all grains twinned.

The ERD shows an apparent permanent decreasing hardening rate characteristic of slip preponderance. The difference between ED and ERD is in contrast with the difference between TTC and IPC typically encountered in compression of *c*-axis fiber textures. In fact, for *c*-axis fiber textures, the TTC loading orientation, equivalent here to ERD, is harder than IPC, because of the necessity of harder slip mode to accommodate deformation along the *c*-axis. Here, upon ERD, basal slip is the predominant deformation mode with a nominal contribution of twinning. The deformation texture in Figure 4.4 substantiates twinning of grains having their *c*-axis around the normal to the ERD (Highest Schmid factors).

After 12% plastic strain, the ERD sample develops an ellipsoidal form with the longer axis along ETD (Figure 4.5) and the shorter axis along ED. This anisotropy is produced by the need of a harder deformation mode to accommodate extension along ED, while basal activity readily accommodates extension along ETD. As such, the sample readily deforms by plane strain compression under ERD, rushing a vertical fracture along ED. This anisotropy induced damage is as such crucial for sheet forming to determine the limiting forming diagrams.

The 30ED sample (figure 4.6a) is clearly inflecting, but with less severity than in the ED. The strain hardening rate versus stress (theta-sigma) curve (figure 4.6b) clearly indicates the amplitude of inflection. Here, the twin-slip interaction led to a nearly constant overall hardening rate starting from well below the inflection point. The 60ED shows a slight inflection point better revealed in the theta-sigma curve. However, Regime III took over quicker. The position of the inflection point in strain

seems to be dependent upon the total twin volume fraction, which is a function of loading orientation.

The ED sample, with profuse twinning, shows a higher saturation stress over all other curves. The 30ED sample broke before a perceptible completion of the saturation behavior. However, the trend indicates an overreaching saturation higher than 60ED curve. The higher saturation stress upon twinning than upon slip was recently reported for basal textured pure magnesium Oppedal et al. [2010]. The 30ED and 60ED stress-strain curves (figure 4.6a) shows not a quite intermediate response between ED and ERD curves. The 60ED starts higher and tends to saturate ultimately lower than 30ED. However, ERD seems to violate this tendency including the saturation regime. The overlapping between curves from all loading orientations is a signature of a complex twin-slip interaction in this rod-textured magnesium alloy.

## 4.4 The polycrystal plasticity model and hardening rules

For all simulations, only slip dislocations lying on the basal and prismatic planes were assumed to provide deformation along the three close packed directions $\langle a \rangle$. Slip deformation along non-basal directions was assumed to be only accommodated by second order pyramidal planes along $\langle c+a \rangle$. As observed in EBSD analyses (see next section), both $\{10\bar{1}2\}\langle 10\bar{1}\bar{1} \rangle$ tensile and $\{10\bar{1}1\}\langle 10\bar{1}\bar{2} \rangle$ compression twins had to be active (Figure 4.13. A sound simulation would minimize the number of modes necessary to acceptable reproduction of the experimental data from mechanical testing and deformation texture.

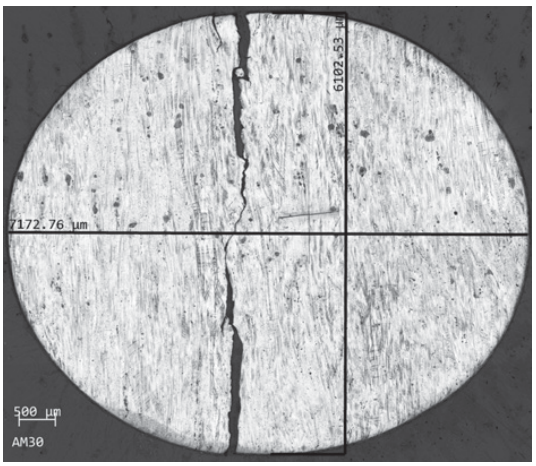


Figure 4.5 Optical micrograph of AM30 sample.

Optical micrograph of an extruded AM30 Mg alloy sample compressed 12% along the Extrusion Radial Direction (ERD). ED and ET are along the vertical and horizontal axes within the plane of view, respectively. Note than the sample extended only 1% along ED versus 19% along ET.

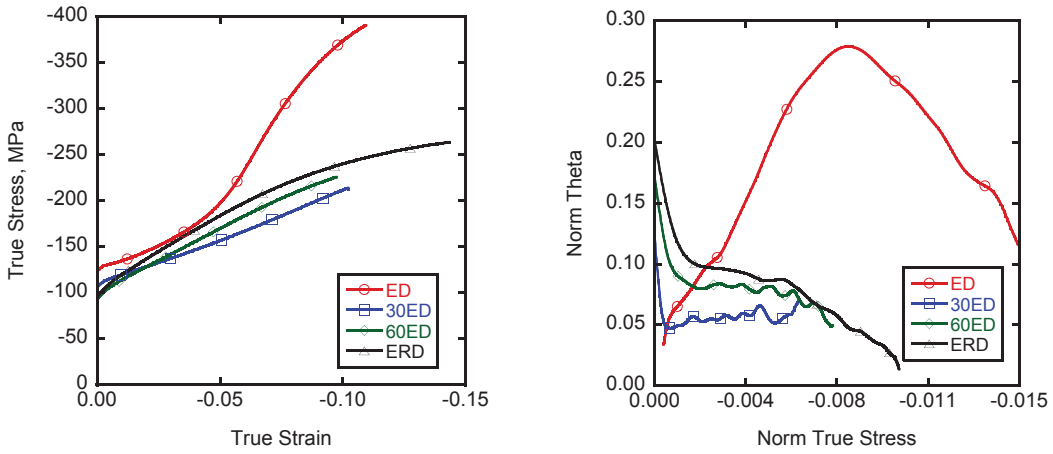


Figure 4.6 AM30 uniaxial compression test results.

Results of experimental uniaxial compression tests of the four samples showing a) true stress versus strain, and b) normalized strain hardening rate versus stress. Stress values were normalized by $\sigma_{\text{normalized}} = (\sigma - \sigma_y)/\mu$ where $\sigma_y$ is yield stress and $\mu$ is shear modulus.

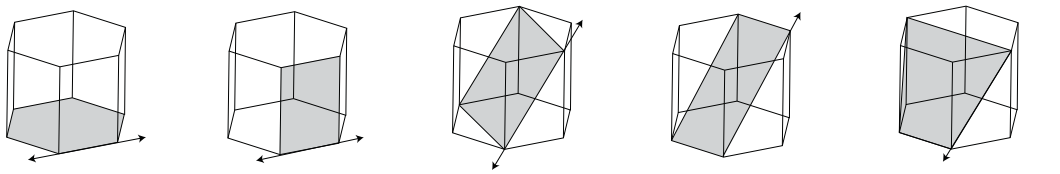

(a) basal $\langle a \rangle$ $\{0001\}\langle 11\bar{2}0\rangle$ (b) prismatic $\langle a \rangle$ $\{10\bar{1}0\}\langle 11\bar{2}0\rangle$ (c) pyramidal $2^{nd}$ $\{11\bar{2}2\}\langle 11\bar{2}3\rangle$ (d) tension twin $\{10\bar{1}2\}\langle 10\bar{1}1\rangle$ (e) compression twin $\{10\bar{1}1\}\langle 10\bar{1}2\rangle$

Figure 4.7 Deformation modes considered in the numerical simulations

Table 4.2 Slip and Twinning Modes used in these simulations for AM30 Mg

| Symbol | Mode | Crystallography | S | No. of Systems | b (nm) |
|---|---|---|---|---|---|
| $\alpha = 1$ | Prismatic $\langle a \rangle$ | $\{10\bar{1}0\}\frac{1}{3}\langle\bar{1}2\bar{1}0\rangle$ | | 3 | 3.21E-01 |
| $\alpha = 2$ | Basal $\langle a \rangle$ | $\{0001\}\frac{1}{3}\langle 2\bar{1}\bar{1}0\rangle$ | | 3 | 3.21E-01 |
| $\alpha = 3$ | Pyramidal $\langle c+a \rangle$ | $\{11\bar{2}2\}\frac{1}{3}\langle\bar{1}\bar{1}23\rangle$ | | 6 | 6.12E-01 |
| $\beta = 1$ | Tensile Twin | $\{10\bar{1}2\}\langle 10\bar{1}1\rangle$ | 0.13 | 6 | 4.92E-02 |
| $\beta = 2$ | Compression Twin | $\{10\bar{1}1\}\langle 10\bar{1}2\rangle$ | 0.1367 | 6 | 1.09E-01 |

As such, from the above EBSD analyses, five deformation modes were selected in the simulations: $\{0001\}\langle 1\bar{2}10\rangle$ (basal $\langle a \rangle$ slip), $\{1010\}\langle 1\bar{2}10\rangle$ (prismatic $\langle a \rangle$ slip), $\{11\bar{2}2\}\langle 11\bar{2}\bar{3}\rangle$ (second order pyramidal $\langle c+a \rangle$ slip), $\{10\bar{1}2\}\langle 10\bar{1}\bar{1}\rangle$ tensile twins, and $\{10\bar{1}1\}\langle 10\bar{1}\bar{2}\rangle$ compression twins. The planes and directions of these deformation modes are illustrated and specified in Figure 4.7 and table 4.2, respectively.

This work uses and compares two different hardening rules and twinning behaviors within the VPSC code. The VPSC code is based on the Visco-Plastic Self-Consistent model to compute stress in grains and can incorporate hardening rules and texture information to simulate the stress-strain behavior and deformation texture evolution together with twinning. The code models polycrystalline aggregates using single crystal

constitutive rules. The VPSC scheme, developed by Molinari et al. [1987] and implemented by Lebensohn and Tomé [1993], estimates the stress, $\sigma$, via micromechanics applied to crystals. The hardening response is based on updating the critical resolved shear stress $\tau^a$ following the constitutive power law that provides the shear strain rate $\dot{\gamma}^a$ in each slip mode $\alpha$ based on the Schmid factor $m^\alpha$ and a constant $\dot{\gamma}_0$ reflecting the macroscopic strain rate:

$$\dot{\gamma}^\alpha = \dot{\gamma}_0 \left| \frac{m^\alpha \overline{\overline{\otimes}} \sigma}{\tau^\alpha} \right|^n \text{sign}\left( m^\alpha \overline{\overline{\otimes}} \sigma \right) \tag{4.1}$$

### 4.4.1 The phenomenological extended Voce hardening model

The first hardening rule used in our simulations is the extended Voce model, described in the original work by Lebensohn and Tomé [1993]. Agnew et al. [2001] used the model in describing the behavior of Magnesium. In the extended Voce model, hardening in individual grains is described by:

$$\hat{\tau}_s = \tau_0^s + \left( \tau_1^s + \theta_1^s \Gamma \right) \left\{ 1 - \exp\left( -\frac{\theta_0^s}{\tau_1^s} \right) \right\} \tag{4.2}$$

where the evolution of the CRSS for each slip system, $s$, are represented by phenomenological parameters reflecting a purely curve fitting approach: $\tau_0^s$, $\tau_1^s$, $\theta_0^s$, and $\theta_1^s$. $\Gamma$ is the accumulated shear strain in each grain.

Latent hardening effects between slip, and slip and twin systems, are incorporated by:

$$\delta\tau^s = \frac{\mathrm{d}\hat{\tau}^s}{\mathrm{d}\Gamma}\sum_{s'} h^{ss'}\delta\gamma^{s'} \tag{4.3}$$

where $h^{ss'}$ is a matrix of latent hardening parameters. Parameters for the Voce model simulations in this work are listed in Table 4.3.

### 4.4.2 The dislocation based model

The dislocation based model uses dislocation densities on different active modes to capture hardening. This model was fully described by Beyerlein and Tomé [2008] where the authors used clock-rolled Zirconium, another HCP metal.

The hardening rule is a temperature and strain rate dependent formulation that assumes the effects of a dislocation forest, dislocation debris (or substructure), a Hall-Petch effect on slip propagation based on dislocation mean free path within the grain, and the effects of slip and Hall-Petch on twin propagation. If $a$ denotes a slip mode having $s$ as a slip system, and $\beta$ denotes a twin mode having $t$ as a twin system, both of these effects are given by the following:

$$\tau_c^{\alpha} = \tau_0^{\alpha} + \tau_{\text{forest}}^{\alpha} + \tau_{\text{sub}} + \tau_{\text{HP}}^{s} \tag{4.4}$$

$$\tau_c^{t} = \tau_0^{\beta} + \tau_{\text{HP}}^{t} + \tau_{\text{slip}}^{\beta} \tag{4.5}$$

The critical resolved shear stresses for the slip resistance equation take the following forms for each of the forest, debris, and Hall-Petch effects, respectively:

$$\tau^{\alpha}_{\text{forest}} = b^{\alpha}\chi\mu\sqrt{\rho^{\alpha}} \tag{4.6}$$

$$\tau^{\alpha}_{\text{sub}} = k_{\text{sub}}\mu b^{\alpha}\sqrt{\rho_{\text{sub}}}\log\left(\frac{1}{b^{\alpha}\sqrt{\rho_{\text{sub}}}}\right) \tag{4.7}$$

$$\tau^{s}_{\text{HP}} = \mu\text{HP}^{\alpha}\sqrt{\frac{b^{\alpha}}{d_g}} \text{ for } s \in \alpha \text{ without twins} \tag{4.8}$$

Here, $b$ is the Burgers vector, $\chi$ is the dislocation interaction coefficient smaller that unity, $\mu$ is the shear modulus, and $d$ is the spacing between twin lamellae.

Dislocation density evolution is modeled by:

$$\frac{\partial\rho^{\alpha}}{\partial\gamma^{\alpha}} = \frac{\partial\rho_{\text{generation}}}{\partial\gamma^{\alpha}} - \frac{\partial\rho_{\text{removal}}}{\partial\gamma^{\alpha}} = \text{TSF}k_1^{\alpha}\sqrt{\rho^{\alpha}} - k_2^{\alpha}(\dot{\varepsilon}, T)\rho^{\alpha} \tag{4.9}$$

The parameter $k_1^{\alpha}$ accounts for the dislocation generation, and the strain rate and temperature dependent $k_2^{\alpha}(\dot{\varepsilon}, T)$ accounts for dislocation removal. The TSF, or Twin Storage Factor, is a parameter first described by Capolungo et al. [2009] for correlations to single crystal Magnesium work by Kelley and Hosford [1968]. Oppedal et al. [2010] performed experiments and numerical simulations on polycrystal pure magnesium and used it as evidence that a dislocation transmutation scheme described in El Kadiri and

Oppedal [2010] was responsible for the rapid strain hardening observed in HCP metals loaded to induce profuse twinning.

$$\frac{k_2^\alpha(\dot{\varepsilon},T)}{k_1^\alpha} = \frac{\chi\, b^\alpha}{g^\alpha}\left(1 - \frac{kT}{D^\alpha (b^\alpha)^3}\log\left(\frac{\dot{\varepsilon}}{\dot{\varepsilon}_0}\right)\right) \tag{4.10}$$

Here $D$ is termed as the drag stress, and $g$ is the activation energy in an Arrhenius type rule for the strain rate dependence. The two critical resolved shear stresses for resistance to twin propagation relate to the Hall-Petch effect and slip and take the following forms, respectively:

$$\tau_{HP}^t = \frac{HP^\beta}{\sqrt{d_g}} \text{ with no twins or when } t \in \beta$$

$$\text{and } t \text{ is the predominant twin system (PTS)} \tag{4.11}$$

$$\tau_{\mathrm{HP}}^t = \frac{HP^{\beta\beta'}}{\sqrt{d_{\mathrm{mfp}}^s}} \text{ when } t \in \beta \text{ and } t \text{ is not the PTS, with PTS } \in \beta' \tag{4.12}$$

$$\tau_{\mathrm{slip}}^\beta = \mu \sum_\alpha C^{\beta\alpha} b^\beta b^\alpha \rho^\alpha \tag{4.13}$$

In these equations, the Hall Petch (HP) terms are used to simulate the hardening response caused by grain segmentation as the twin grows. However, the experimental evidence for this Hall Petch type effect, especially for twin boundaries is not substantiated. In theses simulations, the HP terms are set equal to zero.

In addition slip could affect twinning through the following equation:

$$\tau_{\text{slip}}^{\beta} = \mu \sum_{\alpha} C^{\beta\alpha} b^{\beta} b^{\alpha} \rho^{\alpha} \tag{4.14}$$

The $C^{\beta\alpha}$ term represents the interaction between twin and slip and may be negative or positive depending on whether slip interferes with or contributes to twin growth. In simulation work presented here, we did not consider these two barriers for twin propagation for reasons that will be developed further in this chapter. The parameters related to the generation of debris ($A^{\alpha}$ and $q$), were also not needed in these simulations and were set to zero.

The slip and twinning modes used in the simulations are found in Table 4.2. The dislocation based model parameters with best fits are listed in Tables 4.4 and 4.5.

## 4.5 Results of simulations

In general, correlating the model parameters was conducted by an iterative process with the stress-strain behavior. The fitting process was only applied to the Extrusion Direction (ED) and Extrusion Radial Direction (ERD) experimental data. The experimental stress-strain behavior of the intermediate texture samples were only compared to numerical simulations after the initial fitting to the ED and ERD samples were concluded. The results of the texture evolution and strain hardening rate versus stress plots were not considered until the model correlation was completed. Hence, the

correlations of the texture and strain rate hardening behavior and stress strain behavior of the intermediate texture samples were actual predictions.

### 4.5.1 Voce based model

In this study, we preferred a physical approach for determining the latent hardening parameters. We in fact forced "reasonable" latent hardening values from the literature Agnew et al. [2001] rather than unconstraining them for fitting purposes. In this study, we used latent hardening values of 1 between the different slip systems, and 1.4 between the slip system and the tensile twin. Values substantially higher than these cannot be substantiated physically. The strategy of large latent hardening parameters frequently encountered in the literature to cause a rapid hardening response Proust et al. [2009] was avoided.

The VPSC model with the Voce hardening rule has been used by other researchers studying Magnesium. Only few studies have used the compressive twins as an active deformation mode in the crystal plasticity simulations. Our EBSD analyses reveal profuse nucleation of double twinning but with extremely slow edgewise growth.

The initial simulated values of CRSS are in agreement with those found in the literature for wrought magnesium alloys. In fact, our simulated initial strengths for basal: prismatic: pyramidal: tensile twinning were 23: 95: 111: 67 MPa, or as ratios to the easy basal slip, 1: 4.1: 4.8: 2.9. Agnew et al. [2001] investigating an AZ31 alloy with *c*-axis fiber found initial strength ratios reported to the basal slip of pyramidal and tensile twinning to be 3 and 0.5. Proust et al. [2009] investigating AZ31B and using a

Table 4.3 Voce parameters used in simulations

| Mode | $\tau_0$ | $\tau_1$ | $\theta_0$ | $\theta_1$ | $h^{ss'}$ Prism. | $h^{ss'}$ Basal | $h^{ss'}$ Pyr. | $h^{ss'}$ T. Twin | $h^{ss'}$ C. Twin |
|---|---|---|---|---|---|---|---|---|---|
| Prismatic | 95 | 7 | 462 | 0 | 1 | 1 | 1 | 1 | 0 |
| Basal | 23 | 51 | 683 | 0 | 1 | 1 | 1 | 1 | 0 |
| Pyramidal | 111 | 914 | 3661 | 0 | 1 | 1 | 1 | 1 | 0 |
| Tensile Twin | 67 | 0 | 0 | 0 | 1.4 | 1.4 | 1.4 | 1 | 0 |
| Compression Twin | 315 | 0 | 0 | 0 | 0 | 1 | 1 | 0 | 1 |

"composite grain" variant of the twin model reported values of ratios corresponding to prismatic: pyramidal: tensile twin to be 2.9: 5.2: 2.65.

The fit with the Voce hardening rule to the ED and ERD behaviors is satisfactory. The initial yields for the four loading orientations were all satisfactorily predicted. The hardening rate and overall response were satisfactorily captured for both ED and ERD. However, 30ED and 60ED behaviors were substantially mispredicted. 30ED prediction was the furthest from the test data since the simulated hardening rate in Regime II was of opposite sign to the measured one. It is clear that the current formulation of the Voce model does not incorporate yet a realistic understanding of twin-slip interaction. In fact, an only variation of the Schmid Factor for active deformation modes was sufficient to cause a substantial discrepancy in the prediction of anisotropy. This is atypical to the nature of the crystal plasticity framework. Therefore, it is imprudent to correlate hardening models based only on the two limiting cases of twinning contribution to deformation; intermediate contributions have to be tested as well.

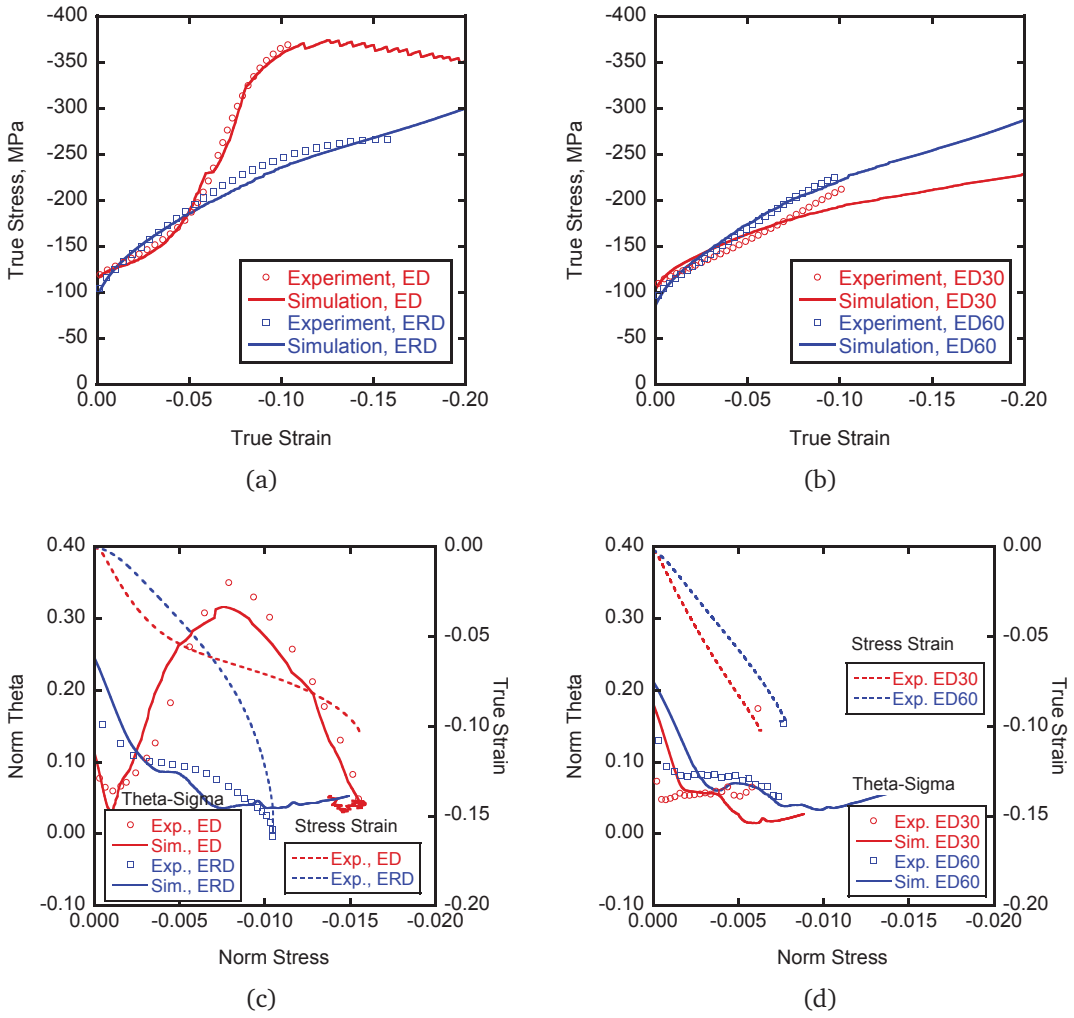


Figure 4.8 Voce hardening rule simulation results.

Stress- strain ((a) and( b)) and strain hardening rate versus stress curves ((c) and (d)) for simulations using VPSC with the Voce hardening rule. In the strain hardening rate versus stress plots, stress values were normalized by $\sigma_{\text{normalized}} = (\sigma - \sigma_y)/\mu$ where $\sigma_y$ is yield stress and $\mu$ is shear modulus.

### 4.5.2 Dislocation based model

Oppedal et al. [2010] used the dislocation based rule to model the behavior of pure Magnesium with $c$-axis fiber. The corresponding initial slip resistances were found to be scalable to the ones simulated for AM30 in this study, although with a $\langle 10\bar{1}0 \rangle$ ||

ED fiber. For each of basal, prismatic, and pyramidal modes, the values producing good correlations for AM30 were 23: 95: 111 MPa (or 1: 4.1: 4.8) compared to 11: 30: 50 MPa (or 1: 3: 4.5) for pure Magnesium. For tensile and compression twins in AM30, $\tau_{crit}$ and $\tau_{prop}$ were 67 and 25 MPa, and 275 and 275 MPa, respectively, compared to 15 and 10 MPa, and 185 and 185 MPa, respectively for pure Magnesium. As a ratio to basal slip, tensile twinning had a higher initial resistance in AM30. i.e 2.91 than in pure Mg i.e., 1.4. This reflects the higher sensitivity to the alloying elements of twinning compared to slip.

In the case of the dislocation density model, reference must be made to the strain hardening rate versus stress plots. Figure 4.20 shows the result of varying the twin storage factor (TSF). It was not possible to correlate simultaneously ED and ERD stress strain behaviors unless a TSF of three was used. The effect of the TSF on the stress strain behavior is illustrated in figures 4.20 and 4.21. Not only under ED was the saturation stress substantially underestimated with TSF=1, but under ERD as well. This is due to nominal tensile twinning under ERD not possible to prohibit under any other loading. This is in variance to the in the *c*-axis fiber where compression along the fiber completely prohibits tensile twinning.

In contrast to the Voce model, the dislocation density based model with the TSF was able to reproduce the mechanical responses under 30ED and 60ED when the fit was done based on ED and ERD behaviors. The robustness of this model is offered by the TSF strategy that hypothesized that the twin hardens more importantly than parent. This hypothesis is of striking consistency with the progressive decrease in the severity

Table 4.4 Dislocation density hardening rule parameters for slip

| | Prismatic ($\alpha = 1$) | Basal ($\alpha = 2$) | Pyramidal ($\alpha = 3$) |
|---|---|---|---|
| $k_1$ $1/m$ | 1.00E+09 | 0.60E+09 | 2.00E+09 |
| $\dot{\epsilon}_0$ $s^{-1}$ | 1.00E+07 | 1.00E+07 | 1.00E+07 |
| $g^\alpha$ | 0.0035 | 0.0035 | 0.003 |
| $D_0^\alpha$ MPa | 3.40E+03 | 10.0E+03 | 0.08E+03 |
| $A^\alpha$ | 0 | 0 | 0 |
| $\tau_0^\alpha$ MPa | 95 | 23 | 111 |
| $\chi$ | 0.9 | 0.9 | 0.9 |
| $q$ | 0 | 0 | 0 |
| $HP^\alpha$ | 0 | 0 | 0 |
| $HP^{\alpha\beta}$ | 0 | 0 | 0 |

of the hardening slope when the loading direction is progressively being deviated from ED toward ERD, i.e., with the progressive decrease of twinning contribution to the overall deformation.

Figure 4.9 show comparisons of the VPSC model with the dislocation based hardening rule and experimental texture data for ED and ERD, respectively. A slight overestimation of texture spread around ED under ED loading is noted. This could be attributed to double twinning that affects tensile twinning which may sharpen more importantly the texture. Double twinning of tensile twinning was not considered in these simulations.

## 4.6 Deformation texture upon profuse twinning (ED)

Figures 4.10, 4.11, 4.12, and 4.13 show IPF maps, image quality (IQ) maps, neutron diffraction pole figures for four level of deformation: 3%, 5.8%, 9% and 12% (rupture), respectively. The general common feature between these IPF maps is the

Table 4.5 Dislocation hardening rule parameters for twinning

| Parameters / Modes | Tensile Twin ($\beta = 1$) | Compression Twin ($\beta = 2$) |
|---|---|---|
| $\tau_0^\beta$ MPa | $\tau_{crit} = 67$, $\tau_{prop} = 25$ | $\tau_{crit} = 275$, $\tau_{prop} = 275$ |
| HP | 0 | 0 |
| $C^{\beta 1}$ | 0 | 0 |
| $C^{\beta 2}$ | 0 | 0 |
| $C^{\beta 3}$ | 0 | 0 |
| Twin Storage Factor | 1, 3 | 1, 3 |

substantial growth of $\{10\bar{1}2\}\langle 10\bar{1}\bar{1}\rangle$ tensile twin with an exclusive predominance of a unique twin system in each grain. As twinning increases upon deformation, the rod-texture develops a strong basal pole until the entire texture is rotated to become a $c$-axis fiber.

At 3% plastic strain (Figure 4.10), the twin volume fraction has already reached approximately 33%. The twins are thin lamellae primarily affecting the parent grain with minimal invasion within recrystallized grains. Most of the lamellae in the parent grains have comparable thickness, in the range of 25 $\mu$m, which depends on the parent grain size. When affected by twins, a recrystallized grain of an average diameter of 30 $\mu$m develops a twin having 3 $\mu$m in thickness. All twins cross the entire grain unless the twin is fragmented into very thin platelets. There is an almost systemic transmission of the twin when the twin edge hits another parent grain Proust et al. [2007] otherwise the twin is stopped at the boundary of a recrystallized grain. A twin lamella curves from one edge to the other as a consequence of the initial misorientation spread within the parent grain. A typical number fraction per parent grain is 200 /mm$^2$ which is characteristic of a steady state growth within Regime I. However, any

possible Hall-Petch hardening due to twin boundaries would be the highest at this level of deformation, namely 3%, and should decrease thereupon. This is in marked contrast with the test data in regime II recording a continuous increase in the hardening rate till inflection at 7% true plastic strain.

At 5.8% of plastic strain (Figure 4.11), the average volume fraction of twins reached 72%, leaving the parent grains as very thin lamellae confined between large coalesced twins. As such, the sample deformation should be mostly accommodated by slip deformation of the twins. The recrystallized grains have undergone important twinning, but still represent the major untwinned portion of the material.

By 9% of plastic strain (Figure 4.12), the parent grains have practically entirely twinned, and the twinned regions form a continuous matrix, which is occasionally interrupted by fine untwinned recrystallized grains.

The IQ maps highlight an important point between the IPF maps of 3% and 5.8%. The polished sample surface after 5.8% plastic strain shows that the twins are swelling with respect to the parent, indicating that twinned regions are harder than the parent grains (Figure 4.11). As such, the twins have higher Confidence Index (CI) than the parent. This situation is reversed at 3% plastic strain. The parent is swelling with respect to the twin as a consequence of harder matrix of the parent than that of the twin. This phenomenon substantiates that dislocation transmutation discriminately induced a hardening increase in the twins.

At 12% of plastic deformation, the recrystallized grains are mostly twinned. The volume fraction of twins reached 98%, and the texture became mostly a *c*-axis fiber

texture. However, Figures 4.14 and 4.16 evidence that part of the deviation from the *c*-axis fiber texture is due to the $\{10\bar{1}1\}$–$\{10\bar{1}2\}$ double twinning. This double twinning was mainly identified by its typical 38° misorientation with respect to the $[2\bar{1}\bar{1}0]$ axis common to the twin and the matrix.

## 4.7 Discussion

Figures 4.18 and 4.19 indicate that the basal slip was substantial along all loading orientations. However, twinning contribution to accommodating strain predominates along ED and was of almost equal extent to basal along 30ED at 3% plastic strain (Figures 4.18a–4.19b). Along 60ED and ERD, at the income of basal slip, twinning contribution markedly decreased, but did not vanish (Figures 4.19c–4.19d). Actually, the twinning activity saturated at approximately 30% under ERD which is the most prohibitive loading orientation for twinning for the rod-texture. This explains the almost unavoidable but mitigating stress-strain curve inflection under all orientations. In the following section, we analyze the behavior along ED and ERD.

### 4.7.1 Behavior under the Extrusion Direction (ED)

From figures 4.18a–4.18b four subsequent regimes of deformation mode activities for compression along the ED direction could be distinguished. In the strain range below 3% plastic strain, basal slip activity is decreasing while twinning activity is increasing up to a maximum relative activity of approximately 65%. This stage corresponded to a deformation mostly accommodated by twinning before twin coalescence

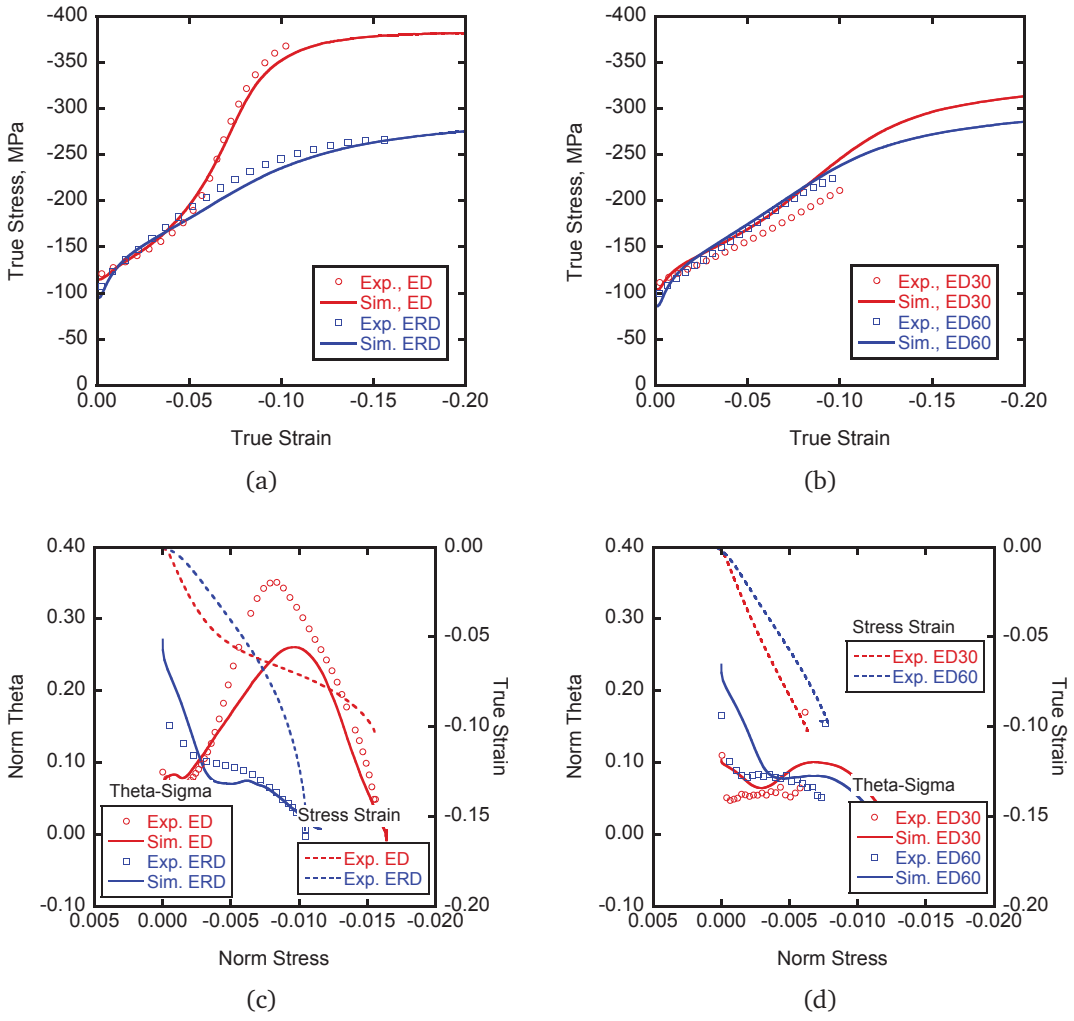


Figure 4.9 Dislocation based hardening rule simulation results.

Stress- strain curves of the (a) extrusion and extrusion radial direction and (b) 30 degrees and 60 degrees from the extrusion direction, and strain hardening rate versus stress curves for the (c) extrusion and extrusion radial direction and (d) 30 degrees and 60 degrees from the extrusion direction for simulations using the dislocation density hardening rule. The simulations used the parameters in Tables 4.4 and 4.5, with twin storage factor equal to 3. In the strain hardening rate versus stress plots, stress values were normalized by $\sigma_{\text{normalized}} = (\sigma - \sigma_y)/\mu$ where $\sigma_y$ is yield stress and $\mu$ is shear modulus.

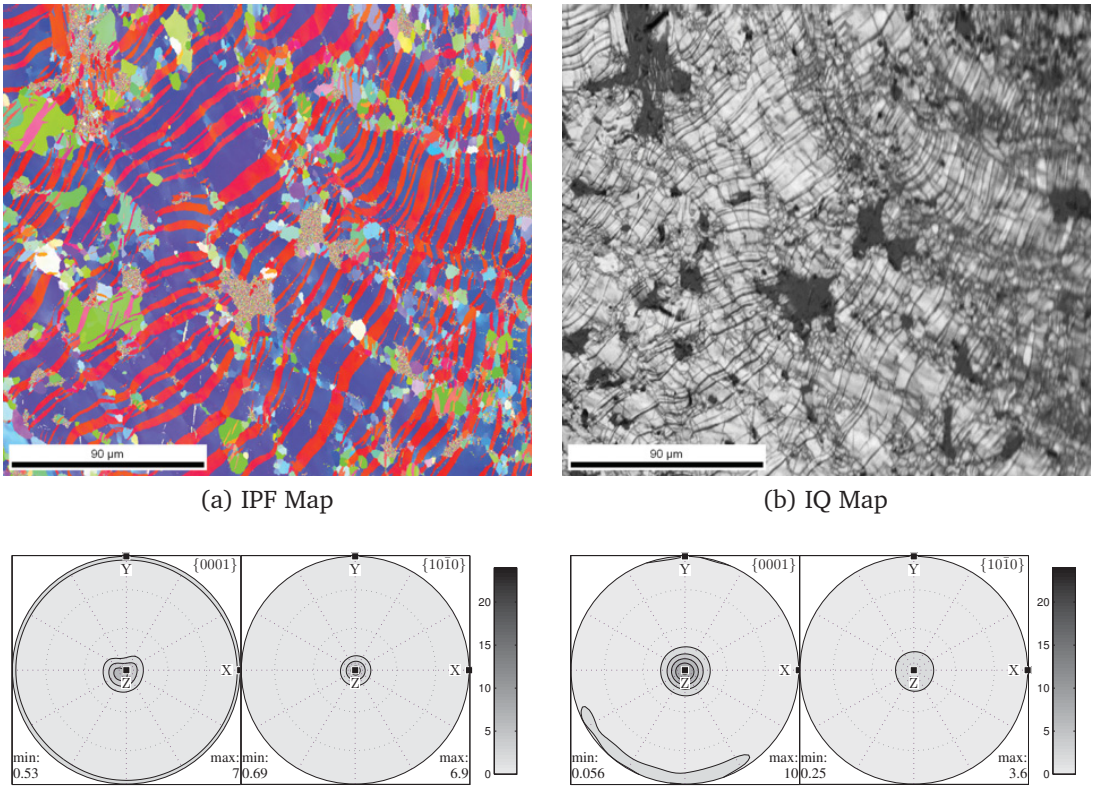


(a) IPF Map

(b) IQ Map

(c) Experiment

(d) Simulation

Figure 4.10 Texture analyses of sample compressed on extrusion direction 3.6%.

Texture analyses using x-ray (XRD) and Electron Backscatter Diffraction (EBSD) of a sample compressed to 3.6% plastic strain along the extrusion direction showing (a) an EBSD IPF map, (b) an EBSD image quality (IQ) map, and {0002} and {10$\bar{1}$0} pole figures obtained by (c) XRD, and (d) VPSC simulations using the dislocation model. Note the important amount of twin lamella affecting the parent grains (in blue), which results in an important ED || {0002} pole. The black regions in the IQ map correspond to non-indexed secondary phase particles.

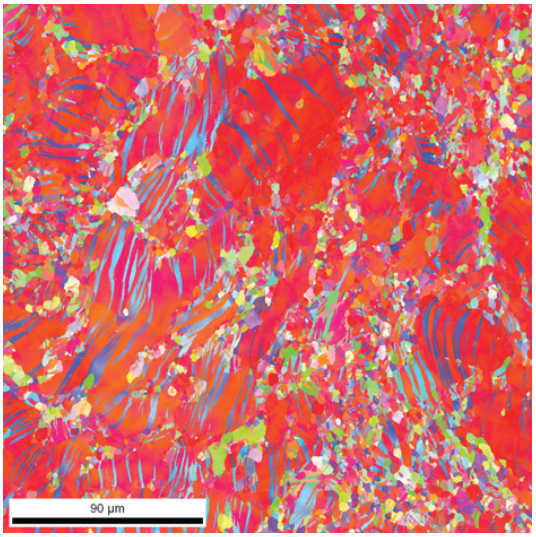


(a) IPF Map

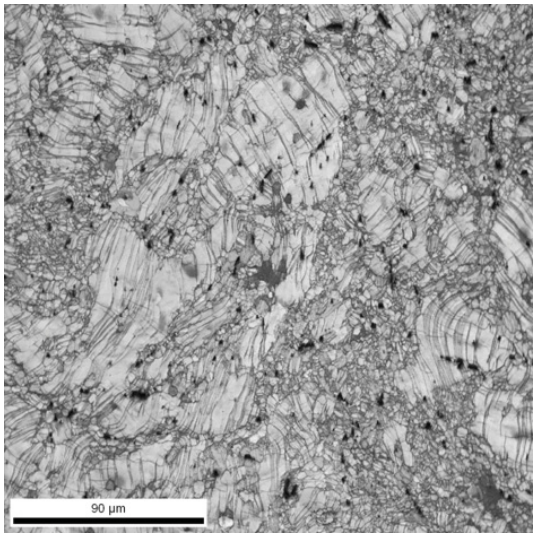


(b) IQ Map

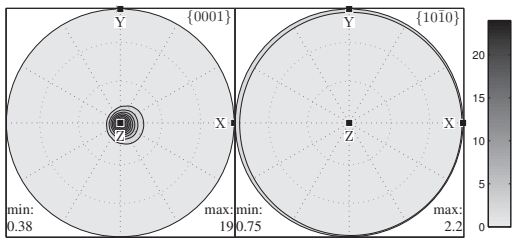


(c) Experiment

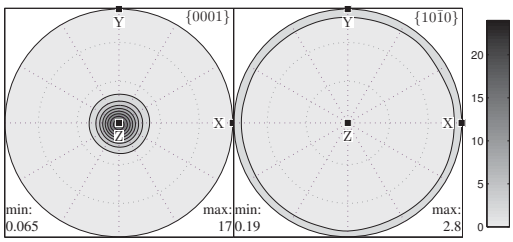


(d) Simulation

Figure 4.11 Texture analyses of sample compressed on extrusion direction 5.8%.

Texture analyses using x-ray (XRD) and Electron Backscatter Diffraction (EBSD) of a sample compressed to 5.8% plastic strain along the extrusion direction showing (a) an EBSD IPF map, (b) an EBSD image quality (IQ) map, and {0002} and {10$\bar{1}$0} pole figures obtained by (c) XRD, and (d) VPSC simulations using the dislocation model. Note that twinning has already started invading the recrystallized grains after invading most of each parent grain volume leaving only extremely fine parent platelets. The ED || {0002} pole has become substantially sharper.

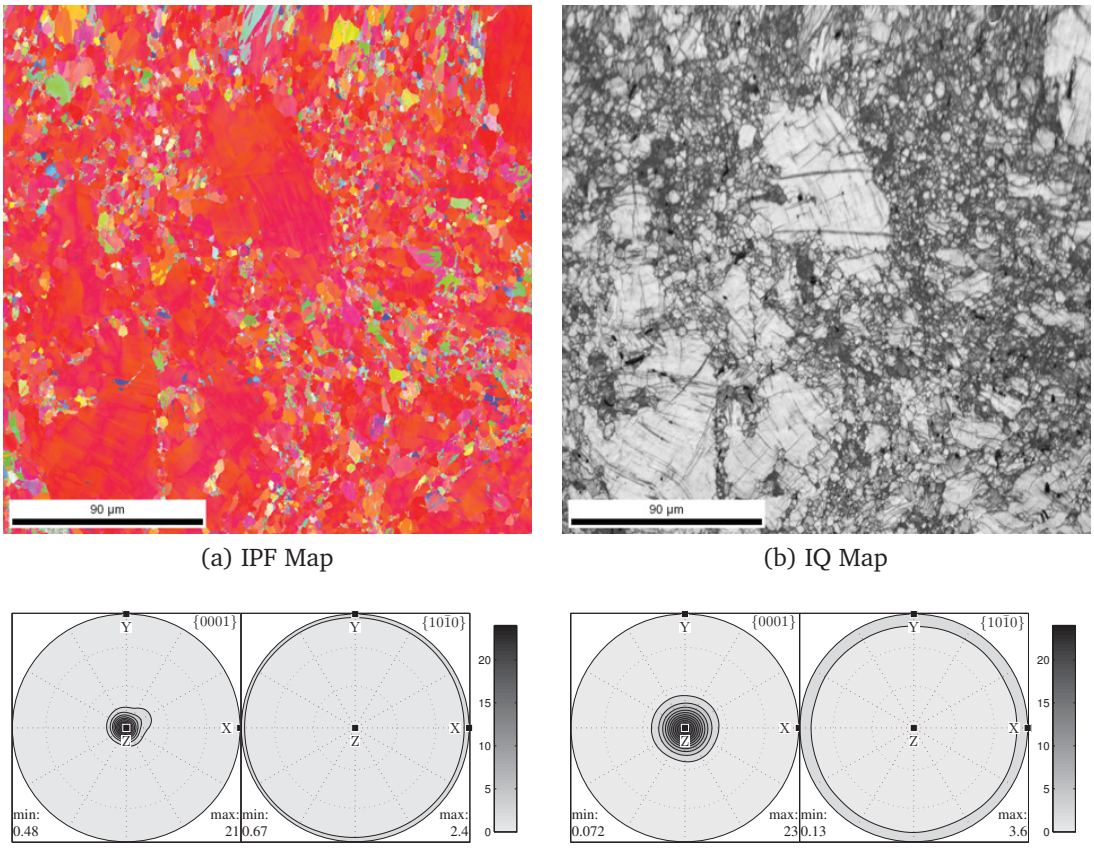


(a) IPF Map

(b) IQ Map

(c) Experiment

(d) Simulation

Figure 4.12 Texture analyses of sample compressed on extrusion direction 8.8%.

Texture analyses using x-ray (XRD) and Electron Backscatter Diffraction (EBSD) of a sample compressed to 8.8% plastic strain along the extrusion direction showing (a) an EBSD IPF map, (b) an EBSD image quality (IQ) map, and {0002} and {10$\bar{1}$0} pole figures obtained by (c) XRD, and (d) VPSC simulations using the dislocation model. Note that twinning has consumed the entire parent structure and most of recrystallized grains. The ED || {0002} pole has become substantially sharper, but other weaker started to develop as a result of compression twins affecting the tensile twins.

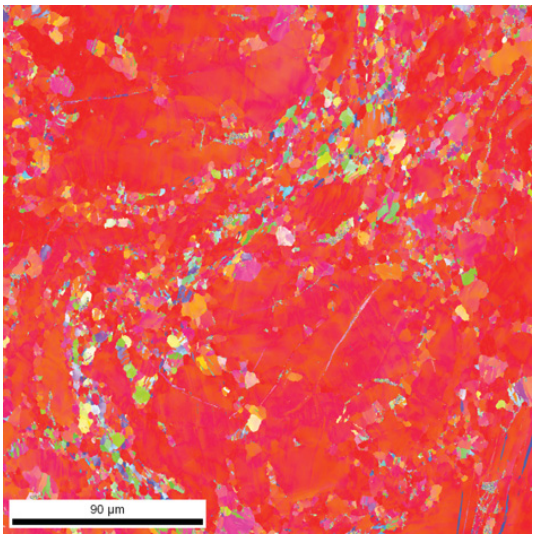


(a) IPF Map

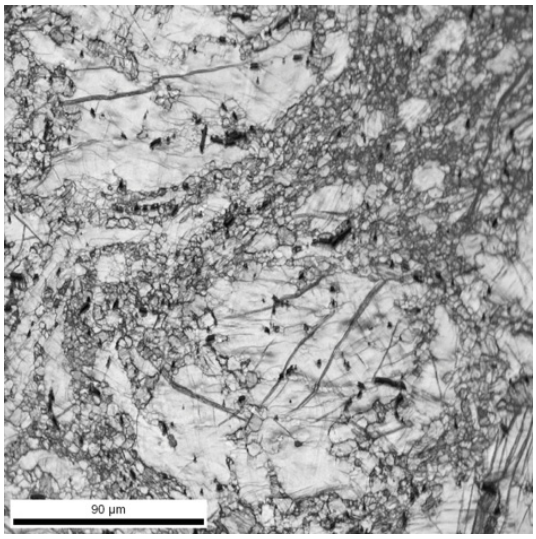


(b) IQ Map

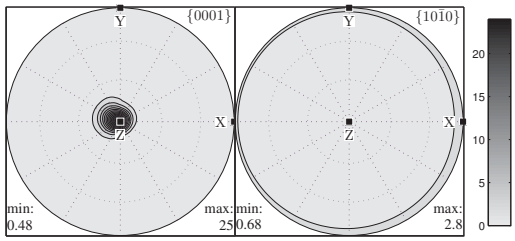


(c) Experiment

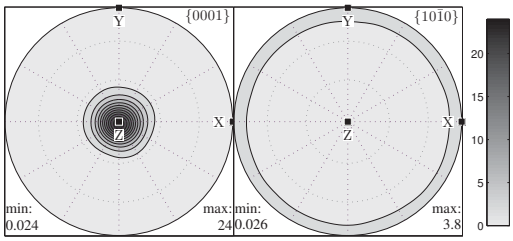


(d) Simulation

Figure 4.13 Texture analyses of sample compressed on extrusion direction 12%.

Texture analyses using x-ray (XRD) and Electron Backscatter Diffraction (EBSD) of a sample compressed to 12% plastic strain along the extrusion direction showing (a) an EBSD IPF map, (b) an EBSD image quality (IQ) map, and {0002} and {10$\bar{1}$0} pole figures obtained by (c) XRD, and (d) VPSC simulations using the dislocation model. Note that twinning has consumed the entire parent structure and nearly all of the recrystallized grains. Nearly all grains reoriented toward the ED || {0002} become except of a more growing compression twins that accelerated the fracture of the sample.

began [Jiang et al., 2007, Proust et al., 2009].The rapid onset of lengthwise thickening of the twins nearly led to a plateau characteristic of Regime I. In the plastic strain range between 3% and 7%, the activity of extension twinning markedly decreased. This corresponds to a mixed stage of twin growth and coalescence where the twinned lamellae grew larger than their relative aspect ratio and merged into each other. The matrix is mostly twinned. Therefore, at least the upper-half of Regime II should be characterized by slip dominance within the twins. This can be verified by the dominance of slip over twinning, which started well before 6% plastic strain.

With slip predominant, Regime II exhibits a substantial and peculiar increase in the hardening rate. When the strain exceeded approximately 7.5%, slip activity exhibits the usual decrease in the hardening rate. The transition was marked by a remarkable inflection into Regime III. A sudden rupture occurred at 12% plastic strain correlated to sudden profuse nucleation of double twinning in tensile twinned matrix (Figure 4.13).

EBSD analyses revealed that both parent and recrystallized grains exhibited segmentation by twinning. This grain refinement seems to peak at 3.5% plastic strain. At higher strains, twin lamella quickly began to coalesce. At approximately 6% plastic strain, the matrix was nearly entirely twinned as shown in Figure 4.11. The highest grain refinement by twinning at lower strains is inconsistent with a possible Hall-Petch effect on hardening in Regime II. Regime II expanded beyond 6% plastic strain, which was beyond twin coalescence regime. This phenomenon questions also the validity of the classical latent hardening approach [Tomé et al., 2001] of twinning on slip used

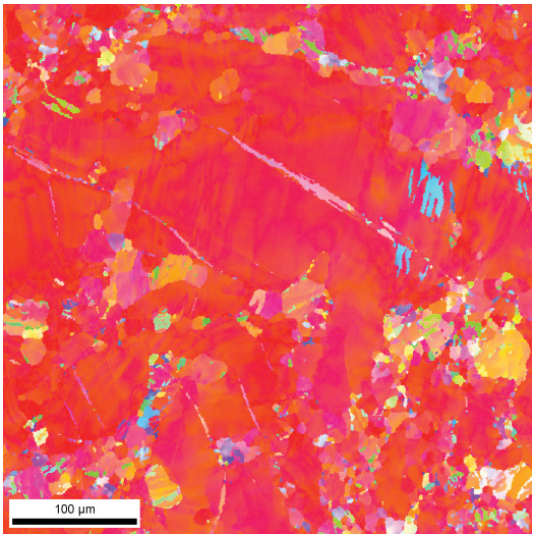


(a) IPF Map

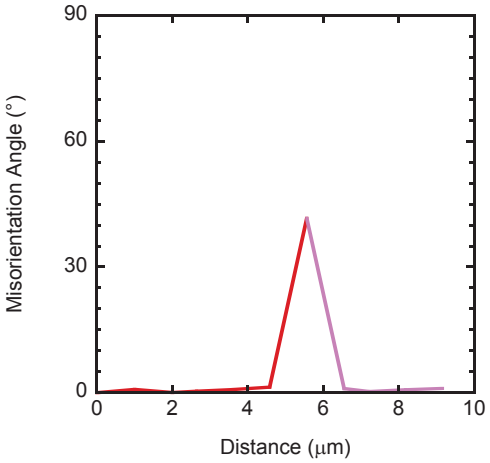


(b) Misorientation Plot

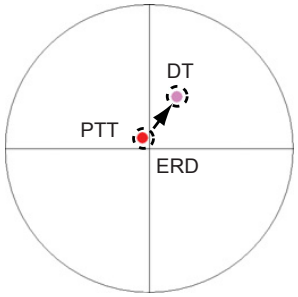


(c) {0001}

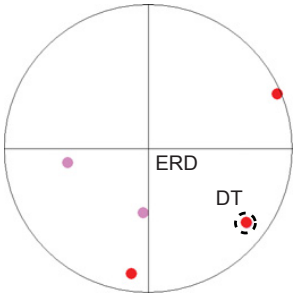


(d) $\{1\bar{2}10\}$

Figure 4.14 Texture analyses of sample compressed on extrusion direction 12%.

Texture analyses using Electron Backscatter Diffraction (EBSD) of an Extrusion Direction (ED) sample deformed to 12% plastic strain revealing double twinning $\{10\bar{1}1\}$–$\{10\bar{1}2\}$ (DT) (a) affecting the primary $\{10\bar{1}2\}$ extension twins (PTT). The colors used here correspond to the colors of the IPF map in Figure 4.11a. The occurrence of this double twinning is confirmed (b) by the common $\{1\bar{2}10\}$ misorientation axis, and (c) by the peak misorientation that is approximately 38°.

in hardening models implemented within the VPSC code, not just the Voce hardening model.

### 4.7.2 Behavior in the Extrusion Radial Direction (ERD)

Under compression along the ERD, basal slip is largely responsible for plastic deformation (up to 67% relative activity at 2% strain) until material rupture took place. However, the relative activity of extension twinning was substantial (up to 23% at 2% strain) and reached over third of that recorded along the ED under the same strain.

The IPF map in Figure 4.15 reveals that the extension twins are actually mostly stopped elastic twins. Residual twins occurred rarely from edge to edge in ERD, while under ED we scarcely observed stopped elastic twins. The lenticular shape and a wedged tip totally embedded within the parent matrix are the main characteristics of a stopped elastic twin. Stopped elastic twinning occurs when the shape change by the twin is accommodated in the matrix before the first twinning dislocations reach the grain boundary, that is, during the lengthwise thickening stage. The twin accommodation is then achieved by slip and not by any type of dislocation-free kinking. Elastic strain could not have accommodated the twin shear either, because the twin would have disappeared upon stress removal, which was not the case here.

The formation of stopped elastic twins in the ERD but not in the ED in grains although having a similar Schmid Factor to that under ED suggests an effect of grain morphology. The stress state for a load acting normal to the elongated grain boundary in the ERD was to induce easier/earlier nucleation of lattice slip dislocations. This would increase the extent of twin-slip interactions during the lengthwise thickening of a twin. The same effect could be promoted by slip dislocations that cross-slipped from

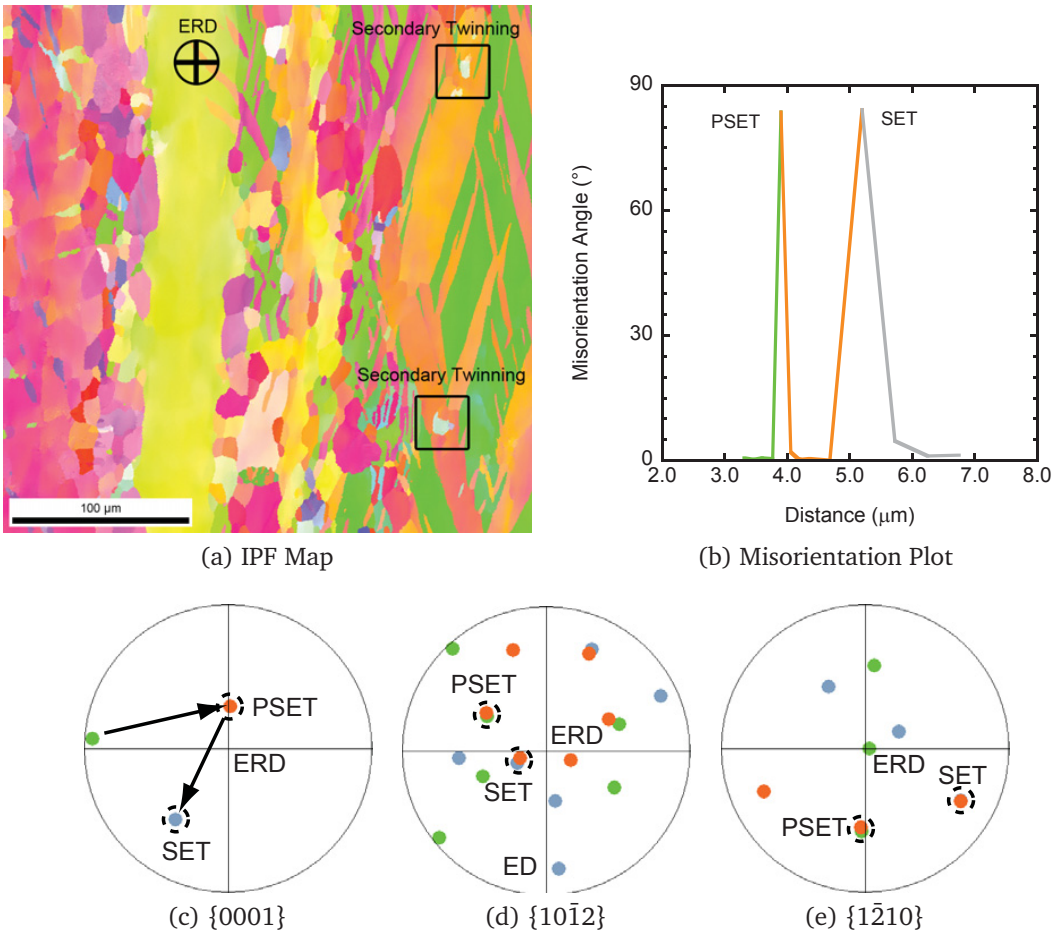


(a) IPF Map

(b) Misorientation Plot

(c) {0001}

(d) $\{10\bar{1}2\}$

(e) $\{1\bar{2}10\}$

Figure 4.15 Texture analyses of sample compressed on extrusion radial direction 5.8%.

EBSD analyses on ERD sample deformed up to 5.8% plastic strain showing (a) an IPF map exhibiting a complex network of multivariant primary "stopped" elastic twins (PSET) neighboring other grains that accommodated strain mostly by slip. The stopped elastic twins induced secondary extension twins in the primary extension twins (SET) at their intersection vertices of the intersecting twins. This twinning sequence is proven by (c - e) the common $\{1\bar{2}10\}$ axis, the common $\{10\bar{1}2\}$ $K_1$ plane, and (b) the characteristic misorientation (87°).

neighboring grains deforming mostly by slip, which is a characteristic misorientation situation encountered in a rod-texture loaded in the ERD.

In either case, the twinning dislocations ahead of the lengthening twin would interact with the substantial lattice slip dislocations to cause a partial recombination of the twinning dislocations ahead of the tapering boundary. Recombination of twinning dislocations was in fact observed at the end of stopped elastic twins either at the edge of a single crystal or at the terminating grain boundary [Hull, 1961]. Here dislocation interactions occur before the twin reaches the other side of the grain boundary.

This situation is similar to that of the emissary dislocation mechanism suggested by Sleeswyk [1962b]. Emissary dislocations, however, form as a homogeneous dissociation in every third twinning disconnection, so they are energetically unfavored. Furthermore, the dissociation suggested by Sleeswyk is appropriate for Body Centered Cubic (BCC) structures where the twin composition plane is an actual slip plane of the structure. That is, the emissary dislocations move away from the twin along $K_1$ to the parent lattice. However, it is interesting to see that a recombination of twinning dislocations whether promoted or not by other slip dislocations could result in a zero net Burgers vector of the twin boundary even if the parent structure is converted into the twin structure. Activation of dislocation sources within the grain ahead of the lengthening tapering boundary of the twin is unlikely here, since the same effect would have occurred in the ED.

Another phenomenon from the IPF map of Figure 4.15 is the systemic formation of multivariant twins not encountered in the ED. The onset of multivariant twinning could have expanded to 6% plastic strain as observed in the load drops in hardening-stress curve of Figure 4.6b. The most common multivariant twinning identified by

EBSD corresponded to 7° misorientation relationship between the two twin variants, and these twins were again mostly stopped elastic twins. The multivariant twinning in the ERD not exhibited in the ED although in grains with similar Schmid factor could also be explained by the normal stresses acting in the elongated grains. In fact, as tacitly implied by the schematic of Abbaschian and Reed-Hill [1991] for necessary accommodating kinks, a high number of surface tilts would be geometrically needed to accommodate strain in an elongated grain than in an equiaxed grain when the stress is acting normal to its main axis. This mandates a higher number fraction of twins and as such multivariant twinning.

An important outcome from the network of intersecting twins is the twin-twin interactions. Further growth of the incoming twin impinging another twin requires accommodation of the incident shear to propagate in the obstacle twin. Generally, it was observed that only a fraction of the incident shear could be transmitted to the obstacle twin so propagation of the incident twin is rendered difficult [Rémy, 1981]. An important conclusion by Mahajan and Chin [1973b] is that the accommodation of the incident shear by slip in the obstacle twin is much more unlikely to occur than secondary twinning. This is consistent with the occurrence of secondary twinning highlighted in the IPF maps of Figure 4.13; only impinging twins with secondary twins at the intersection vertices could noticeably grow by edgewise thickening.

Therefore, the limited growth of twins in the ERD was due to a combined effect of twin-twin interactions and multivariant twinning leading to stopped elastic twins. These mechanisms are beyond the capabilities of the twinning model in the VPSC using

a Voce type law. As such, there was a systemic overestimation of twin activity in the ERD.

This overestimation of twinning activity explains the absence of Regime II in the experimental ERD stress-strain behavior, which underlies a non-Schmid effect of twinning. This could be rationalized by a dislocation transmutation effect on Regime II put forward by El Kadiri and Oppedal [2010]. The limited extent of twin growth would dramatically mitigate transmutation of parent dislocations upon their incorporation in the twins, since the twin boundaries can only sweep a limited volume of the parent. As such, a competition takes place between hardening by transmutation-induced latent hardening and softening due to stoppage of twins. That is, the ERD stress-strain behavior is not purely parabolic but shows a tendency of adopting a linear trend with load drops due to the onset of multivariant twinning before a regime of slip predominance that could take place. The overestimation of twinning caused a substantial misprediction of the ERD hardening-stress curve. As such, although the stress-strain curve seems to be well predicted, none of the stages along ERD were satisfactorily predicted in the rate form.

According to the Hall-Petch effect, the network of multivariant stopped elastic twins should have greatly contributed to induce a Regime II hardening rate in the ERD with probably a similar magnitude as that in the ED. In fact, segmentation in the ERD was finer since growth was limited when compared to that recorded in the ED, and the opposite would be expected if the Hall-Petch effect were in operation. This would induce the twin boundaries to act as more effective barriers thus increasing the ERD

hardening rate. However, there was no type of Regime II in the ERD, and as such a Hall-Petch effect cannot operate by twin segmentation unless the twin boundaries lose coherency with the matrix.

The competition between extension twinning and their impediment by twin-twin interaction and stopped elastic twinning is consistent with the kink observed in the ERD hardening-stress curve at 2.5%. This kink is more marked in the 60ED hardening-stress curve.

The appearance of stopped elastic twins, their limited growth, and their induced twin-twin interaction could explain the overlapping of the stress-strain curves when the loading orientation deviates from ED toward ERD. The stopped elastic twins could also explain the non-monotonic mitigation of the inflection point which is more striking between ED and 30ED.

Figure 4.16 reveals profuse $\{10\bar{1}1\}$–$\{10\bar{1}2\}$ double twinning. It is important to note that double twinning occurred at a considerably lower stress in the ERD than in the ED, which indicates a non-Schmid effect correlated to double twinning. This observation reveals the sensitivity of double twinning to the type and structure of prior dislocations. This is not accounted for in the present formulation of the hardening law in the VPSC code.

If the double twinning affects the elastic stopped twins, then Regime II hardening would be reduced according to the mechanism of preferential latent hardening in the twin by dislocation transmutation. In fact, the $\{10\bar{1}1\}$ contraction twins, a component

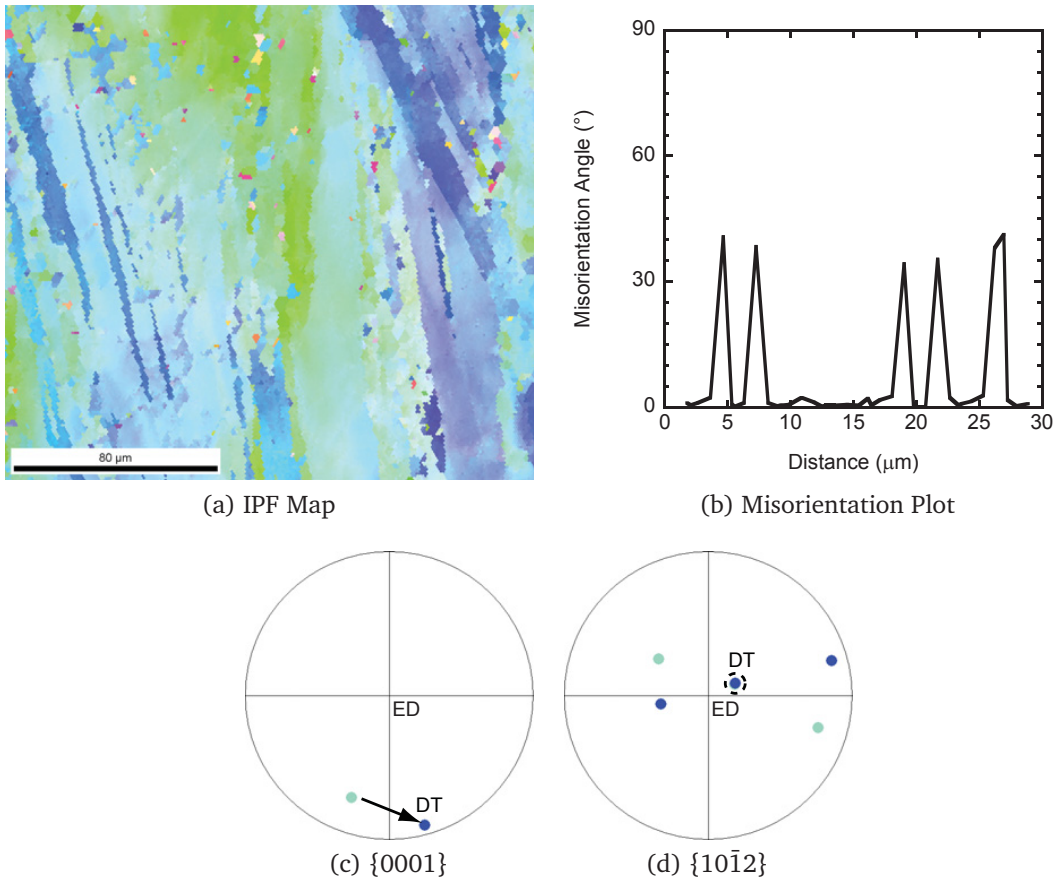


(a) IPF Map

(b) Misorientation Plot

(c) {0001}

(d) {10$\bar{1}$2}

Figure 4.16 Texture analyses of sample compressed on extrusion radial direction 12%.

EBSD analyses on an ERD sample deformed up to 12% plastic strain showing (a) an IPF map exhibiting profuse {10$\bar{1}$1}–{10$\bar{1}$2} double twinning (DT). The double twinning sequence is identified by (b) the characteristic misorientation (38°) around (c) the common {1$\bar{2}$10} axis. The rotation of the *c*-axis by double twinning is shown in the {0001} pole figure of (c).

of the double twins, are known to have significantly smaller growth rates compared to extension twins due to their relatively high characteristic shear [Yoo, 1981].

### 4.7.3 Link to Continuum level modeling

Figure 4.22 shows the yield surface shape changes as the deformation proceeded for the extrusion (Figure 4.22a) and extrusion radial (Figure 4.22b) directions. One can note that the yield surface center shifted indicating some kinematic hardening and an expected Bauschinger effect up to approximately 10% strain, when the stress saturated. One can also note the expansion of the yield surface as the deformation proceeded indicating isotropic hardening up to that point. Finally, one could also note that the shape changed as a function of deformation indicating that the deformation-induced anisotropy from texture changed as well up to 10% strain. If one were to correlate the dislocation and slip activity from Figure 4.18 and4.19 with these yield surfaces in Figure 4.22 can assert that the tensile twinning activity affected the anisotropy from texture and kinematic hardening up 10% strain and the isotropic hardening up that stain level for that matter. After 10% strain, slight isotropic hardening appeared to occur.

## 4.8 Conclusions

The simulations are consistent with the idea of an increased hardening in the twin during profuse twinning caused by the dislocation transmutation idea put forward by El Kadiri and Oppedal [2010].

In the simulations using the dislocation density hardening model, it was not possible to achieve a good model correlation to the experimental data without using a twin storage factor of three. This also gave the desirable effect of correlating fairly

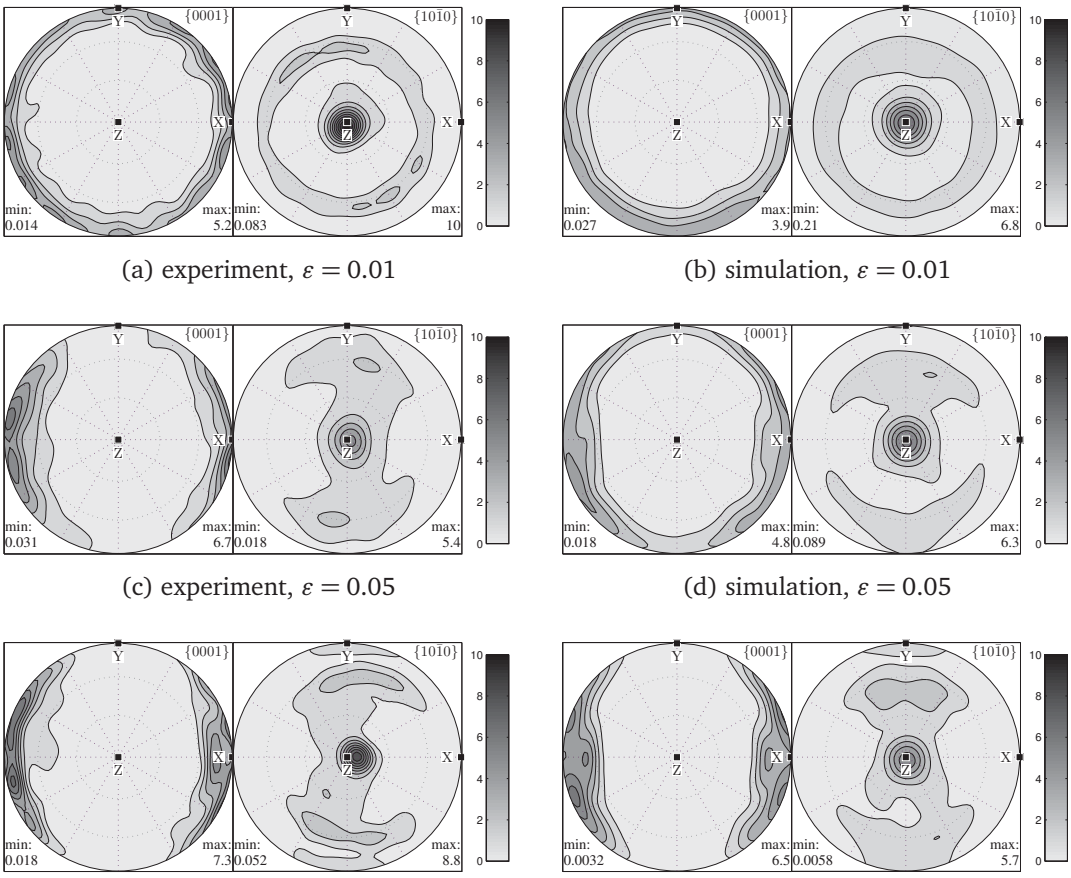


(a) experiment, $\varepsilon = 0.01$

(b) simulation, $\varepsilon = 0.01$

(c) experiment, $\varepsilon = 0.05$

(d) simulation, $\varepsilon = 0.05$

(e) experiment, $\varepsilon = 0.11$

(f) simulation, $\varepsilon = 0.11$

Figure 4.17 Pole figures from samples deformed on extrusion radial direction.

Comparison of {0001} and {10$\bar{1}$0} pole figures of texture obtained by neutron diffraction on samples deformed by uniaxial compression on the extrusion radial direction and predicted by simulations at strain levels of 1, 5, and 11% plastic strain. Z corresponds to extrusion direction; X and Y correspond to extrusion radial directions.

well the strain hardening rate versus stress behavior as well. With a twin storage factor of three, the simulations could reach the proper saturation stress levels that the experimental test data showed. The simulations also predicted well the experimentally observed stress-strain and texture behavior without utilizing a Hall-Petch type effect that has been attributed to the grain refinement by twinning. Also, the Hall Petch

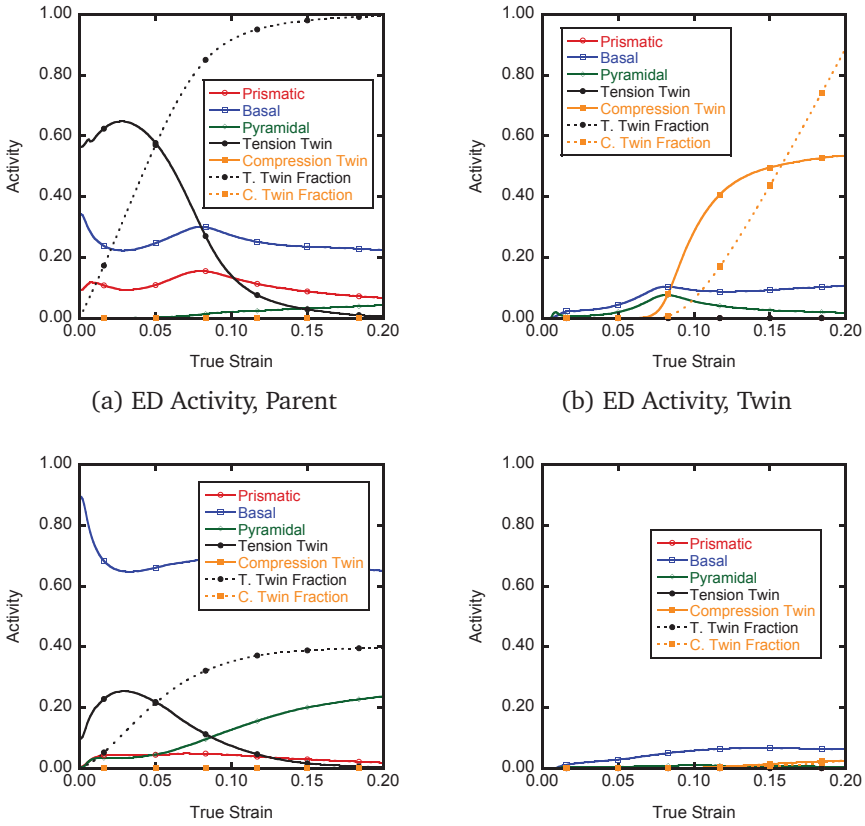


(a) ED Activity, Parent

(b) ED Activity, Twin

(c) ERD Activity, Parent

(d) ERD Activity, Twin

Figure 4.18 Relative activity of slip and twinning in ED and ERD simulations.

Simulation results for the VPSC model using the dislocation density hardening rule with the twin storage factor equal to three showing the relative activities of slip and twinning within the parent and the twin for (a-b) Extrusion Direction compression (ED) and (c-d) Extrusion Radial Direction (ERD), respectively.

effect for magnesium twin boundaries has been experimentally observed to be quite low [Cáceres et al., 2008].

The use of the VPSC simulations with the dislocation density based hardening rule allowed a coupling between slip, twinning, texture, and stress state behavior analysis that has not fully explained by the use of empirical latent hardening parameters such as used in the Voce hardening models. Furthermore, the quantification of the slip

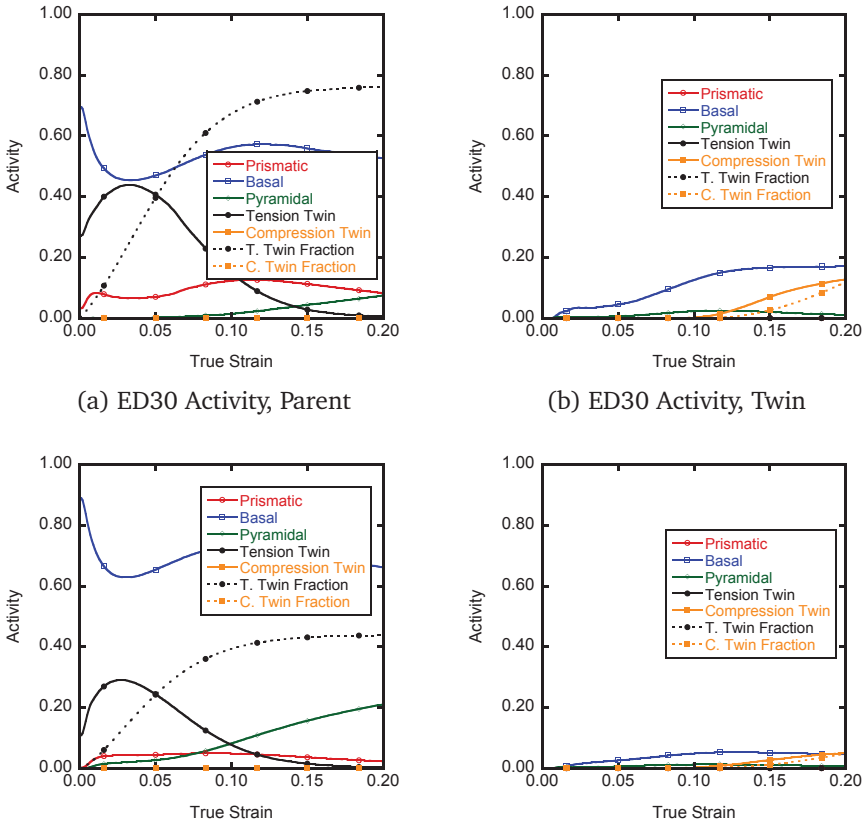


(a) ED30 Activity, Parent

(b) ED30 Activity, Twin

(c) ED60 Activity, Parent

(d) ED60Activity, Twin

Figure 4.19 Relative activity of slip and twinning in 30ED and 60ED simulations.

Simulation results for the VPSC model using the dislocation density hardening rule with the twin storage factor equal to three showing the relative activities of slip and twinning within the parent and the twin for (a-b) Extrusion Direction 30 degree (30ED),(c-d) Extrusion Direction 60 degree (60ED).

activity, twin activity, texture evolution, and hardening as a function of strain allows for macroscale internal state variable.

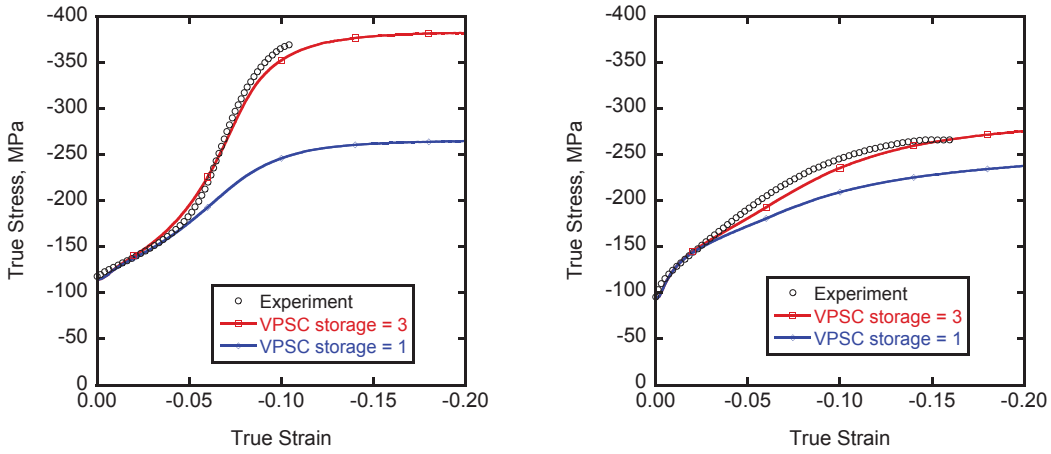


(a) ED (b) ERD

Figure 4.20 Effect of twin storage factor on stress versus strain.

Results of VPSC simulations using the dislocation density hardening rule and experimental results, true stress versus true strain for two different twin storage factors. The simulation and experimental results are from uniaxial compression in a) the Extrusion Direction (ED) and b) Extrusion Radial Direction (ERD). The twin storage parameter strongly affects twin hardening and is markedly apparent in (a).

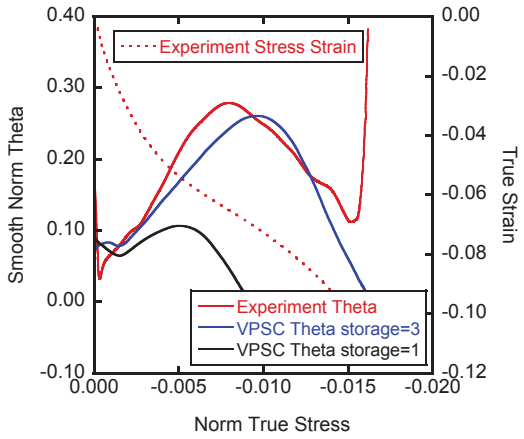


Figure 4.21 Effect of twin storage factor on strain hardening rate versus stress.

Results of VPSC simulations using dislocation density hardening rule and experimental results, plotting strain hardening rate versus stress, for two different values of twin storage factor. The storage factor equal to three provides results significantly closer to the experimentally observed results.

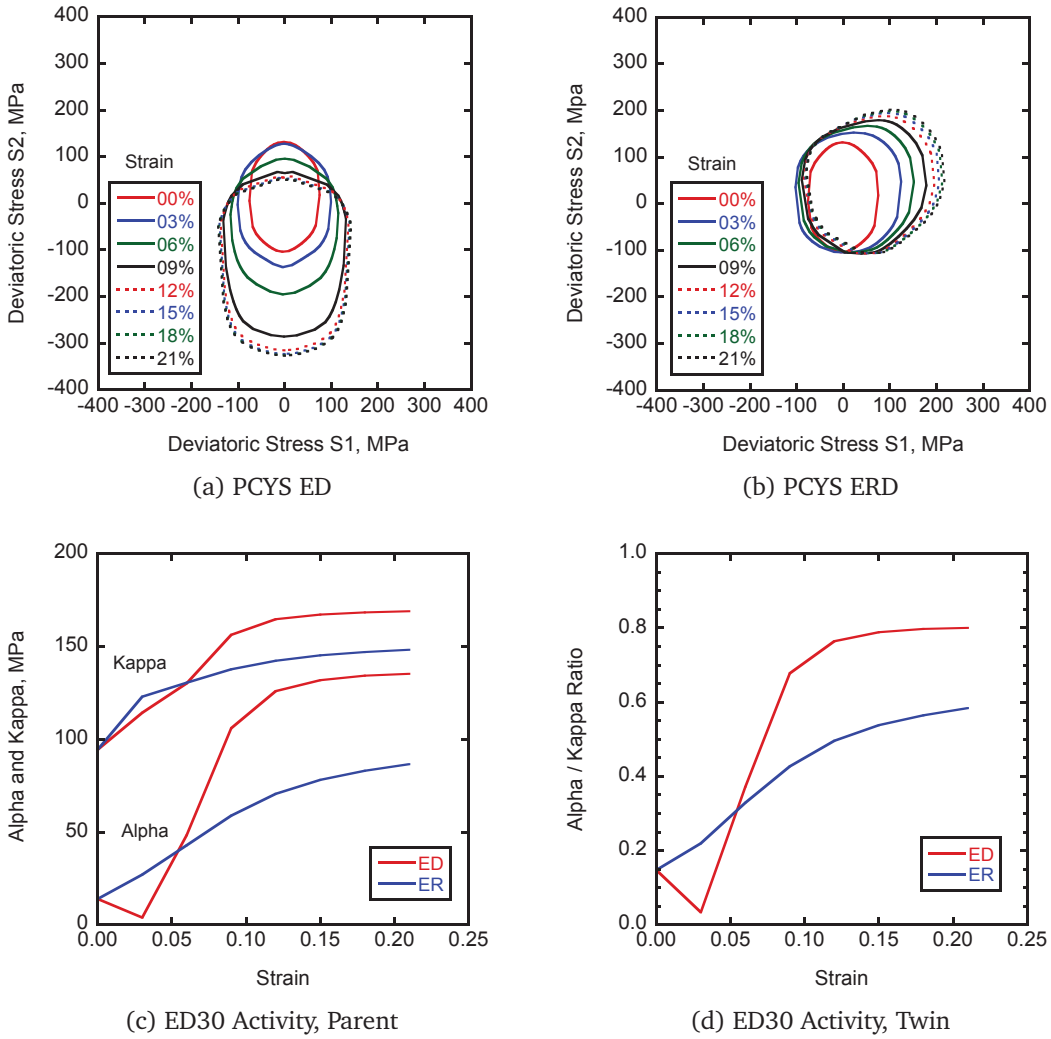


(a) PCYS ED

(b) PCYS ERD

(c) ED30 Activity, Parent

(d) ED30 Activity, Twin

Figure 4.22 Polycrystal yield surface.

Polycrystal yield surface evolution from VPSC simulations using the dislocation density hardening rule. The plot in (a) corresponds to the Extrusion Direction (ED) simulation, and (b) corresponds to the Extrusion Radial Direction (ERD).

CHAPTER 5

SUMMARY AND FUTURE WORK

## 5.1 Summary

A mesoscale crystal plasticity model was used and modified to simultaneously predict, with the same parameters, the mechanical behavior, twin volume fraction evolution and texture evolution in basal textured pure Magnesium and rod textured AM30 Magnesium alloy loaded in multiple load paths to induce profuse twinning. The simulation results are consistent with experimentally observed behavior. Modifications to the model included consideration of a mechanism to date that was neglected in other mesoscale simulations, that of dislocation transmutation, which was caused by the shearing action of the twin boundary as it grows, on the population of dislocations in a parent grain.

Broad discussion of the development of this idea as theory and its mechanism was developed in Chapter II. Fundamental, theoretical research in twinning as early as the 1950's and 1960's described the shearing action on dislocations and the effect upon dislocations in the parent grain as a twin boundary incorporated them into the twin. Recent work has shown experimental evidence of this in FCC crystals, and speculation of the mechanism in HCP crystals, but no researchers incorporated this notion into numerical simulations. The concept of source of dislocations caused by the

plastic accommodation of the twin as it grows in the matrix has also been observed and discussed in the literature but has not been incorporated into simulations. The importance of the twin accommodation effect, and source of dislocations from it, is that during deformation by profuse twinning, the conventional wisdom is that it occurs in the twinning process without evolution of dislocations such as caused by plastic slip deformation. These dislocations caused by the accommodation effect can later be incorporated by the twin as the twin grows thus contributing to the hardening response.

Table 5.1 Summary of testing for pure magnesium

| Loading | Type of Experiment | Purpose |
|---|---|---|
| IP and TT compression | Stress-Strain | Calibration |
| IP and TT compression | Texture | Validation |
| IP compression | Twin volume fraction | Validation |

In Chapter III, observations of the mechanical behavior, twin evolution and texture evolution were made on basal textured, pure magnesium along with numerical simulations that used an empirical factor, the Twin Storage Factor, to incorporate the effect of dislocation transformations. In simulations that used a factor equal to one, i.e. the twin is same as the parent, it was observed that the saturation stress levels of loading that induced and did not induce profuse twinning were nearly identical, contradictory to the experimentally observed behavior. With twin storage factors equal to two and three, the mechanical stress-strain behavior, strain hardening rate versus stress curve, texture evolution, and twin volume fraction evolution in numerical simulations were all

predicted accurately compared to the experimentally observed behavior. Observations made using EBSD confirmed the existence of multivariant and multi-fold twinning that have not been incorporated into numerical simulations.

Table 5.2 Summary of testing for AM30 magnesium

| Loading | Type of Experiment | Purpose |
|---|---|---|
| ED and ERD compression | Stress-Strain | Calibration |
| ED30 and ED60 compression | Stress-Strain | Validation |
| ED, ERD, ED30 and ED60 compression | Texture | Validation |

In Chapter IV, a rod textured AM30 Magnesium alloy was examined. Conventionally, polycrystal studies of HCP materials that undergo loading induced twinning are studied in orthogonal loading configurations that maximize twinning or minimize twinning behavior. Simulations and experimental observations of material at intermediate texture configurations reveal limitations of a twinning induced hardening response. Using the dislocation transformation ideas allowed a contrast of the different twin hardening strategies.

## 5.2 Future Work

As materials such as magnesium are widely adopted in industrial use, their anisotropic mechanical behavior, stemming from their HCP structure and twinning, must be better understood and amenable to higher fidelity material models. In mesoscale simulations of twinning to date, the effect of twinning on the strain harden-

ing response has been modeled via crystallographic reorientation, a Hall-Petch effect caused by grain segmentation, and slip-twin interactions described by latent hardening effects. The effect of dislocation transmutation by the twin boundary described in this work opens new avenues of understanding and research.

### 5.2.1 Electron Backscatter Diffraction (EBSD) analysis of AM30 Magnesium

Mechanical testing and macrotexture and some microstructure analysis was conducted on the AM30 Magnesium samples, along with numerical simulation results. However,a complete EBSD and microtexture analysis was not accomplished in this work, and could reveal mechanisms of deformation. Particular interest is in the intermediate texture samples, and analysis of the multifold and multivariant twinning processes, and twin accommodation effects.

### 5.2.2 Modification to the code to numerically simulate the direct effect of dislocation transmutation and plastic accommodation

In this work we used an empirical "twin storage factor" in the dislocation density evolution equations to model the effect of dislocation transmutation and their latent hardening effect on textured materials loaded to induce profuse twinning. The results are consistent with observed behavior and experiments, but it would be desirable to directly numerically simulate the actual transmutation of dislocations into specific families of new dislocations and their interaction via latent hardening effects. This can be accomplished in modifications to the VPSC code. However, experimental work via

Transmission Electron Microscopy and Molecular Dynamics simulations would reveal the specific transmutation sequences.

### 5.2.3 Direct TEM observations of dislocation population in the twin and parent matrix

What has been presented in this work is theory of the mechanisms, numerical simulations, and meso/macroscale experimental work that is all consistent with explaining the strain hardening behavior of magnesium and HCP metals that deform by profuse twinning. Using TEM observations, it should be possible to directly characterize dislocation substructures in the parent and twin portion of the grain, and this should conclusively prove the theory of the transmutation of dislocations. For FCC metals, work of this kind has been completed [Basinski et al., 1997] and shown to be true. In HCP metals, this has not been conducted but has been predicted theoretically.

### 5.2.4 Molecular Dynamics (MD) Simulations of Twinning

Extensive MD simulations of twinning in magnesium, focusing on twin nucleation and growth, have been conducted [Serra and Bacon, 1996, Wang et al., 2009]. Simulations of twin growth mechanisms are better understood than the actual nucleation mechanism. However, the effect of the twin boundary on dislocations as it shears the population of dislocations in a parent matrix has not been investigated. If this could be done, it would conclusively prove the effect of dislocation transmutation.

### 5.2.5 Strain Path Change experiments

In this study, the focus has been on monotonic testing of materials. The modifications of the code and numerical simulations have been consistent with the experimental evidence. Strain path change experiments, where the material is loaded in one direction, and then loaded in another direction, would be a demanding test of the numerical simulations. Experiments for these have been conducted and await analysis of the results of simulations. The existing code, however, would be challenged to reproduce this well, due to their relatively simplistic modeling of twinning. In addition to the effect of dislocation transmutation described in this work, the code should be modified be account for the effect of dislocation sources by plastic accommodation of the twin, the effect of multiple twin variants instead of requiring that the predominant twin system only being allowed to grow, and the effect of multifold twinning, i.e. a twin that can itself twin one or more times. The effect of twin variants has been described experimentally in the literature recently, and multifold twinning as well, although mainly as a prescribed established sequence as double twinning. Modifications to the code to allow this should be relatively straightforward and fruitful investigative endeavors.

### 5.2.6 Modification to track populations of individual slip systems

Currently, a dislocation model keeps track of a family of slip mode dislocations, e.g. basal dislocations. However, this is limiting and is not representative of the actual material. It is relatively straightforward to keep track of specific slip systems, e.g. the

$(0001)\frac{1}{3}[10-10]$ basal slip system. This would allow one to more faithfully model the path dependent activity such as strain path change simulations as well as the kinematic hardening (Bauschinger effect).

### 5.2.7 Temperature and strain rate dependent investigations

The work presented here has focused on room temperature and quasi-static strain rate testing. The dislocation density model by Beyerlein and Tomé [2008] includes temperature and strain rate dependent features that have not been tested. A relatively straightforward series of tests conducted at different temperatures and strain rates could be done to demonstrate this and is in fact being investigated in the very near future at CAVS, including work at high strain rates on Hopkinson bars.

### 5.2.8 Continuum level modeling efforts

This work has focused on mesoscale modeling but has the capability to provide useful information to continuum level modeling efforts such as yield surface evolution and the effects of twinning on the structure-property relations. The investigation of AZ31 Magnesium in sheet forming modeling and AM30 / AZ61 Magnesium in extrusion process modeling will be should be augmented by characterization of a temperature and strain rate dependent yield surface evolution. From the yield surface evolution, estimates of isotropic / anisotropic and kinematic hardening evolution can be estimated.

# REFERENCES


Abbaschian, R. and R. E. Reed-Hill (1991). *Physical Metallurgy Principles* (3rd ed.). PWS Publishing Company.

Agnew, S. R. and Ö. Duygulu (2005). Plastic anisotropy and the role of non-basal slip in magnesium alloy AZ31B. *International Journal of Plasticity 21*(6), 1161–1193.

Agnew, S. R., M. H. Yoo, and C. N. Tomé (2001). Application of texture simulation to understanding mechanical behavior of Mg and solid solution alloys containing Li or Y. *Acta Materialia 49*(20), 4277–4289.

Armstrong, R. W. and G. T. Horne (1962–1963). Fatigue behaviour in shear of oriented magnesium single crystals. *Journal of the Institute of Metals 91*, 311–315.

Armstrong, R. W. and F. J. Zerilli (1999). Deformation twinning: From atomic modeling to shock wave loading. In S. Ankem and C. S. Pande (Eds.), *Advances in Twinning*, pp. 67–81. The Minerals, Metals & Materials Society.

Basinski, Z. S., M. S. Szczerba, M. Niewczas, J. D. Embury, and S. J. Basinski (1997). The transformation of slip dislocations during twinning of copper-aluminium alloy crystals. *Revue de Metallurgie - Cahiers d'informations Techniques 94*(9), 1037–1043.

Beyerlein, I. J. and C. N. Tomé (2008). A dislocation-based constitutive law for pure Zr including temperature effects. *International Journal of Plasticity 24*(5), 867–895.

Bhattacharyya, D., E. K. Cerreta, R. McCabe, M. Niewczas, G. T. Gray III, A. Misra, and C. N. Tomé (2009). Origin of dislocations within tensile and compressive twins in pure textured Zr. *Acta Materialia 57*(2), 305–315.

Bilby, B. A. and J. W. Christian (1956). *The mechanism of phase transformations in metals*. London: Institute of Metals.

Bunge, H. J. (1982). *Texture Analysis in Materials Science: Mathematical Methods*. Butterworths.

Cáceres, C. H., P. Lukáč, and A. Blake (2008). Strain hardening due to $\{10\bar{1}2\}$ twinning in pure magnesium. *Philosophical Magazine 88*(7), 991–1003.

Capolungo, L., I. J. Beyerlein, and C. N. Tomé (2009). Slip-assisted twin growth in hexagonal close-packed metals. *Scripta Materialia 60*(1), 32–35.

Christian, J. W. and S. Mahajan (1995). Deformation twinning. *Progress in Materials Science 39*(1-2), 1–157.

Clausen, B., C. N. Tomé, D. W. Brown, and S. R. Agnew (2008). Reorientation and stress relaxation due to twinning: Modeling and experimental characterization for Mg. *Acta Materialia 56*, 2456–2469.

El Kadiri, H. and A. L. Oppedal (2010). A crystal plasticity theory for latent hardening by glide twinning through dislocation transmutation and twin accommodation effects. *Journal of the Mechanics and Physics of Solids 58*(4), 613–624.

Eshelby, J. D. (1957). The determination of the elastic field of an ellipsoidal inclusion, and related problems. *Proceedings of the Royal Society of London. Series A, Mathematical and Physical Sciences 241*, 376–396.

Gilman, J. J. (1954). Mechanism of ortho kink-band formation in compressed zinc monocrystals. *Transactions of the Metallurgical Society of AIME 200*, 621– 629.

Hall, E. O. (1951). The deformation and ageing of mild steel: III discussion of results. *Proceedings of the Physics Society B 64*, 747–753.

Hielscher, R. and H. Schaeben (2008). A novel pole figure inversion method: specification of the MTEX algorithm. *Journal of Applied Crystallography 41*(6), 1024–1037.

Holden, J. (1952). Plastic deformation features on cleavage surfaces of metal crystals. *Philosophical Magazine (Series 7) 43*(344), 976–984.

Hull, D. (1961). The initiation of slip at the tip of a deformation twin in $\alpha$-iron. *Acta Metallurgica 9*(9), 909–912.

Jain, A. and S. R. Agnew (2007). Modeling the temperature dependent effect of twinning on the behavior of magnesium alloy AZ31B sheet. *Materials Science and Engineering A 462*(1-2), 29–36.

Jaswon, M. A. and D. B. Dove (1956). Twinning properties of lattice planes. *Acta Crystallographica 9*(8), 621–626.

Jaswon, M. A. and D. B. Dove (1957). The prediction of twinning modes in metal crystals. *Acta Crystallographica 10*(1), 14–18.

Jaswon, M. A. and D. B. Dove (1960). The crystallography of deformation twinning. *Acta Crystallographica 13*(3), 232–240.

Jiang, L., J. J. Jonas, A. A. Luo, A. K. Sachdev, and S. Godet (2007). Influence of $\{10\bar{1}2\}$ extension twinning on the flow behavior of AZ31 mg alloy. *Materials Science and Engineering A 445*, 302–309.

Kaibyshev, R. and O. Sitdikov (1994). Dynamic recrystallization of Magnesium at ambient temperature. *Zeitschrift für Metallkunde 85*(10), 738–743.

Kalidindi, S. R., A. A. Salem, and R. D. Doherty (2003). Role of deformation twinning on strain hardening in cubic and hexagonal polycrystalline metals. *Advanced Engineering Materials 5*(4), 229–232.

Karaman, I., H. Sehitoglu, A. J. Beaudoin, Y. I. Chumlyakov, H. J. Maier, and C. N. Tomé (2000). Modeling the deformation behavior of Hadfield steel single and polycrystals due to twinning and slip. *Acta Materialia 48*(9), 2031–2047.

Kelley, E. W. and W. F. Hosford, Jr. (1968). Plane-strain compression of magnesium and magnesium alloy crystals. *Transactions of the Metallurgical Society of AIME 242*(1), 5–13.

Klimanek, P. and A. Pötzsch (2002). Microstructure evolution under compressive plastic deformation of Magnesium at different temperatures and strain rates. *Materials Science and Engineering A 324*(1–2), 145–150.

Kocks, U. and H. Mecking (2003). Physics and phenomenology of strain hardening: the FCC case. *Progress in Materials Science 48*(3), 171–273.

Kocks, U. F. (1970). The relation between polycrystal deformation and single-crystal deformation. *Metallurgical Transactions 1*, 1121–1143.

Kocks, U. F., J. S. Kallend, H. R. Wenk, A. D. Rollett, and S. I. Wright (1995). *popLA Preferred Orientation Package – Los Alamos* (LA-CC-89-18 ed.). Los Alamos National Laboratory.

Lavrentev, F. F. (1975). *Deformatsionnoje uprochnenie i dinamika dislokatsii v geksagonalnykh plotno upakovannykh metallakh*. Doctor's thesis, Fiziko-Tekhnicheskii Institut Nizkilch Temperatur, Akademiya Nauk Ukrainskoi SSR, Kharkov.

Lavrentev, F. F. (1980). The type of dislocation interaction as the factor determining work hardening. *Materials Science and Engineering 46*(2), 191–208.

Lavrentev, F. F. and Y. A. Pokhil (1975a). Effect of "forest" dislocations in the $\{11\bar{2}2\}\langle 11\bar{2}3\rangle$ system on hardening in Mg single crystals under basal slip. *Physica Status Solidi (a) 32*(1), 227–232.

Lavrentev, F. F. and Y. A. Pokhil (1975b). Relation of dislocation density in different slip systems to work hardening parameters for Magnesium crystals. *Materials Science and Engineering 18*(2), 261–270.

Lavrentev, F. F., O. P. Salita, and S. V. Sokolsky (1978). Effect of "deformational" and thermal annealing on the stability of dislocation structure in Zn crystals. *Materials Science and Engineering 33*(2), 199–205.

Lavrentev, F. F. and V. L. Vladimirova (1970). Role of dislocations in the plastic deformation of zinc single crystals. *Fizika Metallov i Metallovedenie 29*(1), 150–156.

Lebensohn, R. A. and C. N. Tomé (1993). A self-consistent anisotropic approach for the simulation of plastic deformation and texture development of polycrystals: application to Zirconium alloys. *Acta Metallurgica et Materialia 41*(9), 2611–2624.

Li, B. and E. Ma (2009). Pyramidal slip in magnesium: Dislocations and stacking fault on the $\{10\bar{1}1\}$ plane. *Philosophical Magazine 89*, 1223–1235.

Livescu, V., C. M. Cady, E. K. Cerreta, B. L. Henrie, and G. T. Gray III (2006). The high strain rate deformation behavior of high purity magnesium and AZ31B magnesium alloy. In A. A. Luo, N. R. Neelameggham, and R. S. Beals (Eds.), *Magnesium Technology 2006*, pp. 153–158. The Minerals, Metals & Materials Society.

Ma, Q., H. El Kadiri, A. L. Oppedal, J. C. Baird, and M. F. Horstemeyer (2010). Twinning effects in a rod-textured AM30 Magnesium alloy. Submitted.

Madec, R., B. Devincre, and L. P. Kubin (2002). From dislocation junctions to forest hardening. *Physical Review Letters 89*(25), 255508–1 255508–4.

Mahajan, S. (1971). Twin-slip and twin-twin interactions in Mo-35 at.% Re alloy. *Philosophical Magazine 23*(184), 781–794.

Mahajan, S. (1975). Fragmented twins in Mo-35 at.% Re alloy. *Acta Metallurgica 23*, 547–552.

Mahajan, S. (1981). Accommodation at deformation twins in BCC crystals. *Metallurgical and Materials Transactions A 12*(3), 379–386.

Mahajan, S. and G. Y. Chin (1973a). Formation of deformation twins in FCC crystals. *Acta Metallurgica 21*(10), 1353–1363.

Mahajan, S. and G. Y. Chin (1973b). Twin-Slip, Twin-Twin and Slip-Twin interactions in Co-8 Fe alloy single crystals. *Acta Metallurgica 21*(2), 173–179.

McCabe, R. J., E. K. Cerreta, A. Misra, G. C. Kaschner, and C. N. Tomé (2006). Effects of texture, temperature and strain on the deformation modes of zirconium. *Philosophical Magazine 86*(23), 3595–3611.

McCabe, R. J., G. Proust, E. K. Cerreta, and A. Misra (2009). Quantitative analysis of deformation twinning in zirconium. *International Journal of Plasticity 25*, 454–472.

Mecking, H. and U. F. Kocks (1981). Kinetics of flow and strain-hardening. *Acta Metallurgica 29*(11), 1865–1875.

Michel, J. P. and G. Champier (1975). Effect of the pyramidal dislocation forest on the basal slip of Zn at 198 K. *Memoires Scientifiques de la Revue de Metallurgie 72*(2), 111–114.

Michel, J. P. and G. Champier (1976). Effect of a forest of pyramidal dislocations on basal slip in Zn. In *4th Int. Conf. Strength of Metals and Alloys*, pp. 94 – 97.

Molinari, A., G. R. Canova, and S. Ahzi (1987). A self consistent approach of the large deformation polycrystal viscoplasticity. *Acta Metallurgica 35*(12), 2983–2994.

Mordike, B. L. and T. Ebert (2001). Magnesium properties –applications–potential. *Materials Science and Engineering A 302*(1), 37–45.

Mori, T. and H. Fujita (1980). Dislocation reactions during deformation twinning in Cu-11at.% Al single crystals. *Acta Metallurgica 28*(6), 771–776.

Niewczas, M. (2007). Dislocations and twinning in face centered cubic crystals. In F. R. N. Nabarro and J. P. Hirth (Eds.), *Dislocations in Solids*, pp. 263. Elsevier Science.

Oppedal, A. L., H. El Kadiri, Q. Ma, and M. F. Horstemeyer (2010). Limitation of current hardening models in predicting anisotropy by twinning in hcp metals: Application to a rod-textured AM30 magnesium alloy. in preparation.

Oppedal, A. L., H. El Kadiri, C. N. Tomé, G. C. Kaschner, S. C. Vogel, J. C. Baird, and M. F. Horstemeyer (2010). Hardening mechanisms upon profuse twinning in pure magnesium. submitted.

Parisot, R., S. Forest, A. Pineau, F. Grillon, X. Demonet, and J. M. Mataigne (2004). Deformation and damage mechanisms of zinc coatings on hot-dip galvanized sheets: Part I. deformation modes. *Metallurgical and Materials Transactions A 35A*, 797–811.

Partridge, P. G. and E. Roberts (1964). Slip and deformation twinning in magnesium. In *Third European Regional Conference on Electron Microscopy*, pp. 213–214. Czechoslovak Academy of Sciences.

Petch, N. J. (1953). The cleavage strength of polycrystals. *Journal of the Iron and Steel Institute 174*, 25–28.

Pratt, P. L. and S. F. Pugh (1952). Twin accommodation in zinc. *Journal of the Institute of Metals 80*, 653–658.

Proust, G., C. N. Tomé, A. Jain, and S. R. Agnew (2009). Modeling the effect of twinning and detwinning during strain-path changes of Magnesium alloy AZ31. *International Journal of Plasticity 25*(5), 861–880.

Proust, G., C. N. Tomé, and G. C. Kaschner (2007). Modeling texture, twinning and hardening evolution during deformation of hexagonal materials. *Acta Materialia 55*(6), 2137–2148.

Reed-Hill, R. E. (1973). Role of deformation twinning in determining the mechanical properties of metals. In R. E. Reed-Hill (Ed.), *The Inhomogeneity of Plastic Deformation*, Metals Park, OH, pp. 285–311. American Society for Metals: American Society for Metals.

Rémy, L. (1977). Twin-slip interaction in FCC crystals. *Acta Metallurgica 25*(6), 711–714.

Rémy, L. (1981). The interaction between slip and twinning systems and the influence of twinning on the mechanical behavior of FCC metals and alloys. *Metallurgical and Materials Transactions A 12*(3), 387–408.

Roberts, C. S. (1960). *Magnesium and its Alloys*. New York: John Wiley & Sons.

Robertson, I. M. (1986). Microtwin formation in deformed nickel. *Philosophical Magazine A 54*(6), 821 – 835.

Rosenbaum, H. S. (1961). Non-basal slip and twin accommodation in zinc crystals. *Acta Metallurgica 9*(8), 742–748.

Rosenbaum, H. S. (1964). Nonbasal slip in HCP metals and its relation to mechanical twinning. In R. E. Reed-Hill, J. P. Hirth, and H. C. Rogers (Eds.), *Deformation Twinning*, pp. 43 – 76. New York: Gordon and Breach Science Publishers.

Sachs, G. (1928). Zur ableitung einer fliessbedingung. *Zeitschrift des Vereines Deutcher Ingenieure 72*, 734–736.

Salem, A. A., S. R. Kalidindi, and R. D. Doherty (2003). Strain hardening of titanium: role of deformation twinning. *Acta Materialia 51*(14), 4225–4237.

Saxl, I. (1968). The incorporation of slip dislocations in twins. *Czechoslovak Journal of Physics 18*, 39–49.

Serra, A. and D. J. Bacon (1996). A new model for twin growth in HCP metals. *Philosophical Magazine A 73*(2), 333–343.

Sleeswyk, A. W. (1962a). Emissary dislocations: Theory and experiments on the propagation of deformation twins in $\alpha$-iron. *Acta Metallurgica 10*(8), 705–725.

Sleeswyk, A. W. (1962b). Twinning and the origin of cleavage nuclei in $\alpha$-iron. *Acta Metallurgica 10*, 803–812.

Stohr, J. F. and J. P. Poirier (1972). Etude en microscopie electronique du glissement pyramidal $\{11\bar{2}2\}\langle 11\bar{2}3\rangle$ dans le magnesium. *Philosophical Magazine 25*, 1313–1329.

Taylor, G. I. (1938). Plastic strain in metals. *Journal of the Institute of Metals 62*, 307–324.

Tomé, C. N. (2008). *Program Pole (version 8b)*. Los Alamos National Laboratory.

Tomé, C. N., R. A. Lebensohn, and U. F. Kocks (1991). A model for texture development dominated by deformation twinning: application to Zirconium alloys. *Acta Metallurgica et Materialia 39*(11), 2667–2680.

Tomé, C. N., P. J. Maudlin, R. A. Lebensohn, and G. C. Kaschner (2001). Mechanical response of Zirconium–I. derivation of a polycrystal constitutive law and finite element analysis. *Acta Materialia 49*(15), 3085–3096.

Tomsett, D. I. and M. Bevis (1969). The incorporation of basal slip dislocations in twins in zinc crystals. *Philosophical Magazine 19*(157), 129–140.

USAMP AMD 604 (2006). Magnesium front end project. Technical report, USAMP.

Vladimirova, V. L. and F. F. Lavrentev (1973). Interaction of primary dislocations with forest dislocations in Zn at 1.5 k. *Fizika Tverdogo Tela 15*(2), 549–551.

Von Dreele, R. B. (1997). Quantitative texture analysis by Rietveld refinement. *Journal of Applied Crystallography 30*, 517–525.

Wang, J., J. P. Hirth, and C. N. Tomé (2009). $(\bar{1}012)$ twinning nucleation mechanisms in hexagonal close-packed crystals. *Acta Materialia 57*, 5521–5520.

Wenk, H. R., L. Lutterotti, and S. Vogel (2003). Texture analysis with the new HIPPO TOF diffractometer. *Nuclear Instruments and Methods in Physics Research Section A 515*(3), 575–588.

Wonsiewicz, B. C. and W. A. Backofen (1967). Plasticity of magnesium single crystals. *Transactions of the Metallurgical Society of AIME 239*, 1422–1431.

Yoo, M. H. (1969). Interaction of slip dislocations with twins in hcp metals. *Transactions of the Metallurgical Society of AIME 245*, 2051–2060.

Yoo, M. H. (1981). Slip, twinning, and fracture in hexagonal close-packed metals. *Metallurgical and Materials Transactions A 12*(3), 409–418.

Yoo, M. H. and C. T. Wei (1966). Growth of deformation twins in zinc crystals. *Philosophical Magazine 14*(129), 573–587.